Techno-Economic Assessment of Polyolefin-Rich Plastic Waste Pyrolysis to Naphtha- and Jet-Fuel-Range Blendstocks in the Netherlands

Gate-to-gate steady-state modelling and minimum selling price estimation for two outlet intents

Bram Geveke
4565118

Delft University of Technology

TU Delft

Abstract

In the Netherlands, packaging dominates the plastic waste stream and is rich in polyolefins such as polyethylene and polypropylene. Mechanical recycling remains the predominant route, but it faces challenges for packaging waste due to contamination, material degradation, and multilayer complexity, motivating pyrolysis-based routes that can recover hydrocarbon value from streams that are difficult to recycle mechanically.

This thesis assesses a fixed, gate-to-gate plastic pyrolysis and upgrading configuration and compares two outlet intents, producing either a single naphtha-range blendstock or a split slate with an additional jet-fuel-range blendstock cut. A steady-state mass and energy balance is developed for a fixed four-area plant topology (A100 pyrolysis, A200 hydrotreating, A300 hydrocracking and final fractionation, and A400 utilities and integration), and plant-boundary flows are monetised in a discounted cash flow model. The minimum selling price (MSP) is defined as the main-product price required for break-even at net present value equal to zero; one-at-a-time sensitivity is applied to key levers, and a pedigree-based lens is used to qualify claim strength.

At a common 40 kt/y plastic feed basis and 8,000 h/y utilisation, total saleable liquid production is essentially unchanged between outlet intents (2,807.73 kg/h versus 2,816.11 kg/h), while the jet-oriented intent mainly redistributes the liquid pool and increases electricity demand (112.40 to 219.92 kW). The resulting MSP is 2,134 EUR/t for the naphtha pathway and 4,940 EUR/t for the jet-fuel pathway, with the difference driven primarily by MSP closure and main-product basis in the split slate rather than by higher overall liquid yield. Sensitivity results show that scale and fuel-gas export monetisation dominate MSP: reducing capacity from 40 to 20 kt/y increases MSP by 28.2% (naphtha) and 37.7% (jet), and removing the fuel-gas export credit increases MSP by 10.8% and 14.3%, respectively. Results are screening-level, steady-state, and gate-to-gate; they are not investment-grade, exclude full life-cycle assessment, and do not imply certification or aviation-fuel compliance.

Contents

1

Introduction

Since the development of petrochemical routes to produce polymers, plastics have become a cornerstone of modern society. Valued for low cost, low weight, durability, and versatility, plastics are widely used across consumer, industrial, and infrastructure applications [1]. These properties have driven global plastic production from approximately 2 $\mathrm{Mt\,y^{-1}}$ in 1950 [2] to over 400 $\mathrm{Mt\,y^{-1}}$ today [3], with forecasts suggesting production could double by 2050 if current patterns persist [4].

However, these benefits are accompanied by growing environmental concerns associated with plastic production and end-of-life management. Widespread use of plastic products generates large quantities of plastic waste. By 2015, approximately 6,300 Mt of plastic waste had been generated; around 9% had been recycled, 12% incinerated, and 79% accumulated in landfills or released into the natural environment [5]. Plastic debris has been found in all major ocean basins [6], from the deep sea to near the summit of Mount Everest, and even within the atmosphere [7]. Due to their resistance to natural degradation, plastics persist for decades or longer, leading to widespread and long-term pollution [8]. Even when plastics degrade through weathering, they fragment into microplastics that can disrupt food chains and adversely affect human and environmental health [2].

In addition, greenhouse gas (GHG) emissions from plastic manufacturing contribute to climate change. In 2015, plastic manufacturing was responsible for an estimated 1.7 Gt CO_2-equivalent emissions, accounting for roughly 4% of global carbon emissions [9]. If current trends continue, this figure could rise to 6.5 Gt CO_2 eq by 2050, at which point plastics would consume around 15% of the global carbon budget for limiting warming to below 2 °C [10].

The plastics sector is also strongly path-dependent on fossil fuels for both feedstock and energy, resulting in carbon lock-in [11]. Over 90% of plastic feedstock is derived from fossil sources [12]. Moreover, an estimated 6% of global oil production is used for plastics production, with roughly half used as material feedstock and half as fuel for production processes [10]. If growth continues as expected, oil consumption by the plastics sector could reach 20% of total oil consumption by 2050 [10].

These combined impacts, resource dependence, GHG emissions, and persistent pollution, motivate a transition from today's linear model of *extract–manufacture–use–discard* toward a circular plastics economy. In a circular economy, waste plastics are recovered and repurposed as feedstock for remanufacturing, such that raw materials remain in use and material value is retained within the value chain [8], [13].

One of the clearest examples of linearity in plastics use is packaging. Packaging represents a large share of total plastic consumption and is characterized by short use cycles and high disposability [14]. In the Netherlands, packaging dominates the plastic waste stream, with polyolefins such as polyethylene (PE) and polypropylene (PP) representing the bulk of this flow [15], [16]. Mechanical recycling

is currently the predominant recycling route, but it faces challenges for packaging waste due to contamination, material degradation, and the complexity of multilayer structures [17], [18]. In addition, repeated processing can degrade mechanical properties, contributing to down-cycling into lower-value applications [19].

As a result, despite considerable sorting and recycling efforts in the Netherlands, large volumes of plastic packaging waste are currently incinerated with energy recovery. It remains a primary end-of-life option for plastic packaging [20]. In 2017, 229 kt of household packaging waste was incinerated with energy recovery, representing 57% of the total share [21]. While this approach can recover heat and electricity, it does not mitigate demand for virgin plastics [22] and is associated with emissions of up to 3 kg CO_2 per kilogram of plastic incinerated [23]. Incineration also removes plastics from the material cycle, undermining circularity objectives.

In response to the limitations of current waste management, advanced recycling technologies have emerged to address hard-to-recycle plastic streams that are commonly destined for incineration or suffer from the drawbacks of mechanical recycling. Among the most prominent options is pyrolysis [24], [25]. Pyrolysis involves thermal decomposition of plastic waste in the absence of oxygen, producing an oil-like liquid spanning a wide range of hydrocarbons, alongside a non-condensable gas fraction and solid residues [26].

The liquid intermediate from pyrolysis can be upgraded into valuable liquid blendstocks for different markets. One key product intent is upgrading toward a *naphtha-range blendstock*, motivated by the role of naphtha as a primary steam-cracker feedstock for producing light olefins such as ethylene and propylene. In this context, pyrolysis-based recycling provides a potential route to reduce reliance on virgin fossil feedstock and to redirect plastic waste from incineration toward material re-entry into petrochemical value chains, while leveraging existing petrochemical infrastructure.

A second strategic product intent is upgrading toward a *jet-fuel-range blendstock*. Aviation is widely regarded as hard to abate because aircraft will continue to require high-energy-density liquid fuels for the foreseeable future, while direct electrification and hydrogen face major deployment constraints for long-haul aviation [27]. Pyrolysis of polyolefin-rich waste can yield a liquid with material in the jet-fuel boiling range, but practical use in fuel supply chains is governed by stringent property windows and impurity constraints, which typically require fractionation and more extensive upgrading [28]. In this thesis, the jet outlet is treated as a jet-fuel-range blendstock objective under specification intent. The purpose is to compare the technical and economic implications of a more stringent upgrading target, not to claim fuel certification or compliance, which lies outside the scope of this work.

Despite growing interest in plastic pyrolysis, its techno-economic performance at industrial scale remains uncertain, particularly when assessments are translated into specific national contexts and when alternative product intents are compared under consistent boundaries and modeling conventions. Reported studies often differ in feedstock definition, upgrading representation, and boundary treatment, which complicates like-for-like comparison of outcomes and obscures the drivers of economic feasibility.

To address these gaps, this thesis assesses the techno-economic performance of pyrolysis-based recycling of a representative Dutch residual plastic fraction. The quantitative assessment uses a pretreated, polyolefin-rich feed derived from DKR 350 (formal feedstock definition in Chapter 5) and adopts a reference facility scale of 40 kt y^{-1} within the Dutch industrial context. Two pathways are evaluated under a single shared gate-to-gate process topology: (i) a *naphtha pathway* targeting a cracker-relevant naphtha-range blendstock, and (ii) a *jet-fuel pathway* targeting a jet-fuel-range blendstock while co-producing naphtha. The pathways differ only by upgrading severity and fractionation cut logic; detailed stream numbering and area definitions are introduced in Chapter 5.

A screening-level techno-economic assessment (TEA) framework is applied to quantify (i) technical performance using Technical Performance Metrics (TPMs) and (ii) economic performance using the minimum selling price (MSP) under a consistent discounted cash flow (DCF) basis. Robustness is

tested using a focused one-at-a-time (OAT) sensitivity analysis in which one economic parameter is varied at a time while all other technical and financial assumptions remain fixed. This thesis does not perform a full life-cycle assessment (LCA). Environmental relevance is therefore discussed as context, while the quantitative scope is restricted to the gate-to-gate system defined in Chapters 4–5.

The feasibility of pyrolysis-based recycling also depends on how the system is positioned within the value chain. Key stakeholders include (i) waste management and sorting actors supplying the residual feedstock at battery limits, (ii) the plant operator responsible for conversion and upgrading, (iii) suppliers of imported hydrogen and purchased utilities, (iv) offtakers in petrochemical and refinery value chains receiving liquid blendstocks, and (v) regulators and policy actors shaping incentives and constraints for waste diversion and circularity. These stakeholder interfaces influence boundary choices and the economic interpretation of contracting conditions (e.g., gate fee versus paid feedstock) and offtake assumptions for liquid products and byproducts.

Guided by this framing, the thesis addresses the following main research question:

> *What is the techno-economic performance of producing a cracker-relevant naphtha-range blendstock and a jet-fuel-range blendstock through pyrolysis-based recycling of polyolefin-rich plastic waste in the Netherlands under a consistent gate-to-gate screening TEA basis?*

The corresponding sub-research questions and the phased methodology used to answer them are defined in Chapter 4.

This work aligns with the objectives of the MSc Sustainable Energy Technology program by applying system-level analysis to a conversion technology at the interface of waste management, industrial energy use, and chemical/fuel value chains. The emphasis is on transparent modeling and auditable techno-economic interpretation of near-term integration options, rather than investment-grade valuation or lifecycle quantification.

The remainder of this thesis is structured as follows. Chapter 2 introduces the plastics system context and motivates the Dutch residual feedstock and product intents. Chapter 3 reviews the literature and synthesizes evidence gaps and constraints that inform modeling choices. Chapter 4 defines the research questions, scope, and TEA methodology. Chapter 5 establishes the gate-to-gate system design, feedstock specification, and the pathway-defining choices that are held fixed in subsequent chapters. Chapter 6 reports steady-state technical performance and TPMs for both pathways. Chapter 7 translates these technical outcomes into economic results using an MSP-based screening TEA under a consistent DCF basis. Finally, Chapter 8 tests robustness through an OAT sensitivity analysis, comparing how MSP responds to a focused set of high-leverage parameters in the naphtha pathway and the jet-fuel pathway.

2

Background

Chapter 1 introduced the environmental burden of plastic waste, with particular attention to short-lived packaging applications dominated by polyolefins. It also positioned thermochemical recycling, and pyrolysis in particular, as a route that can convert polyolefin-rich waste into a hydrocarbon intermediate that may be used as an energy carrier or as a chemical feedstock. Building on that foundation, this chapter provides the conceptual background needed to motivate the system and feedstock choices assessed in later chapters. It first summarizes how plastics are produced, classified, and used across sectors, emphasizing why packaging dominates waste generation. It then discusses why polyolefins are central to packaging, and outlines the main end-of-life pathways and their input-quality requirements. The chapter concludes by clarifying what background elements are fixed for this thesis and where the formal system definition is provided.

2.1. The Current Plastic System

2.1.1. Plastic Types and Characteristics

Plastics are synthetic or semi-synthetic materials composed of organic polymers, formed through polymerization of monomers into long chains of repeating units. The term *plastic* originates from the Ancient Greek word πλαστικός (*plastikos*), meaning “capable of being shaped or molded,” reflecting their malleability. Depending on molecular structure and processing conditions, plastics can be extruded into films, molded into rigid objects, thermoformed into flexible packaging, or spun into synthetic fibers.

Plastics are commonly categorized into thermoplastics and thermosets based on their physico-chemical behavior under heat treatment [29]. Thermoplastics consist of polymer chains that are not chemically cross-linked, allowing them to soften and melt reversibly upon heating. This enables reshaping and reprocessing and makes thermoplastics recyclable *in principle*, provided sufficient input quality [30]. Common thermoplastics include PE, PP, polyethylene terephthalate (PET), polystyrene (PS), and polyvinyl chloride (PVC). PE can be further classified into high-density (HDPE), medium-density (MDPE), low-density (LDPE), and linear low-density (LLDPE) grades, based on density and the morphology of the polymer backbone.

Figure 2.1 shows the global distribution of plastics production by polymer family in 2021. For this thesis, the key implication is that thermoplastics dominate total production, supporting a focus on thermoplastic waste streams and, within those, the major commodity polymers relevant to packaging [3].

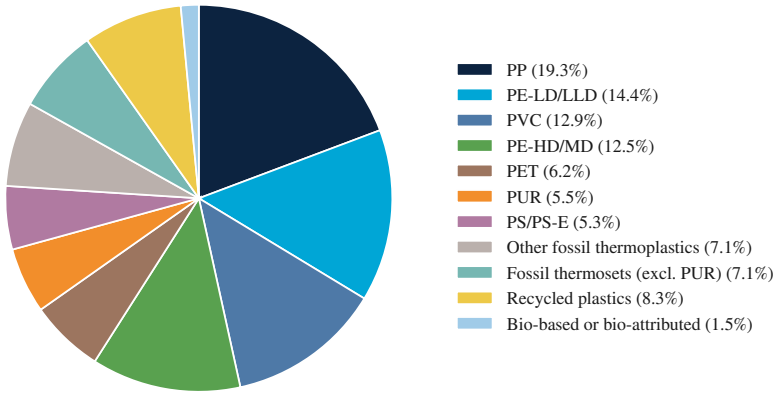

Figure 2.1: Global plastic production by polymer family, 2021. Adapted from PlasticsEurope (2024) [3].

Thermosets, in contrast, form three-dimensional networks of cross-linked polymer chains. Once cured, they harden permanently and cannot melt upon reheating; instead, they degrade irreversibly [31]. This makes thermosets unsuitable for conventional mechanical recycling. Consequently, thermosets are typically disposed of through incineration, landfilling, or niche reuse as inert fillers [32]. Due to these limitations, thermosets are of limited relevance to this study and to recycling-focused literature more broadly, where the term *plastics* is often used to refer primarily to thermoplastics.

2.1.2. Plastic Production and Processing

Plastics can also be classified by the chemical pathways through which they are synthesized from fossil feedstocks. Production begins with the extraction of hydrocarbons, typically crude oil or natural gas, which are refined and distilled into fractions. Among these, naphtha is a key intermediate for plastics production, while lighter gases such as ethane and propane are also used. In steam crackers, these feedstocks undergo thermal cracking to produce light olefins (e.g., ethylene, propylene, butadiene) and aromatics (e.g., benzene, toluene, xylene) that serve as precursors for polymer synthesis. Olefins can be used directly as monomers, whereas aromatics are typically converted into functionalized compounds such as terephthalic acid, ethylene glycol, and diisocyanates.

These monomers are polymerized via two principal routes: addition polymerization and condensation polymerization. In addition polymerization, monomers with unsaturated bonds undergo a chain-growth process in which successive monomers add to the reactive end of a growing polymer chain. The repeating unit retains the full atomic composition of the monomer, meaning no small molecules are released during the reaction [30], [33]. This process may be initiated by free radicals, cations, anions, or coordination catalysts [34]. Figure 2.2 provides a schematic representation of addition polymerization. For this thesis, the relevance is that major packaging polymers such as PE and PP are produced via addition polymerization, which also influences the set of feasible chemical recycling routes discussed later.

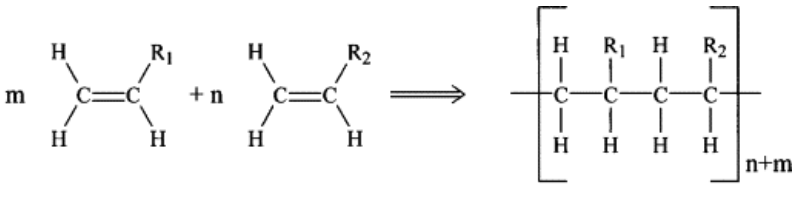

Figure 2.2: Schematic representation of addition polymerization. Adapted from [35].

The production method influences polymer structure and properties. LDPE is synthesized through high-pressure free-radical polymerization, resulting in a highly branched structure. This branching inhibits tight chain packing, giving LDPE its flexibility, softness, and relatively low density. In contrast, HDPE is produced at lower pressures using catalytic polymerization, yielding more linear chains with higher crystallinity [30], [36].

PP is produced by catalytic polymerization of propylene, typically using Ziegler–Natta catalysts. The presence of a methyl group on every other carbon atom in the repeating unit increases stiffness and melting temperature relative to PE, supporting applications requiring greater rigidity and thermal stability [30], [36].

In condensation polymerization, bifunctional monomers react to form a polymer chain while eliminating a small molecule such as water, methanol, or HCl as a byproduct; the repeating unit therefore differs in atomic composition from the original monomers [31]. This mechanism is common for polyesters (e.g., PET), polyamides (e.g., Nylon), and polyurethanes. Figure 2.3 illustrates the principle of condensation polymerization. For this thesis, the key implication is that condensation polymers (e.g., PET) enable depolymerization routes that are typically not applicable to polyolefins.

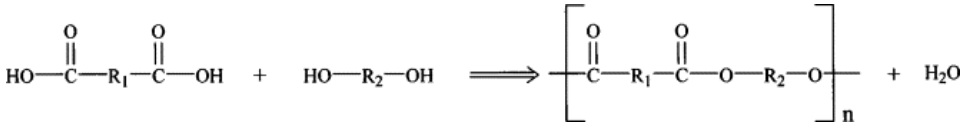

Figure 2.3: Schematic representation of condensation polymerization. Adapted from [35].

After polymerization, raw polymers are typically produced as pellets or powders and blended with additives such as plasticizers, stabilizers, colorants, and flame retardants to achieve desired properties [37]. These additives are relevant to end-of-life processing because they influence contamination, sorting performance, and the quality constraints on recycling outputs. Final products are then manufactured via extrusion, injection molding, blow molding, or thermoforming.

2.1.3. Plastic Applications and Packaging Material

Plastics are used across packaging, construction, automotive, electronics, household goods, and agriculture. Their low cost, durability, and ease of processing have enabled substitution for traditional materials such as metals, glass, and wood. Figure 2.4 shows the global distribution of plastics demand by application in 2021. The key implication for this thesis is that packaging dominates demand and is characterized by short product lifetimes, making it a major contributor to near-term waste generation [16].

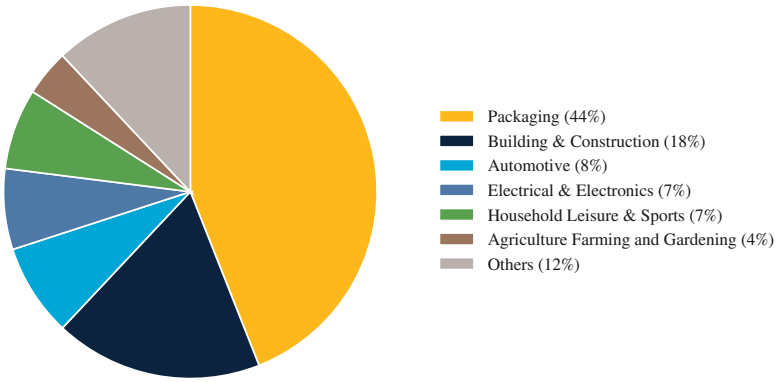

Figure 2.4: Distribution of global plastics use by application in 2021 [16].

Packaging plastics are typically designed for single-use or short-lived purposes, resulting in rapid transition from use to disposal. In contrast, plastics in construction or automotive remain in use for years or decades. This short functional lifespan contributes to a predominantly linear packaging system, where materials are extracted, used once, and then discarded. Packaging waste also poses specific recycling challenges due to low weight, frequent contamination, and widespread use of multilayer or multi-material structures.

Packaging materials are dominated by polyolefins, primarily PE and PP. Together, these accounted for approximately 55% of plastic packaging in 2021 [16]. Figure 2.5 shows their general chemical structures. For this thesis, the key implication is that the hydrocarbon nature of polyolefins makes them compatible with thermochemical conversion to hydrocarbon intermediates, while the additive/contaminant burden and heterogeneity of packaging remain binding constraints for downstream upgrading.

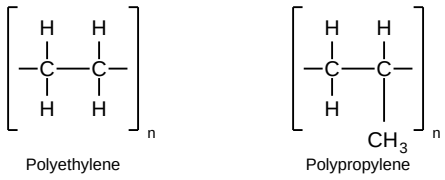

Figure 2.5: General chemical structure of polyethylene and polypropylene [36].

PE is widely used in packaging due to its ductility, chemical resistance, and ease of processing, with LDPE and HDPE grades suited for flexible and rigid packaging, respectively. The low density and flexibility of LDPE make it appropriate for films and bags, while the higher crystallinity and tensile strength of HDPE support use in containers and crates [30], [36].

PP is similarly important in packaging, particularly where higher stiffness and thermal resistance are required. The methyl substituent in the PP backbone increases rigidity and melting point relative to PE, supporting applications such as food containers, caps, labels, and rigid or semi-flexible packaging formats [30], [36].

2.1.4. Transition Options and Strategic Considerations

The dominance of short-lived polyolefin packaging highlights the need for system-level strategies that address both resource use and end-of-life handling. Two broad approaches are often discussed: (1)

improving the circularity of existing fossil-based plastics through recycling, and (2) substituting fossil-derived plastics with alternatives such as bio-based or biodegradable polymers. Bio-based plastics may reduce fossil feedstock dependence and are sometimes cited as a route to lower life-cycle impacts, but their adoption remains limited; as of 2022, they accounted for less than 2% of global plastic production [3]. Key constraints include production cost, feedstock availability, land-use trade-offs, and compatibility with existing recycling infrastructure.

Most bio-based plastics are chemically identical to fossil-based thermoplastics (drop-in materials) and therefore face similar end-of-life challenges. Others, such as biodegradable plastics, require controlled composting conditions that are often not available in practice. As a result, recycling remains the most immediate strategy for reducing plastic waste volumes and increasing circularity within the current system, especially for high-volume packaging applications. However, the heterogeneity and contamination typical of post-consumer packaging waste limit the performance of conventional mechanical recycling and motivate interest in advanced recycling technologies, including thermochemical routes such as pyrolysis.

2.2. Plastic Recycling

Within current system constraints, recycling remains a central option for mitigating the impacts of plastic waste. Its performance depends not only on conversion technologies, but also on upstream stages of collection, sorting, and pretreatment, which determine both the quantity and quality of material available for reuse. These stages also determine which recycling routes are technically and economically feasible. The following sections summarize collection and sorting and then introduce the main technological recycling pathways and their input-quality requirements.

2.2.1. Plastic Collection

Collection is the first operational step in recycling systems and influences both the volume and quality of plastic waste available for further processing. Collection strategies can be broadly divided into source separation (separation at the point of disposal) and post-collection recovery (extraction from mixed municipal solid waste, MSW).

Within the European Union, source-separation systems are generally preferred because they can deliver higher-quality material streams that require less intensive downstream sorting [38]. Examples include curbside or drop-off household schemes and deposit-refund systems that recover low-contamination, single-polymer streams [30]. Household separation can also provide good material quality, though effectiveness depends heavily on public participation and correct disposal behavior [22].

In contrast, post-collection recovery systems can increase the overall volume of plastics collected by mechanically separating them from mixed MSW, but such streams tend to be more contaminated and typically yield lower-quality recyclates unless additional cleaning and sorting steps are applied.

The Netherlands employs a hybrid system combining household separation of lightweight packaging waste, mechanical recovery from residual MSW, and a deposit-refund system for PET beverage bottles [39]. This combination increases collection volumes, but the resulting streams differ significantly in quality. Deposit-refund PET streams are relatively homogeneous and can support closed-loop recycling, while mixed household-collected and MSW-derived streams often require intensive sorting and are more likely to be directed to open-loop applications or advanced recycling routes.

2.2.2. Plastic Sorting

After collection, plastics are sorted into fractions of sufficient purity. The required degree of homogeneity depends on the downstream recycling route and targeted product quality. Sorting can be performed manually or through automated systems that exploit material properties to separate large volumes efficiently [40].

Automated sorting techniques can be grouped into direct and indirect methods. Direct sorting separates materials based on intrinsic properties such as size, density, magnetism, or conductivity. Representative examples include air classification, magnetic and eddy current separation (for metal removal), and density-based separation such as float–sink and hydrocyclones [41].

Indirect sorting methods identify materials using sensing and detection technologies prior to separation. In practice, these are dominated by optical and spectral approaches for polymer identification (e.g., near-infrared and hyperspectral imaging), supported by X-ray-based methods where elemental information is needed [41]. Performance can be limited by contamination, coatings, and dark plastics.

Sorting lines are frequently integrated with pretreatment steps such as shredding or granulation, washing to remove organic/inorganic contaminants, and drying [30]. For this thesis, the key implication is that sorting and pretreatment determine not only polymer purity, but also the residual contaminant burden (e.g., additives, multilayers, and trace elements) that constrains feasible recycling pathways and, for advanced recycling, the upgrading requirements for intermediate products.

2.2.3. Recycling Strategies and Technologies

Once plastic waste is sorted into fractions of varying purity, it can be directed to different recycling routes. These strategies are commonly categorized into four levels: primary, secondary, tertiary, and quaternary recycling [22]. Each route differs in the extent to which it preserves the original polymer structure and in its contribution to material circularity.

Primary Recycling

Primary recycling (reuse or re-extrusion) requires exceptionally clean and homogeneous streams and involves reintegration of single-polymer waste into production. Because the polymer retains its original properties, this approach can enable products comparable to those made from virgin material and is therefore a closed-loop pathway [42]. In practice, it is typically limited to pre-consumer waste such as production off-cuts or process scrap and is rarely feasible for most post-consumer packaging waste due to strict purity requirements [32].

Secondary Recycling

Secondary recycling, commonly referred to as mechanical recycling, converts post-consumer plastic waste into new products through physical reprocessing while retaining the polymer backbone [42]. Pretreated streams (sorted, washed, and size-reduced) are melted and re-extruded into flakes or pellets. Recyclate quality depends strongly on upstream sorting and cleaning, since incompatible polymers and impurities compromise melt behavior and mechanical properties [42].

Mechanical recycling is the dominant recycling route today, but it faces limitations [43]. Polymer chains degrade under thermal and mechanical stress during use and reprocessing, reducing achievable product quality [44]. As a result, downcycling to lower-value products is common, and most thermoplastics can only undergo a limited number of recycling cycles before properties deteriorate [32]. Packaging waste is particularly challenging due to multilayers, pigments, additives, and organic residues, which increase sorting/cleaning requirements and reduce the likelihood of producing high-quality recyclate [42]. Closed-loop recycling is therefore typically limited to selective collection systems that deliver clean mono-material streams, such as deposit-refund PET. In the Netherlands, the *statiegeld* system reported a closed-loop recycling rate of 99% for PET bottles in 2017 [15].

Tertiary Recycling

When plastics are too contaminated or compositionally complex for mechanical recycling, tertiary recycling provides routes that convert polymers into chemical feedstocks. Also referred to as chemical or feedstock recycling, tertiary recycling includes chemical depolymerization and thermochemical conversion processes that produce monomers or other intermediates that can be used to produce plastics, chemicals, or fuels.

Chemical depolymerization uses combinations of solvents, reagents, and heat to cleave polymers into monomers or oligomers, which can then be purified and reintroduced as secondary raw materials [45]. It is particularly suited to condensation polymers such as PET and polyamides, whose ester or amide bonds can be cleaved under relatively mild conditions. For PET, established pathways include glycolysis to bis(2-hydroxyethyl) terephthalate (BHET), methanolysis to dimethyl terephthalate (DMT), and hydrolysis to terephthalic acid (TPA), all of which can be repolymerized. Polyamides such as nylon-6 can be recovered as ε-caprolactam, while other nylons often require harsher conditions and yield less selectively. Because depolymerization performance depends on monomer recovery and purification, it is best suited to relatively homogeneous, uncontaminated waste streams [45], [46].

Thermochemical recycling methods, including pyrolysis, gasification, and hydrothermal liquefaction, apply heat (and sometimes catalysts) under controlled atmospheres to convert plastic waste into fuels or chemical feedstocks. Compared to mechanical recycling and chemical depolymerization, thermochemical processes can accommodate more heterogeneous and contaminated streams, though pretreatment and contaminant management remain important [37].

Pyrolysis (typically 400–800 °C, oxygen-free) converts plastics into condensable vapors (oil), non-condensable gases, and char [47]. For polyolefins such as PE and PP, pyrolysis yields hydrocarbon mixtures that can be upgraded and introduced into petrochemical value chains, including steam cracking routes, to recover olefins such as ethylene and propylene [24], [25]. Gasification converts plastics at high temperatures (typically $>$700 °C) in the presence of limited oxygen or steam to produce synthesis gas (CO and H_2), which can be used for power generation or synthesis routes such as methanol production and Fischer–Tropsch conversion [37]. Hydrothermal liquefaction operates in water at moderate temperatures (typically 250–400 °C) and high pressures, yielding crude-like oils that may be further refined [47].

Quaternary Recycling

When neither mechanical nor tertiary recycling routes are feasible, plastics are often diverted to quaternary recycling, where energy is recovered through incineration in waste-to-energy (WtE) facilities. This utilizes the calorific value of plastics for heat and electricity generation but results in irreversible material loss and associated emissions. From a circularity perspective, it is generally the least favorable option.

In the Netherlands, landfilling of recoverable waste has been prohibited since 2009 [48]. When recycling is infeasible, incineration is therefore a primary alternative. Despite increased packaging recycling from 2006 to 2020, around 35% of plastic packaging waste remains unrecycled and is largely incinerated [16]. Polyolefins such as HDPE, LDPE, and PP have high calorific values (above 40 MJ/kg), supporting their use as WtE fuels [47], [49]. In the Netherlands, WtE facilities generate around 10 PJ annually, supplying approximately 2.4% of national electricity [23]. Incineration releases around 3 kg CO_2 per kilogram of plastic combusted, alongside other air pollutants [23].

2.2.4. Scope and Handover

This chapter has outlined the plastic system from production to end-of-life, emphasizing (i) the dominance of short-lived packaging applications and (ii) the central role of polyolefins (PE and PP) within packaging waste. It also summarized how the feasibility of recycling routes depends on upstream collection and sorting and on the input-quality requirements of mechanical recycling, depolymerization, and thermochemical conversion.

For this thesis, the key background implication is that a substantial share of post-consumer packaging remains heterogeneous and contaminated after collection and sorting, limiting closed-loop mechanical recycling and motivating advanced recycling approaches that can produce hydrocarbon intermediates. Accordingly, the quantitative assessment in later chapters focuses on pyrolysis-based conversion of a representative Dutch residual plastic fraction: a pretreated, polyolefin-rich feed derived from DKR 350 (formal feedstock definition and system boundary in Chapter 5). The assessment evaluates two product intents for the upgraded liquid intermediate, a naphtha-range blendstock and a jet-fuel-range blend-

stock, within a consistent gate-to-gate techno-economic scope defined in Chapters 4–5.

The following chapter reviews the literature relevant to these pathways and the Dutch context, identifying evidence gaps and constraints that inform the modelling choices used in the system design and assessment chapters.

3

Literature Review

This chapter critically reviews the state of the art on thermochemical recycling of plastics, with emphasis on polyolefin-rich packaging waste in the Dutch context and on pathways that valorise the liquid fraction through hydroprocessing. The chapter first compares hydrothermal liquefaction (HTL), gasification, and pyrolysis, and motivates pyrolysis as the most relevant route for producing hydrocarbon liquids that can be upgraded into specification-oriented blendstocks. It then examines feedstock and pretreatment, explaining why polyolefins are technically favourable, how Dutch sorting practices shape available streams, and why the residual DKR 350 fraction provides a policy-relevant reference basis. Next, it reviews pyrolysis operation and reactor design, focusing on variables that govern yield, distillation behaviour, and the balance between condensables and light gases, while highlighting limitations of batch-dominated evidence. The chapter then synthesises pyrolysis products and product quality constraints, showing why liquid upgrading is primarily driven by olefinicity and trace contaminants for real residual feeds. Building on this, it frames upgrading against specification intent for two outlet objectives implemented in this thesis as a *naphtha pathway* (cracker-relevant naphtha-range blendstock) and a *jet-fuel pathway* (jet-fuel-range blendstock), and it reviews hydrotreating and hydrocracking evidence with explicit attention to what is transferable into model-ready indicators. Finally, it reviews TEAs of plastic pyrolysis, identifies comparability limitations that originate in non-aligned upgrading and boundary assumptions, and synthesises cross-cutting knowledge gaps that motivate the modelling and assessment approach used in later chapters.

3.1. Thermochemical recycling routes for plastics

Building on the overview of thermochemical reactor technologies given in Chapter 2, this section compares HTL, gasification, and pyrolysis for polyolefin-rich packaging waste, with a focus on technical suitability, scalability, and implications for downstream upgrading and system integration.

3.1.1. Hydrothermal liquefaction

HTL employs water under subcritical conditions (250–370 °C, 10–25 MPa) or supercritical conditions ($>$374 °C, $>$22 MPa) to depolymerise plastics into oil-like products [50], [51]. While PET and PC readily undergo hydrolysis in subcritical water, polyolefins and polystyrene are resistant under these conditions and generally require supercritical environments to achieve high conversion [24]. Under optimised supercritical conditions, oil yields above 90 wt% have been reported for polyethylene and polypropylene, with product fractions spanning naphtha and diesel boiling ranges [24]. These conditions demand high pressures and temperatures, implying high-pressure equipment, elevated energy demand, and increased CAPEX and OPEX relative to atmospheric pyrolysis. In addition, oils produced from polyolefins in HTL can exhibit diesel-like density and heating value, but oxygenated compounds

formed through radical reactions in the aqueous matrix have also been reported, complicating direct integration with conventional refinery and petrochemical units [51]. Compared with pyrolysis and gasification, plastic HTL remains at an earlier development stage, with most studies still at laboratory scale [51]. Overall, HTL is technically promising but faces deployment barriers associated with high-pressure operation, energy intensity, and limited commercial evidence for plastics.

3.1.2. Gasification

Gasification converts plastics into syngas, primarily a mixture of hydrogen and carbon monoxide, by partial oxidation at high temperatures of roughly 700–1500 °C [24], [52]. Operating with oxygen, steam, or air, it produces synthesis gas that can be used for heat and power or upgraded into chemicals such as methanol and Fischer–Tropsch liquids [50], [51]. The process can treat heterogeneous and contaminated waste streams [24], but its high operating temperature increases energy demand and cost relative to pyrolysis [52]. Tar formation and syngas cleaning requirements further complicate operation and increase capital intensity [53]. From a material circularity perspective, converting polyolefin carbon chains into syngas breaks down hydrocarbons into single-carbon species and requires additional synthesis steps to return to liquid fuels and chemicals. Although gasification is well established for coal and biomass, its application to plastics is comparatively novel and less mature [24]. Overall, gasification offers feedstock flexibility and a versatile intermediate, but its high energy intensity, cleaning demands, and different circularity logic reduce its relevance for near-term liquid upgrading routes.

3.1.3. Pyrolysis

Compared with HTL and gasification, pyrolysis aligns more closely with polyolefin-rich packaging waste and with the objective of producing hydrocarbon liquids that can be upgraded into petrochemical and fuel-range blendstocks [18], [24], [50]. Pyrolysis operates at moderate temperatures in the absence of oxygen, enabling thermal decomposition of polyolefins into condensable hydrocarbons that can be fractionated into naphtha-range material and heavier cuts [18], [54], [55]. Unlike HTL, pyrolysis avoids high-pressure water systems; unlike gasification, it avoids the intermediate step of syngas production. Reviews of industrial practice emphasise continuous reactor concepts and heat integration as central implementation themes, while also noting persistent challenges related to feed contamination and product quality [18], [37]. For these reasons, the remainder of this chapter focuses on pyrolysis feedstock and pretreatment, operating conditions and reactor design, product distributions and quality constraints, upgrading framed by specification intent, and TEA evidence.

3.2. Feedstock and pretreatment

3.2.1. Feedstock suitability and limitations of laboratory evidence

As discussed in Chapter 2, polyolefins are a technically suitable feedstock class for producing hydrocarbon liquids by pyrolysis. This suitability is often motivated using proximate and ultimate analysis. Proximate analysis evaluates moisture, volatile matter, ash, and fixed carbon, while ultimate analysis provides elemental composition. Table 3.1 summarises representative proximate and elemental analyses and degradation temperature ranges for common polymers. The values are compiled from Dai et al. [56], while the original data sources are indicated in the reference column.

Table 3.1 indicates high volatile matter and low ash for most polymers. In pyrolysis, volatile matter correlates with liquid yield, whereas ash can promote char formation and influence gas composition [47]. Polyolefins are distinguished in ultimate analysis by consisting primarily of carbon and hydrogen, yielding a high H/C ratio and avoiding oxygen, nitrogen, and chlorine. This supports production of alkanes and alkenes without intrinsically generating oxygenated or halogenated compounds. In contrast, PET and PVC can introduce oxygenated compounds and hydrogen chloride upon degradation, respectively, which can degrade liquid stability and increase corrosion and impurity-management requirements [18], [47], [70]. PS tends to produce more aromatic oils; these may be valuable in specific chemical markets but are not inherently aligned with cracker-relevant naphtha objectives and may constrain jet-fuel-range

Table 3.1: Proximate and elemental analysis of different polymers, with degradation temperatures. Values are compiled from Dai et al. [56], while the original data sources are indicated in the reference column.

Plastic type	Proximate analysis[1]	Elemental analysis[2]	Degradation T (°C)	Ref.
Polyethylene terephthalate (PET)	0.46 / 86.83 / 7.77 / 0.02	C 62.5, H 4.2, O 33.3	370–530	[57], [58]
High-density polyethylene (HDPE)	0.00 / 99.81 / 0.01 / 0.18	C 85.6, H 14.4	450–520	[59], [60]
Polyvinyl chloride (PVC)	0.80 / 93.70 / 6.30 / 0.00	C 38.5, H 4.9, Cl 56.6	280–350	[61], [62]
Low-density polyethylene (LDPE)	0.30 / 99.70 / 0.00 / 0.00	C 85.6, H 14.4	400–500	[63], [64]
Polypropylene (PP)	0.15 / 95.08 / 1.22 / 3.55	C 85.7, H 14.3	350–500	[64], [65]
Polystyrene (PS)	0.25 / 99.63 / 0.12 / 0.00	C 92.3, H 7.7	350–500	[66], [67]
Acrylonitrile butadiene styrene (ABS)	–	C 87.5, H 8.5, N 4.0	350–500	[68], [69]
Polyamide (PA, Nylon)	–	C 63.0, H 8.0, O 13.0, N 16.0	380–500	[69]

blending depending on required property envelopes [71]. For these reasons, many pyrolysis studies restrict PVC and PET to low shares in mixtures, often assuming 1–2 wt% and targeting < 5 wt% [70].

While these compositional arguments support polyolefin-rich feedstocks, a central limitation of the literature is the dominance of virgin, single-polymer experiments. Laghezza et al. [18] report that 79% of studies examine virgin resins, largely in batch experiments at around 500 °C, with polyethylene and polypropylene dominating. This bias provides mechanistic insight but reduces applicability to real post-consumer waste, which is heterogeneous and contains additives, fillers, and residues. Mixed feeds can exhibit polymer interactions that shift decomposition behaviour and product slates. Martínez-Narro et al. [72] show that mixed waste exhibits polymer–polymer interactions, where radicals from PS destabilise polyolefins and shift decomposition to lower temperatures. Hussein et al. [73] find that kinetic parameters differ substantially between mixtures and individual polymers, complicating reactor modelling. Mirkarimi et al. [74] emphasise that even small PET or PVC fractions can reduce liquid yields and degrade oil quality.

A further distinction is between virgin polymers and real waste. Xayachak et al. [75] note that much knowledge is derived from additive-free virgin polymers, whereas post-consumer waste is mechanically and thermally aged and contains variable contamination. Comparative studies show higher liquid yields and lower char for virgin samples than for real waste. Das and Tiwari [76] report liquid yields of 82.25 wt% for virgin plastics versus 74.98 wt% for real waste, with char residues of 3.66 wt% compared with 19.55 wt% for waste-derived PP. Yan et al. [77] similarly report much higher char yields for real PP and LDPE than for virgin counterparts. Tai and Yeh [78] report that real PP degraded at 406 °C with an activation energy of 12.07 kcal/mol, versus 471 °C and 39.91 kcal/mol for virgin PP.

To structure this evidence, Xayachak et al. [75] classify feedstocks into four categories: Group A (virgin, single polymers), Group B (virgin, mixed polymers), Group C (real waste, sorted by polymer type), and Group D (real waste, unsorted). Across 20 studies, Groups A and B generally achieve liquid yields above 80 wt%, while Groups C and D show lower and more variable performance. This supports a thesis-relevant conclusion: laboratory evidence on virgin polymers tends to overestimate condensable yields and underestimate quality-driven upgrading requirements relative to real residual waste streams. Bridging this gap requires explicit attention to sorting and pretreatment, which determine contaminant burden and therefore downstream compatibility and upgrading severity.

3.2.2. Sorting and pretreatment in the Dutch context

Sorting and pretreatment determine the composition and contaminant load of pyrolysis feedstocks and therefore influence both product quality and upgrading requirements. In the Netherlands, household plastic packaging is collected together with metals and drink cartons (PMD) and processed at large-scale sorting plants. These facilities produce monostream fractions such as DKR-329 (PE), DKR-324 (PP), and DKR-328 (PET) that are prioritised for mechanical recycling [15], [39]. After recovery of these higher-value streams, the residual DKR 350 fraction remains as a mixed category that is less suitable for mechanical recycling but relevant for chemical recycling via pyrolysis. DKR 350 typically contains 50–70 wt% polyolefins (PE and PP) with variable shares of PET, PS, PVC, multilayer laminates, and non-plastic contaminants such as paper, aluminium, pigments, and residues [79], [80], [81]. Fixed-bed

pyrolysis of DKR 350 at 500 °C has produced 66–69 wt% oil and wax, with about 27% of condensables in the naphtha to gasoline range (<200 °C) [82].

Additional sorting can enrich polyolefins and reduce oxygen- and chlorine-containing polymers. Van Akker et al. [81] enriched DKR 350 to about 81 wt% PE+PP and produced about 48 wt% aliphatic-rich oil in a continuous fluidised-bed system. Van Strien et al. [80] report that polyolefin enrichment combined with pretreatment can yield oils containing up to 94% aliphatic compounds and chlorine levels reduced to 17–32 ppm, although their work is based on laboratory-scale batch operation. These results indicate that enrichment and pretreatment can materially reduce contaminant burden and improve the starting point for downstream upgrading.

Pretreatment choice also matters. Conventional washing reduces surface contamination but is less effective at removing inorganics and additives. Genuino et al. [82] show that washed DKR 350 can still produce oils with >150 ppm chlorine and 8–14 wt% oxygen, which are far above cracker-relevant heteroatom and halogen limits and imply substantial impurity-focused upgrading. Dry-washing has been reported to be more effective in the DKR 350 context. Van Strien et al. [80] show that dry-washing reduced ash to <4 wt% and lowered chlorine in oils to 17–32 ppm while increasing liquid yield and aliphatic content.

Feedstock variability is an additional practical consideration. Since DKR 350 is the residual fraction after sorting, its composition fluctuates with upstream recovery rates and local collection systems. Genuino et al. [79] compare three Dutch DKR 350 batches and report variation in PET, PS, and multilayer content. Despite this, they find that overall yields are relatively stable, while impurity levels vary moderately. Oils contain chlorine in the range of 17–33 ppm, alongside measurable oxygen, nitrogen, and sulfur attributed to multilayers, additives, and minor non-polyolefin fractions [79]. This supports treating DKR 350 as a representative Dutch residual feedstock basis for comparative assessment, provided that pretreatment and the resulting contaminant burden are made explicit.

3.2.3. Summary: what the Dutch feedstock evidence implies

Two implications follow from the Dutch sorting and pretreatment literature. First, DKR 350 provides a practically relevant reference basis because it is the residual stream after recovery of mechanically recyclable monostreams [15], [39]. Second, pretreatment and enrichment can materially shift impurity burden and liquid quality in ways that propagate directly into upgrading requirements [79], [80], [81], [82]. These implications motivate using a defined DKR 350 basis (and explicitly stated pretreatment assumptions) when translating literature into model-ready upgrading indicators and TEA boundary assumptions.

3.3. Pyrolysis operation and reactor design

This section reviews operating conditions and reactor configurations that shape pyrolysis yields and liquid quality, with emphasis on variables that affect the distillation profile, olefinicity, and the distribution of light gases and heavy fractions. Where quantitative comparisons are made, the focus is on directionality and mechanisms. In later chapters, the steady-state model is anchored to a single continuous reference dataset for internal consistency across the technical assessment and TEA; this section therefore emphasises which operating variables most strongly affect the data that must be anchored.

3.3.1. Temperature

Temperature is consistently identified as a major parameter controlling cracking extent and therefore the balance between liquids, gases, and solids [18], [47], [54], [55]. Laghezza et al. [18] report that low temperatures favour wax formation, while increasing temperature raises liquid production until a maximum is reached, after which gas yields increase due to secondary cracking. Across their dataset, 400–550 °C is most common, with 500 °C applied in 46% of studies. Temperatures above 600 °C are generally employed when the objective is to maximise gas yields [18]. Gong et al. [55] similarly note that many studies operate near 500–550 °C.

For polyolefins, a narrower window is often associated with maximum liquid yields. Xayachak et al. [75] emphasise that PE and PP liquid yields are generally maximised between 450 and 500 °C, with higher temperatures favouring secondary cracking to gases and lower temperatures leaving waxes. Zhao et al. [83] show for polyethylene that increasing temperature from 500 to 600 °C increased gas yields from 8.2 to 56.8 wt% while reducing liquid yield from 81.2 to 28.5 wt%. Al-Salem [84] reports maximum oil yield from HDPE at 550 °C and maximum gas yield at 700 °C. For polypropylene, Aisien et al. [85] report an oil yield of 83.4 wt% at 400 °C, and Martynis et al. [86] report 80–89 wt% at similar temperature. Increasing temperature does not necessarily increase PP oil yield, consistent with the onset of secondary cracking rather than improved liquid production [87].

A key limitation is that much evidence is based on virgin polymers. Real post-consumer plastics can decompose at lower temperatures due to chain degradation and additive effects [75], [78]. Butler et al. [37] report that many commercial plants do not exceed 500 °C, reflecting a practical balance between energy demand, liquid yield, and controlling secondary cracking.

For polyolefin-rich mixed streams such as DKR 350, temperature trends are consistent with polyolefin behaviour. Genuino et al. [79] compare pyrolysis of DKR 350 at 500 and 600 °C in a pilot-scale fluidised bed. At 500 °C, condensable yields are approximately 55 wt% with about 35 wt% gas, whereas at 600 °C liquids drop to about 40 wt% and gas rises to about 50 wt%. The higher temperature shifts oils toward lighter hydrocarbons, indicating increased secondary cracking [79]. Overall, 450–500 °C emerges as a broadly representative window for maximising liquids from polyolefin-rich feeds, while acknowledging that reactor design and residence time determine how temperature translates into effective severity.

3.3.2. Residence time and heating regime

In addition to temperature, vapour residence time and the effective heating regime shape product slates by controlling the balance between primary depolymerisation and secondary cracking or recombination [18], [47]. In batch systems, “heating rate” is typically reported as a programmed ramp (for example °C/min) and is entangled with reactor thermal inertia, particle heat transfer, and mixing. In continuous reactors, heating is better interpreted through effective heat flux and solids handling, while vapour residence time is governed by hydrodynamics and quench effectiveness rather than by a simple batch hold time.

Longer vapour residence times generally promote secondary cracking of condensable vapours into lighter gases and can shift liquid composition toward lighter fractions. This contributes to the recurring observation that pilot-scale continuous studies often report lower condensable yields than laboratory batch work at nominally similar temperatures [79], [81]. From a modelling perspective, residence-time effects change not only total yields, but also the distribution between naphtha-range and heavier fractions, which in turn affects the scale and severity of downstream upgrading.

3.3.3. Catalysis and industrial relevance

Catalytic pyrolysis has been widely studied as a means to influence selectivity and liquid composition compared with thermal operation [18], [75]. Zeolites such as ZSM-5 and USY are frequently studied due to strong acidity and shape selectivity. These catalysts often reduce liquid yields while shifting liquids toward gasoline-range or aromatic-rich compositions. Seo et al. [88] report that pyrolysis of HDPE with HZSM-5 at 450 °C produced 35 wt% liquids and 65 wt% gas, while at 500 °C liquid yield dropped to 4.4 wt% and gas yield rose to 86.1 wt%. FCC catalysts and other industrial by-product catalysts have also been applied, but selectivity and reproducibility vary across studies and operating contexts [18], [89], [90], [91].

Despite extensive laboratory work, transferability to realistic feeds and continuous operation remains a central limitation. Laghezza et al. [18] report that catalysts appear in a substantial share of studies, but predominantly at lab scale. Butler et al. [37] emphasise catalyst deactivation by coke and poisoning by heteroatoms such as chlorine, nitrogen, and oxygen as critical challenges for real waste. In addition,

the Dutch residual-feed literature motivating this thesis (DKR 350 and enriched derivatives) is primarily based on thermal pyrolysis operation when providing continuous pilot-scale datasets [79], [81]. Therefore, catalytic pyrolysis is treated here as an important research direction, but not the baseline for the present assessment. This scope choice is anchored in three literature-based criteria: (i) most catalytic evidence remains laboratory-dominated [18], [75]; (ii) deactivation and poisoning risks are repeatedly highlighted for heterogeneous plastic waste [37]; and (iii) the most directly applicable Dutch continuous datasets used to ground comparative modelling in later chapters are based on thermal operation [79], [81].

3.3.4. Reactor design and representativeness of evidence

Reactor configuration governs heat and mass transfer, vapour residence time, solids handling, and scalability. The literature distinguishes batch, semi-continuous, and continuous operation in fixed-bed, mechanically stirred, auger, and fluidised-bed reactors [18], [47], [75].

Batch reactors dominate laboratory studies due to simplicity and parameter control, but they are limited in industrial relevance due to poor heat transfer and discontinuous operation [75]. Continuous reactor concepts provide more industrially relevant evidence. Fluidised-bed reactors repeatedly emerge as suitable for scale-up due to strong heat flux, continuous feeding, and efficient gas–solid contact [18], [37], [47]. Laghezza et al. [18] report that fluidised and mechanically fluidised beds dominate pilot-scale studies, supporting their role as an industrial benchmark configuration.

Evidence from DKR 350 highlights systematic differences between batch and continuous operation. Van Strien et al. [80] report up to 78 wt% liquid yields for dry-washed DKR 350 in a laboratory autoclave, while Genuino et al. [79] report lower liquid yields in a 5 kg h^{-1} continuous fluidised-bed plant at 500 °C, attributed in part to longer vapour residence times and secondary cracking. Van Akker et al. [81] report intermediate yields for polyolefin-enriched DKR 350 streams in continuous fluidised-bed operation. Collectively, this indicates that batch evidence tends to overestimate condensable yields relative to continuous pilot operation and supports prioritising continuous pilot data when anchoring system modelling and TEA comparisons.

3.3.5. Summary and knowledge gaps in pyrolysis operation

Three uncertainties recur in the literature in ways that matter for model anchoring and TEA translation: (i) operating “severity” is not consistently comparable because temperature, heating regime, and residence time are variably defined [18], [47]; (ii) catalytic findings are extensive but weakly demonstrated on realistic feeds under continuous operation [18], [37]; and (iii) batch evidence dominates despite systematic differences in yields and slates compared with continuous pilot systems [75], [79]. These uncertainties motivate treating operating parameters as embedded in a selected continuous reference dataset in later chapters, while using literature primarily for mechanistic interpretation and for bounding plausible outcome ranges.

3.4. Pyrolysis products and product quality constraints

Pyrolysis produces condensable liquids, non-condensable gases (NCG), and solid char. Their proportions and composition depend on feedstock and operating conditions, but they also determine upgrading requirements and system economics. Since this thesis evaluates pathways that valorise the liquid fraction, emphasis is placed on liquid composition, distillation behaviour, and impurity burden. NCG and char are discussed primarily in relation to boundary choices that propagate into TEA results.

3.4.1. Condensable liquid fraction

Polyolefin pyrolysis liquids span broad boiling point ranges and are typically dominated by aliphatic hydrocarbons. Chang [54] reviews PE and PP oils as rich in paraffins, isoparaffins, and olefins, with aromatics increasing under more severe conditions or when non-polyolefins are present. Gong [55] similarly emphasises that pyrolysis liquids can be distilled into cuts from sub-200 °C naphtha to heavier

fractions and that high olefinicity drives instability and downstream hydrogenation needs. Laghezza et al. [18] synthesise that product slates shift with operating severity and feed composition even when nominal temperatures are similar, underscoring the difficulty of comparing oil quality without context.

For Dutch-relevant mixed streams, DKR 350 studies provide compositionally resolved evidence that links liquid quality constraints to real residual feedstocks. Van Strien et al. [80] analyse oils from polyolefin-enriched, dry-washed DKR 350 using GC$\times$GC-TOFMS (PIONA) and elemental analysis, reporting aliphatic-rich oils with ppm-level chlorine after pretreatment. Genuino et al. [82] show that washed but otherwise untreated DKR 350 can yield oils with elevated heteroatoms, reporting approximately 8–14 wt% oxygen and more than 150 ppm chlorine attributed to multilayers, traces of PET and PVC, inks, and additives. At pilot scale, Van Akker et al. [81] process polyolefin-enriched DKR 350 in a continuous fluidised bed and report aliphatic-dominant oils that can be fractionated toward naphtha-range cuts, while noting that impurity constraints remain a decisive barrier for petrochemical integration.

These compositional features motivate upgrading requirements. Gong [55] highlights that unsaturated matrices and residual heteroatoms necessitate hydrotreating and dehalogenation and, where boiling-range reshaping is required, hydrocracking or tailored fractionation. Chang [54] similarly links upgrading severity to target outlet and impurity burden. Laghezza et al. [18] emphasise that reported oil quality metrics are not comparable unless linked to feed pretreatment and to an indicator set that includes distillation behaviour and elemental impurities.

3.4.2. Non-condensable gas fraction

NCG from plastic pyrolysis consists predominantly of light hydrocarbons (C_1 to C_4) with variable H_2 and minor CO and CO_2. For polyolefins, the stream is typically rich in ethylene and propylene and exhibits a high heating value; reviews report values on the order of 45–50 MJ/kg and increasing gas yields under more severe conditions [18]. Such off-gases are often assumed to be combusted for process heat in TEA studies and can offset part of the endothermic heat duty of pyrolysis [92].

DKR 350 evidence confirms similar composition tendencies. Van Strien et al. [80] report NCG dominated by C_2 to C_4 olefins for dry-washed, polyolefin-enriched DKR 350 in batch operation. Van Akker et al. [81] find propylene and ethylene as major components in a continuous fluidised-bed pilot, with C_4 fractions increasing at higher temperature. Genuino et al. [79] observe comparable light-gas signatures in continuous pilot operation, with NCG representing a material fraction of the mass balance.

Routing choices for NCG vary across TEAs (see Section 3.6). Fivga and Dimitriou [17] combust NCG and char to meet reactor heat duty, while other TEAs assume internal heat recovery, CHP generation, export power, or alternative handling of light ends [93], [94]. While recovery of hydrogen or light olefins may be of interest, such pathways require additional separations and are rarely treated transparently in TEA models of plastic pyrolysis [94], [95].

Because boundary assumptions for off-gases strongly affect both mass-balance storytelling and TEA comparability, this thesis applies a consistent battery-limits convention in later chapters. As defined in Chapter 5 and carried through Chapters 6–8, Stream 423 is treated as an *exported byproduct fuel gas at battery limits* (creditable in the TEA), while a separate vent/purge stream leaves to battery limits (flare header outlet) for offsite handling. No on-site flare combustion is modelled, and no flare CO_2 is claimed. When CO_2 is reported as a metric later in the thesis, it is restricted to direct on-site combustion as explicitly modelled, excluding exported gas combustion, offsite vent handling, and upstream emissions.

3.4.3. Char fraction

Char yields are typically below 10 wt% for polyolefins but increase for mixed waste streams due to fillers, additives, and inorganics [18]. Char consists of unconverted fragments, ash, and condensed carbonaceous residues. Most TEA studies treat char as a low-value by-product that is combusted for heat recovery together with NCG or disposed of, implying that its economic role is secondary relative to liquid valorisation [17], [94]. Higher-value applications have been proposed, including adsorption

and composite applications [96], [97], but these are market- and specification-dependent and are not treated as robust base-case levers in most plastic pyrolysis TEAs.

3.4.4. Synthesis: quality constraints as a precursor to specification intent

Across the literature, the decisive uncertainty for liquid valorisation is specification-driven rather than yield-driven. Polyolefin-rich feeds produce aliphatic liquids with substantial olefinicity, while mixed residual feeds such as DKR 350 introduce persistent heteroatoms and halogens that can remain binding even after pretreatment [80], [81], [82]. For NCG, the key uncertainty is not calorific value but how scale-relevant heat self-sufficiency and any surplus routing are represented within a consistent boundary story [17], [93], [94]. For char, promising applications exist but are not yet supported by widely adopted, specification-defined markets that are consistently represented in the TEA literature [96], [97]. Accordingly, the next section frames upgrading against specification intent and reviews hydroprocessing evidence in terms of outcome metrics that can be translated into a steady-state model, including impurity removal, olefin saturation, heavy-pool conversion, gas make, and associated yield penalties.

3.5. Liquid upgrading framed by specification intent and target indicators

The preceding section showed that pyrolysis liquids are typically olefin-rich and may retain heteroatoms and halogens that remain decisive for downstream compatibility, even when polyolefin-rich feedstocks and pretreatment are applied. In upgrading literature, these challenges are commonly framed against specification intent, because specification categories determine whether a liquid can be handled within petrochemical and fuel infrastructures and because they shape both required upgrading severity and recoverable product yield. This section reviews how specification intent is used to motivate upgrading and how hydrotreating and hydrocracking studies report operating windows and outcomes. Emphasis is placed on what can be generalised across studies and what remains under-specified in ways that limit comparative TEA.

3.5.1. Why upgrading is required: specification intent rather than boiling range

A recurring conclusion is that usability is not defined by boiling range alone. It is defined by stability- and contaminant-related constraints that are outlet-specific and that directly shape upgrading severity and yield penalties. Two intents recur in the literature and align with this thesis: (i) a cracker-relevant naphtha-range blendstock intent (implemented as the *naphtha pathway*) and (ii) a jet-fuel-range blendstock intent where kerosene-range material is evaluated against jet-driven property categories without claiming certification (implemented as the *jet-fuel pathway*).

For the cracker-relevant naphtha intent, binding constraints are commonly expressed as ppm-level limits on heteroatoms and trace contaminants, combined with stability requirements that disfavour olefin-rich feeds. Kusenberg et al. [26] summarise representative industrial limits for steam cracker feedstocks and report nitrogen at 100 ppm for naphtha (2000 ppm for gas oils), sulfur at 500 ppm, oxygen at 100 ppm, chlorine at 3 ppm, and phosphorus at 0.5 ppm. They also cite an operator-informed maximum allowable olefin concentration of 2 wt% in naphtha-range feedstocks due to fouling and coke formation [26]. These values illustrate why plastic-derived liquids are generally not treated as cracker feed without stabilisation and impurity management. Belbassai et al. [98] report plastic pyrolysis oil with high olefin content (approximately 60 wt%) and interpret this olefinicity as a primary reason that the oil is unsuitable for fuel use or steam-cracker integration prior to hydrotreatment. Halogens form a second recurring barrier due to corrosion risks and catalyst disruption. Zeb et al. [99] emphasise halogens as a critical contamination category, note corrosion risks, and report that chlorine in transportation fuels should not exceed 10 ppm. They also describe how PVC-derived pathways can form chlorinated aromatics (for example chlorobenzenes) that can partition into light fractions, implying that distillation alone does not guarantee removal of problematic chlorine species [99]. For mixed residual feeds such as DKR 350, pretreatment reduces but does not necessarily eliminate these contaminant categories

[79], [80], [82]. Overall, the literature most defensibly frames the naphtha outlet as a cracker-relevant blendstock objective. Hydrotreating is positioned as enabling stabilisation and impurity reduction, while hydrocracking and fractionation manage the boiling-range envelope and heavy-tail behaviour that governs recoverable product slates.

For the jet-fuel-range blendstock intent, usability is framed through cold-flow operability, combustion performance, and distillation control, again expressed via specification-style categories. Jeon et al. [100] summarise representative targets, including minimum net heat of combustion of 42.8 MJ kg^{-1}, density of 775–840 kg m^{-3}, freezing point at most -47 °C, and kinematic viscosity at -20 °C below 8 mm^2 s^{-1}. Chevron [101] illustrates that specification intent can be yield-limiting through cut definition, noting that Jet A has a maximum freezing point of -40 °C whereas Jet A-1 is -47 °C, and that the lower freezing point requirement can constrain the usable distillation cut. Halimi et al. [102] reproduce a compact set of ASTM D7566 requirement categories and show that specification tables alone are not evidence of compliance, as their simulated 100% waste-wood-derived SAF violates the reproduced final boiling point cap and is interpreted as requiring blending with conventional jet fuel [102]. Liu and Wang [103] similarly report pyrolysis-derived aviation fuel after thermal cracking and fractionation that falls within ASTM ranges except for freezing point and density, indicating that cold-flow and bulk property windows can remain limiting even when a kerosene-range fraction exists.

A further practical constraint is that property measurement and compositional characterisation methods may not be transferable to plastic-derived fractions without prior stabilisation. Tameesh et al. [104] develop a GC method for total aromatics in kerosene-range material (150–250 °C) that is restricted to samples containing less than 0.1% olefins and/or heteroatomic compounds. Lissitsyna et al. [105] show that GC$\times$GC-TOFMS can provide hydrocarbon-class and carbon-number distributions for kerosene samples, enabling class-based comparison. Together, these methodological constraints support the interpretation that meaningful evaluation against jet-fuel-range property categories often presupposes stabilisation and impurity reduction rather than treating these as optional polishing steps.

Two limitations follow from this intent framing. First, many studies cite specification limits but do not report a consistent, comparable set of measured properties for plastic-derived fractions, particularly when blending is assumed or when cut definitions are incompletely disclosed [100], [103]. Second, even where specification categories are clear, the literature does not provide a generalisable relationship between pyrolysis-oil quality and pretreatment history and the upgrading severity required to approach these categories while consistently quantifying hydrogen use, gas make, and yield penalties.

3.5.2. Hydrotreating: stabilisation and impurity removal

Across upgrading studies on plastic-derived liquids, hydrotreating is used to stabilise an olefin-rich matrix and to remove heteroatoms and halogens by converting them into separable products (for example H_2O, NH_3, and HCl). Sun and Yoon et al. [106] demonstrate this stabilisation function for waste plastic pyrolysis oil using sulfided NiMo/γ-Al_2O_3 at 350 °C, reporting large reductions in nitrogen (2570 wppm to 97 wppm) and chlorine (220 wppm to 5 wppm) after hydrotreating. They also report a pronounced shift in the naphtha-range hydrocarbon class distribution away from olefins and toward paraffins, with paraffins in the naphtha portion reaching 60.2 vol%, consistent with extensive olefin saturation [106]. A TEA-relevant implication is that these improvements are not achieved without phase redistribution and losses: the authors report an oil loss of around 5 wt% attributed mainly to conversion of heteroatom-containing compounds into gaseous or aqueous products under high hydrogen partial pressure [106].

Transferability of nominal operating windows is limited because hydrotreating outcomes depend strongly on feed matrix, hydrogen availability, and reactor mode. Luo et al. [107] quantify sensitivity in batch hydrotreating of LDPE pyrolysis oil using a Ni/biochar catalyst, showing that increasing initial H_2 pressure from 1 to 2 MPa at 300 °C increases selectivity to C_5–C_{15} paraffins from 61.6% to 76.1% while driving C_5–C_{15} and C_{16}–C_{20} olefins to 0%. They also report non-monotonic temperature behaviour at constant 2 MPa, where C_5–C_{15} paraffin selectivity peaks at 300 °C but declines at 350 °C with increased aromatic content, linked to competing oligomerisation, condensation, and aromatisation [107]. These

trends indicate that selecting typical temperature and pressure values from batch studies is not robust when secondary reactions compete with saturation.

Continuous evidence further complicates comparison because many studies treat plastic-derived material as a blend component rather than a neat feed. Tomášek et al. [108] study continuous hydrogenation of cracked PE or PP fractions blended into straight-run kerosene (10–30% cracked fraction) over commercial in situ sulfided NiMo/Al_2O_3/P catalyst. Within 200–300 °C, 40 bar, LHSV 1.0–3.0 h^{-1}, and H_2/hydrocarbon ratio 400 Nm^3/m^3, they report practically sulfur- and olefin-free products at 300 °C and reduced aromatic contents, and report freezing points for PP-derived blends substantially below typical jet constraints [108]. This provides evidence that hydrogenation can render plastic-derived blend components compatible with kerosene property envelopes, but it is not directly transferable to neat pyrolysis oils with higher impurity burdens or different boiling distributions.

Overall, hydrotreating studies demonstrate stabilisation and impurity reduction, but they report outcomes on heterogeneous bases and under non-aligned feed and reactor contexts. Hydrogen use, phase losses, and gas formation are not consistently disclosed on comparable bases across studies, restricting direct translation into comparative assessments that require consistent yield accounting and utility implications [106], [107], [108].

3.5.3. Hydrocracking: boiling-range reshaping and severity trade-offs

Hydrocracking is introduced when stabilisation alone is insufficient and the product slate must be reshaped, particularly by reducing heavy tails and redistributing carbon toward naphtha and, for jet-fuel-range intent, kerosene-range material. Outcomes depend not only on nominal severity (temperature, pressure, space velocity, residence time) but also on catalyst architecture and the extent of secondary cracking. This determines the trade-off between desired liquids and gas make and therefore affects both product value and energy integration.

Palos et al. [109] illustrate these trade-offs in an autoclave study on a PPO/VGO blend at 80 bar and 420–440 °C. They define boiling cuts using ASTM D2887-based ranges, with naphtha (35–216 °C), LCO (216–343 °C), and HCO ($>$343 °C), and define conversion as reduction of the HCO fraction to lighter products and coke [109]. At 420 °C, their best-performing catalyst achieves 53.1% conversion with 18.3 wt% naphtha and 33.8 wt% LCO while limiting gas to 5.5 wt%. At 440 °C, conversion rises to 75.9% with higher naphtha and LCO yields, but gas increases to 9.8 wt% [109]. For less favourable catalysts, gas yields rise markedly at higher temperature, indicating stronger overcracking and reduced liquid selectivity [109]. This matters for system modelling because gas make changes not only liquid yield but also separation loads, hydrogen management, and utility integration.

Kim et al. [110] provide a two-step perspective (hydrotreating followed by hydrocracking) aimed at producing high-quality naphtha from WPPO. In hydrocracking of hydrotreated WPPO at 420 °C over sulfided NiMo supported on micro- versus mesoporous HZSM-5, the mesoporous catalyst yields naphtha with 75.0 wt% paraffins, 9.7 wt% aromatics, and 0.5 wt% olefins, compared with 65.4 wt% paraffins, 22.1 wt% aromatics, and 1.4 wt% olefins for the microporous analogue [110]. They also report that microHZSM-5 can increase aromaticity relative to the hydrotreated feed, consistent with shape-selective aromatisation pathways [110]. This is relevant for both cracker-relevant naphtha objectives, where aromatics and olefins may be constrained, and for jet-fuel-range blending, where aromaticity can be limited by property windows.

Sajdak et al. [111] demonstrate optimisation framing for tire pyrolysis oil using aviation-fuel-motivated criteria, targeting reduced aromatics and naphthalenes below 3% in a two-stage route (HDO followed by hydrocracking). Their results show that when the feed is intrinsically aromatic, meeting jet-fuel-motivated compositional targets can remain difficult even under severe conditions [111]. Methodologically, the study makes optimisation targets explicit, but it reinforces that transferability across feed matrices is limited and that outcome reporting bases vary substantially.

Overall, hydrocracking studies qualitatively agree on the trade-off between heavy-fraction conversion,

liquid yields, and gas make, but they do not provide a standardised severity framework transferable across feedstocks and catalyst families. Differences in cut definitions, reporting conventions, and incomplete disclosure of gas and hydrogen metrics limit direct translation into consistent product slates for steady-state modelling [109], [110].

3.5.4. Synthesis and knowledge gap: need for outcome-based translation into model-ready indicators

Three conclusions follow. First, specification intent is necessary because cracker-relevant naphtha-range blendstocks and jet-fuel-range blendstocks are constrained by different binding categories. Cracker-relevant naphtha is dominated by ppm-level heteroatom and halogen limits and low-olefin requirements [26], while jet-fuel-range intent includes cold-flow and distillation endpoint constraints that can be yield-limiting even when a kerosene-range fraction exists [101], [102]. Second, hydroprocessing severity is multi-dimensional. Hydrotreating can reduce nitrogen and chlorine by orders of magnitude and convert olefin-rich fractions toward paraffin-dominant compositions, but outcomes depend on feed matrix, catalyst state, hydrogen availability, and reactor mode [106], [108]. Hydrocracking can be expressed through heavy-fraction conversion and linked to naphtha and middle-distillate yields, yet gas make and liquid composition shifts are strongly catalyst-dependent and sensitive to cut definition [109], [110].

Third, and most important for comparative assessment, the literature lacks a transferable, specification-anchored way to connect pyrolysis-oil quality and pretreatment history to hydroprocessing outcomes expressed in a consistent indicator set. Hydrogen use is often missing or not comparable, gas make and composition are frequently under-reported, phase losses are inconsistently disclosed, and naphtha and middle-distillate ranges are defined on non-aligned bases [107], [109], [111]. This limitation propagates into TEA models, where upgrading severity is often simplified while hydrogen, gas routing, and yield penalties are treated with non-aligned assumptions [18], [95]. The present thesis therefore adopts an outcome-based translation approach in later chapters, reformulating literature-reported upgrading effects into comparable indicators for stabilisation, impurity removal, heavy-pool conversion, and gas formation to enable consistent comparison across the naphtha and jet-fuel pathways.

3.6. Techno-economic analysis evidence and comparability limits

TEA combines mass and energy balance information with economic parameters, including CAPEX, OPEX, and product revenues, to evaluate economic performance using indicators such as NPV, IRR, payback period, and minimum selling prices [112]. There is growing academic and industrial interest in the economics of pyrolysis for waste plastics [94], but reviews highlight a limited number of transparent TEAs and a persistent disconnect between laboratory evidence and commercial implementation [8], [17], [95]. Laghezza et al. [18] emphasise that the key unresolved question is economic sustainability at scale.

A central comparability limitation is that many TEAs adopt non-aligned assumptions on liquid upgrading and specification intent. Some studies omit explicit upgrading trains and implicitly price oils as generic fuels or intermediates, while others assume stabilisation or deep upgrading without consistently accounting for hydrogen consumption, gas make, phase losses, and cut definition effects. Since these variables are precisely the outcome metrics needed to translate upgrading into model-ready indicators, TEA comparisons across product pathways can be structurally unstable if upgrading severity and boundary choices are not explicitly harmonised.

TEAs in the plastic pyrolysis literature differ in feedstock, operating conditions, location, and end product. Fivga and Dimitriou conduct a TEA for a UK-based pyrolysis plant processing 100 kg/h of mixed plastic waste using a continuous thermal fluidised-bed reactor at 530 °C to produce heavy oil [17]. Yield data were confidential. Aspen HYSYS and APEA were used for simulation and economics. Assumptions include a selling price of £0.55/kg oil, zero-cost feedstock, and internal use of pyrolysis gases and char for heat. A secondary fluidised-bed combustor burns NCG and char to meet reactor heat duty,

and no hydrotreating or hydrocracking block is modelled. The base case is unprofitable, while scale-up scenarios show improved economics.

Lubongo et al. assess a plant processing PP, HDPE, LDPE, and PS under comparable reactor technology [40]. Their base case is a fluidised-bed catalytic configuration (silica–alumina) and the oil is valued on a fuel-spec basis without an explicit upgrading train. NCG is combusted for process heat and char is landfilled. They evaluate market-priced feedstock versus zero-cost feedstock and find that feedstock cost strongly governs profitability, with larger plants becoming viable under the zero-cost scenario.

Larrain et al. model pyrolysis within open-loop and closed-loop recycling pathways [93]. In the closed-loop scenario, the process aims to produce naphtha as a substitute for fossil naphtha in virgin plastic production, while the open-loop pathway produces waxes replacing fossil paraffin waxes. They find stronger economic performance for the open-loop pathway, largely due to higher product value. Their closed-loop route includes hydrogenation to meet substitutability, and NCG is sent to a gas engine for CHP, while char is outside the model boundary.

Yadav et al. discuss a catalytic fast pyrolysis system with a capacity of 240 metric tons/day of mixed plastic waste [94]. They model scenarios targeting naphtha, mixed products, aromatics-rich products, and olefins-rich products. They report high minimum selling prices relative to fossil counterparts and identify feedstock cost, co-product sales prices, separation CAPEX, and operating costs as key drivers. In their process, separations and upgrading drive economics, while utilities rely on purchased energy and NCG and char are not treated as principal economic levers.

Overall, the TEA literature indicates that profitability is sensitive to scale, feedstock cost, and boundary assumptions. However, results are difficult to benchmark because many studies rely on laboratory yields, generic mixed feeds, or omit explicit upgrading trains. Assumptions on specification intent, upgrading severity, hydrogen costs, gas routing, and char handling vary widely. This reinforces the need for transparent, specification-anchored modelling that links feed pretreatment and pilot-scale yields to explicit upgrading outcome metrics and consistent TEA boundary choices.

3.7. Synthesis of knowledge gaps and implications for the thesis

Across the literature, a persistent mismatch remains between research conditions and industrial practice. Evidence is dominated by virgin polymers and batch studies, while industrially relevant feeds are heterogeneous (for example DKR 350) and operation is continuous. Recent DKR 350 work begins to address this gap, but a consistent framework linking upstream sorting and pretreatment to downstream performance under continuous operation remains limited.

Operating windows and representativeness compound uncertainty. Temperature, heating regime, and vapour residence time are variably defined and reported, and batch studies tend to overestimate liquid yields relative to continuous systems. For catalysis, extensive laboratory exploration contrasts with sparse demonstration on real-waste feeds under continuous operation. Catalyst stability, regeneration, and cost–performance trade-offs therefore remain unresolved at scale.

Product constraints are specification-driven. For liquids, comparable datasets connecting pretreatment and operating context to PIONA, distillation profile, and impurities (O/N/Cl/S) are scarce, and the mapping from these quality indicators to model-ready upgrading metrics (hydrogen use, gas make, phase losses, aligned cut definitions) is not harmonised. For NCG, composition and heating value are broadly known, but scale-relevant quantification of heat self-sufficiency and a clear routing hierarchy for surplus remain unresolved. For char, potential uses exist but near-term, specification-defined markets are uncertain.

Finally, TEAs are not fully comparable. Many omit explicit upgrading trains or treat upgrading with non-aligned assumptions, while boundary choices for NCG and char vary widely. Together, these gaps motivate a standardised, specification-anchored assessment grounded in continuous pilot data for a defined Dutch feedstock and translated into explicit, outcome-based upgrading indicators that support

consistent steady-state modelling and TEA comparison across pathways.

3.8. Synthesis of knowledge gaps and implications for the thesis

3.8.1. Cross-cutting knowledge gaps from the literature

Across the literature, a persistent mismatch remains between research conditions and industrial practice. Evidence is dominated by virgin polymers and batch studies, while industrially relevant feeds are heterogeneous (for example DKR 350) and operation is continuous [18], [75]. Recent DKR 350 work begins to address this gap, but a consistent framework linking upstream sorting and pretreatment to downstream performance under continuous operation remains limited [79], [80], [81].

Operating windows and representativeness compound uncertainty. Temperature, heating regime, and vapour residence time are variably defined and reported, and batch studies tend to overestimate condensable yields relative to continuous systems [18], [79]. For catalysis, extensive laboratory exploration contrasts with sparse demonstration on real-waste feeds under continuous operation; catalyst deactivation and poisoning are repeatedly highlighted as key barriers [18], [37].

Product constraints are specification-driven. For liquids, comparable datasets connecting pretreatment and operating context to distillation profile and impurities (O/N/Cl/S) remain scarce, and the mapping from these quality indicators to model-ready upgrading metrics (hydrogen use, gas make, phase losses, aligned cut definitions) is not harmonised [18], [95]. For NCG, composition and heating value are broadly known, but TEAs differ materially in how off-gases are treated within the system boundary [17], [93], [94]. For char, potential uses exist but near-term, specification-defined markets are uncertain and are not consistently represented as robust base-case assumptions [96], [97].

Finally, TEAs are not fully comparable. Many omit explicit upgrading trains or treat upgrading with non-aligned assumptions, while boundary choices for NCG and char vary widely [18], [95]. Together, these gaps motivate a standardised, specification-anchored assessment grounded in continuous pilot data for a defined Dutch feedstock and translated into explicit, outcome-based upgrading indicators that support consistent steady-state modelling and TEA comparison across pathways.

3.8.2. Implications for modelling choices

The literature review motivates three modelling choices used in the remainder of this thesis.

Defined Dutch feedstock basis. Because feed composition and pretreatment drive impurity burden and liquid quality, the assessment is grounded in a defined Dutch residual feedstock basis (DKR 350 and explicitly stated pretreatment assumptions) rather than generic “mixed plastic” feeds [15], [39], [79].

Continuous reference anchoring for yields and slates. Because batch evidence tends to overestimate condensable yields and differs systematically in gas/condensable splits and distillation behaviour, later chapters anchor the steady-state model to a single continuous reference dataset to preserve internal consistency when comparing the naphtha and jet-fuel pathways [75], [79], [81].

Outcome-based upgrading translation under specification intent. Because hydroprocessing studies do not provide a transferable severity framework with consistently reported hydrogen use, gas make, and phase losses, later chapters express upgrading through outcome indicators consistent with specification intent: stabilisation and impurity removal for hydrotreating, and heavy-pool conversion with associated yield penalty and gas make for hydrocracking [18], [106], [109]. This approach supports consistent comparison of pathway outcomes using Technical Performance Metrics (TPMs) in Chapter 6 and consistent economic closure using MSP in Chapter 7.

3.8.3. Research aim

This study delivers a specification-anchored assessment of continuous polyolefin-rich plastic pyrolysis on a defined Dutch residual feedstock basis (DKR 350). Using the literature-based constraints

and gaps synthesised above, the thesis compares two pathways implemented under a shared process topology: a *naphtha pathway* targeting a cracker-relevant naphtha-range blendstock and a *jet-fuel pathway* targeting a jet-fuel-range blendstock (without making certification claims). The assessment links feed and pretreatment evidence in the Dutch context to liquid quality constraints and then translates upgrading into outcome-based indicators for hydrotreating (stabilisation and impurity removal) and, where required by outlet intent, hydrocracking (heavy-pool conversion and associated yield penalties). These technical outcomes are evaluated using TPMs (Chapter 6) and converted into economic outcomes via an auditable MSP-based TEA with explicit basis and coefficients (Chapter 7), with robustness tested through a focused OAT sensitivity set (Chapter 8).

3.8.4. Main research question

The subsequent research question is formulated as follows:

What is the techno-economic performance of producing a cracker-relevant naphtha-range blendstock and a jet-fuel-range blendstock through pyrolysis-based recycling of polyolefin-rich plastic waste in the Netherlands?

4

Research Questions and Methodology

4.1. Research Sub-Questions

To structure the research process, the main research question is broken down into four interdependent sub-questions. Each sub-question corresponds to a distinct research phase, ensuring a logical sequence that ultimately leads to answering the overarching research question.

1. *What are the system boundaries, process configurations, and input–output relationships for producing naphtha-range and jet-fuel-range blendstocks from pyrolysis of polyolefin-rich plastic waste?*
2. *What are the technical characteristics of producing naphtha-range and jet-fuel-range blendstocks from pyrolysis of polyolefin-rich plastic waste?*
3. *What are the economic performance outcomes of the naphtha pathway and jet-fuel pathway, and what do these imply for their feasibility under a consistent assessment basis?*
4. *How sensitive are the economic outcomes of each pathway to variations in key assumptions, and which parameters are the primary drivers of feasibility?*

4.2. Research Design

The research adopts a structured, phased methodology grounded in a TEA framing consistent with Van Dael et al. [113]. The four TEA elements (market framing, process design/simulation, economic evaluation, and sensitivity analysis) are implemented here as four research phases aligned with the sub-research questions in section 4.1. In this thesis, the “market” element is operationalised as an explicit set of unit-price coefficients and scenario assumptions used in the DCF model (Chapter 7), rather than as a standalone market study.

The methodological design is intentionally proportionate to the objective of the thesis. The aim is to develop a transparent, internally consistent, and decision-oriented comparison of two pathway intents under a common gate-to-gate basis, rather than to produce a detailed first-principles process design, a full market forecast, or a full life-cycle assessment. For that reason, the methodology prioritises traceability, comparability, and auditability across phases. Where the available evidence base does not support more mechanistic detail at a consistent level across the full A100–A400 system, the thesis adopts screening-level representations that are sufficiently detailed to preserve boundary completeness and economic handover consistency, while avoiding an unsupported impression of precision.

The methodology relies primarily on secondary data from peer-reviewed literature, technical reports, and industry sources. These inputs are integrated into spreadsheet-based models to quantify steady-state mass and energy balances, pathway performance, and DCF-based economic outcomes. The

two study cases are referred to consistently as the *naphtha pathway* and *jet-fuel pathway*. They share a common overall flowsheet topology, while differing in downstream upgrading severity and product cut logic used to report the naphtha-range and jet-fuel-range blendstocks. Detailed stream numbering and area definitions are introduced in Chapter 5.

Figure 4.1 summarises the four-phase research design adopted in this thesis and highlights how the outputs of each phase provide the primary inputs to the subsequent phase.

The literature review in Chapter 3 provides the foundation for Phase 1 by synthesising the state of the art on plastic pyrolysis, upgrading, and TEA conventions. These findings are used to establish system boundaries, define process configurations, and parameterise input–output relationships for two pathways, resulting in clearly defined systems and representative process flow diagrams (PFDs) (Chapter 5).

In Phase 2, the process definitions are translated into internally consistent steady-state mass and energy balances using a screening-level, black-box modelling approach. This phase is designed to generate complete and auditable plant-boundary handover quantities under a shared system definition, using a level of representation that is consistent with the available secondary data and with the comparative objective of the thesis. The resulting flows are used to quantify technical performance in terms of product yields, auxiliary resource and utility requirements (e.g., imported hydrogen and electricity), byproduct energy export potential, and plant-boundary waste/discharge streams (Chapter 6).

In Phase 3, the technical outputs are mapped onto a DCF TEA framework to quantify investment and operating costs, revenues, and break-even economics. While conventional TEA indicators (NPV, IRR, payback) are defined for completeness, the economic comparison in this thesis is anchored on the minimum selling price as the break-even product price that satisfies the DCF closure condition (Chapter 7). This provides a pathway-consistent economic comparison under a shared financial basis, while keeping the interpretation tied directly to the designated focal product in each pathway.

Phase 4 applies a one-at-a-time (OAT) sensitivity analysis on the same economic basis to identify the dominant drivers of MSP and thus feasibility under uncertainty (Chapter 8). The sensitivity phase is intended to rank the importance of a limited set of high-leverage assumptions and to clarify which project and market levers most strongly shape the results under the adopted screening basis, rather than to provide a full probabilistic uncertainty analysis. Each phase builds on the outcomes of the previous one, enabling a consistent, stepwise evaluation of the two pathways.

4.3. Research Methods

This section describes how the four research phases are implemented and fixes the common study conventions used throughout the remainder of the thesis. In particular, it defines the shared system boundary, reporting basis, and interpretation rules that are applied consistently in Chapters 5–8 before detailing the methods used in each phase.

The quantitative assessment is gate-to-gate: the boundary begins where pre-processed plastic waste enters the conversion section and ends at battery limits where the naphtha-range and jet-fuel-range blendstocks, byproducts, and waste/discharge streams leave the system. Upstream waste management steps (collection, sorting, washing) and downstream refining, blending, and product use are excluded from the quantitative model and discussed qualitatively for context.

Results are reported as steady-state flowrates (e.g., kg/h, kW) and as normalised intensities (e.g., kg/kg feed, MJ/kg feed, kWh/t feed) to enable comparison across pathways. The common scale basis used throughout the technical and economic assessment is 40 kt/y plastic feed and 8,000 h/y operation, consistent with the design basis and DCF assessment basis used in later chapters.

Two gas-related boundary conventions are applied consistently throughout the thesis to avoid ambiguity in mass balance, emissions interpretation, and economic crediting. First, an exported byproduct fuel-gas stream at battery limits may be credited economically as an energy byproduct in the TEA (Chapter 7)

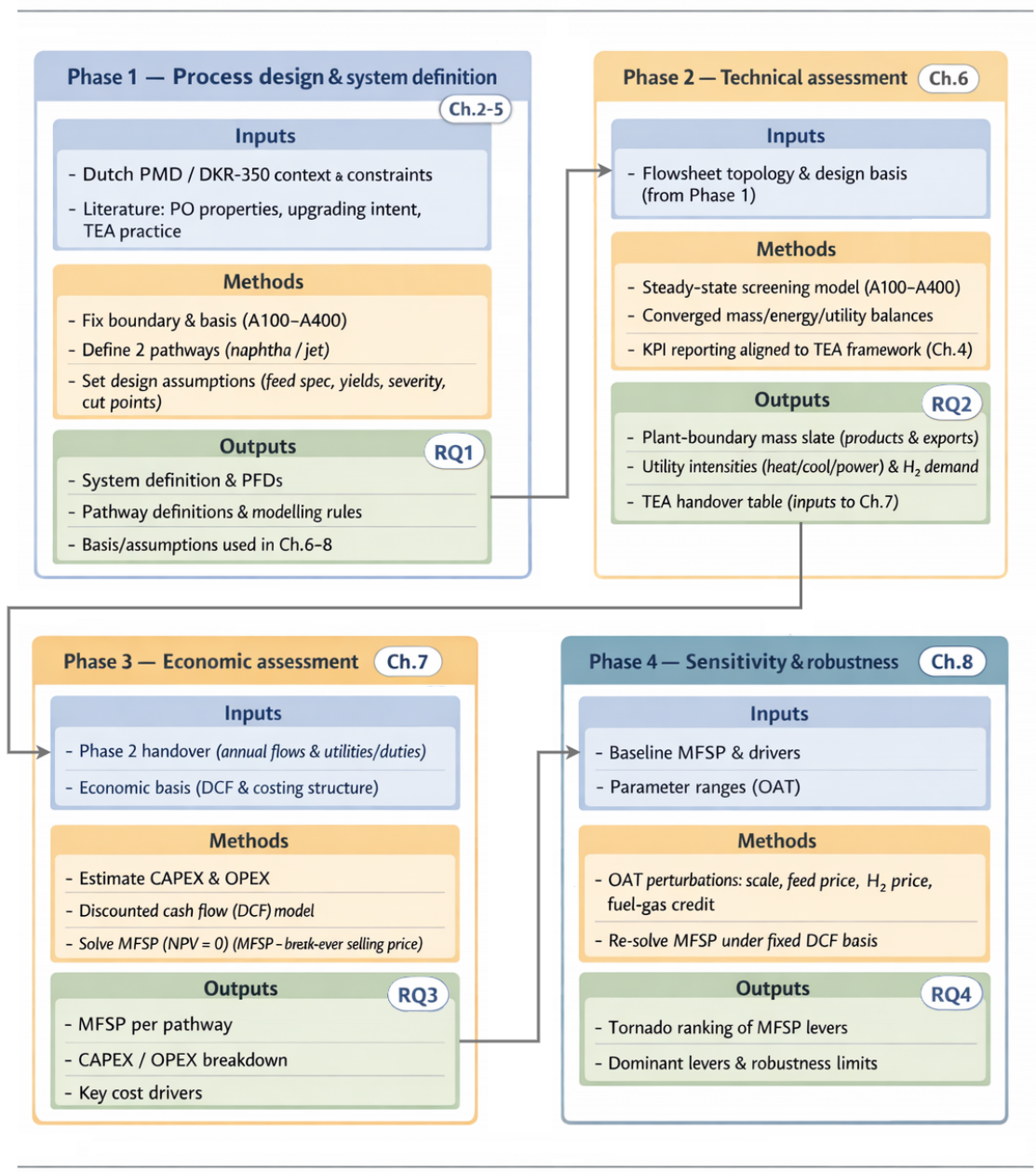

Figure 4.1: Research diagram showing the four-phase methodology used in this thesis. Each phase maps to a sub-research question and follows an input–methods–outputs logic, with outputs from one phase providing the primary inputs to the next.

and treated as a sensitivity lever (Chapter 8). Second, any continuous vent/purge gas routed to a flare header is treated as vent/purge to battery limits for offsite handling; baseline modelling does not include on-site flare combustion or destruction, and no flare emissions are claimed. When a CO_2 emissions metric is reported, it is restricted to direct on-site combustion only as explicitly modelled; CO_2 present as a component in exported or vented gas streams is not automatically interpreted as an emitted quantity within the gate-to-gate scope.

4.3.1. Phase 1: System Design and Configuration

The first phase addresses the initial sub-research question:

> *What are the system boundaries, process configurations, and input–output relationships for producing naphtha-range and jet-fuel-range blendstocks from pyrolysis of polyolefin-rich plastic waste?*

This phase serves a dual purpose: (i) to collect and critically evaluate the technical, economic, and contextual data required to represent the conversion system at study level; and (ii) to translate these findings into a fixed, simplified, and internally consistent reference configuration for the two product pathways. This step is methodologically necessary because the available literature does not provide a single ready-made process definition that can be transferred directly into the later technical and economic phases. Instead, heterogeneous evidence on feedstock quality, pyrolysis operation, upgrading requirements, and study boundaries must first be consolidated into one coherent gate-to-gate system basis before pathway comparison becomes meaningful.

The literature review in Chapter 3 provides the main evidence base and is distilled into three categories of inputs used throughout the remainder of the thesis. First, feedstock characteristics and pretreatment requirements are derived from studies on Dutch DKR 350 plastic waste streams. Evidence on polyolefin dominance, contaminant levels (e.g. chlorine and heteroatoms), and the role of additional sorting and dry-washing is used to define representative feedstock assumptions that form part of the system boundary. Second, process conditions and reactor design choices are drawn from experimental and pilot-scale literature. Reported operating windows for thermal pyrolysis of polyolefins (e.g. temperature range, reactor type, and residence time considerations) inform the choice of a thermal baseline suitable for screening-level assessment. Third, product yields, compositions, and upgrading requirements are derived from reported pyrolysis oil characterisation and upgrading studies. These define the pathway input–output relationships and the scope of downstream upgrading steps included in the model.

For the naphtha pathway, the review motivates an upgraded naphtha-range cut compatible with steam-cracker feed framing. For the jet-fuel pathway, the review motivates a jet-fuel-range cut definition and upgrading severity consistent with a jet-motivated blendstock framing, noting that certification (e.g., full ASTM compliance) is outside the scope of a screening TEA. The two pathways are therefore not defined as entirely separate plants, but as two pathway intents implemented on a shared gate-to-gate topology with pathway-specific upgrading severity and product cut logic. This preserves comparability by ensuring that later differences in technical and economic performance can be interpreted against a common reference configuration rather than against changing system boundaries or independently designed process layouts.

Where necessary for transparency, the classes of secondary data used in the model (yields and conversions, utility and resource factors, screening-level cost factors, and price coefficients) are documented in the model documentation provided with the spreadsheet files (appendix) and summarised in Chapter 7 for the economic inputs. Based on these inputs, representative PFDs are developed in Chapter 5 to define major unit operations, their interconnections, and the gate-to-gate system boundary. The outcome of Phase 1 is therefore a pair of consistent pathway definitions (boundary, configuration, and key input–output relationships) that can be implemented in the technical and economic models. In this way, Phase 1 establishes the common study basis that is held constant in later chapters, allowing Chapters 6–8 to remain traceable to an explicitly defined and pathway-consistent system design.

4.3.2. Phase 2: Technical Assessment

This phase addresses the second sub-research question:

> *What are the technical characteristics of producing naphtha-range and jet-fuel-range blendstocks from pyrolysis of polyolefin-rich plastic waste?*

The objective of Phase 2 is to quantify the technical performance of the two pathways by translating the Phase 1 process definitions into steady-state mass and energy balances. The technical model is deliberately formulated at screening level: it is intended to produce complete and internally consistent plant-boundary flow information that supports a transparent technical assessment (Chapter 6) and provides the basis for the TEA calculations in Phase 3 (Chapter 7), rather than to reproduce detailed plant dynamics or rigorous thermodynamics.

This modelling choice is deliberate and follows directly from the scope and evidence base of the thesis. The purpose of the technical assessment is to compare two pathway intents under a shared gate-to-gate boundary and to generate a complete set of auditable handover quantities for subsequent economic evaluation, not to develop a detailed design package for a specific plant. A more mechanistic model would require aligned kinetic, compositional, and equipment-design data across pyrolysis, hydrotreating, hydrocracking, gas handling, and fractionation that are not available in a sufficiently consistent form for the Dutch DKR 350-based system assessed here. Much of the available evidence base is experimental, pilot-scale, pathway-specific, or reported under different feedstock and boundary assumptions. Under these conditions, a screening-level steady-state representation is methodologically appropriate because it preserves transparency, internal consistency, and comparability across pathways without implying a level of predictive precision that would not be supported by the available secondary data.

Modelling scope and steady-state boundary

The model covers all unit operations within the gate-to-gate process boundary defined in Chapter 5. All units are evaluated at steady state; inventories, dynamic effects, and transient operation are not represented. The model is formulated to report a complete plant-boundary slate, including liquid products as well as byproducts, utilities, and waste/discharge streams required for mass-balance auditability and TEA handover.

This scope is consistent with the role of Phase 2 in the overall research design. The intention is not to simulate all physical phenomena that may influence plant behaviour in practice, but to construct a pathway-consistent representation of the conversion system that makes the technical consequences of the adopted design choices visible at plant boundary. By fixing the boundary and operating basis, the technical assessment ensures that later differences in economic performance can be traced back to pathway-specific upgrading and product-recovery logic rather than to changes in system definition.

Black-box representation and verification

A spreadsheet-based black-box modelling approach is used for both pathways. Unit operations are represented by aggregate transformation and separation rules that map inlet streams to outlet streams while satisfying overall conservation principles. Reactors are represented by literature-informed conversion and yield relationships, and separation units by split factors anchored to the adopted reporting basis (i.e. the cut definitions used to report naphtha-range and jet-fuel-range material). The intent is not to emulate detailed kinetics or equilibrium behaviour, but to maintain transparency and consistency between the pathway definitions, the computed balances, and the indicators reported in Chapter 6.

The use of black-box representations is appropriate here because the thesis compares pathway behaviour at the level of integrated plant-boundary outcomes rather than at the level of detailed unit-operation physics. In other words, the methodological requirement is not to resolve internal reactor fields or rigorous phase equilibria, but to represent how the adopted process configuration transforms plastic feed into saleable products, byproducts, and utility burdens under a common reporting basis.

The black-box structure therefore serves as a transparent translation layer between the heterogeneous literature inputs compiled in Phase 1 and the system-level quantities needed in Chapters 6–8.

Where necessary for reporting and internal consistency, streams are tracked on a unified component basis that preserves boiling-range ordering and supports the definition of product cuts. In practice, this is implemented through a consistent bookkeeping structure (e.g. lumped hydrocarbon families and/or pseudo-components by carbon number/boiling range), combined with explicit tracking of key non-hydrocarbon species (e.g. hydrogen, light gases, and water). This common basis ensures that streams can be mixed, split, and transformed without loss of accounting consistency across the flowsheet.

Before results are reported, each pathway solution is checked for mass-balance closure across the plant boundary, internal consistency of split definitions and recycle handling, and consistency of units and normalisations between absolute flows (kg/h, kW) and reported intensities (kg/kg feed, kWh/t feed). These checks are necessary to confirm that the integrated flowsheet is numerically coherent and that the resulting plant-boundary slate can be interpreted and transferred consistently into the TEA. They should not, however, be read as a substitute for rigorous thermodynamic validation or plant-operability proof; rather, they confirm bookkeeping integrity within the adopted screening representation.

Pedigree analysis of evidence base and model structure

Numerical closure and bookkeeping consistency checks are necessary to ensure that reported plant-boundary slates are internally coherent, but they do not by themselves communicate the strength of the underlying evidence base (for example whether key relationships are supported by direct measurements or by proxies). To make these strengths and limitations explicit, this thesis applies a *pedigree analysis* as a qualitative complement to quantitative uncertainty evaluation approaches such as validation and sensitivity analysis [114]. Van der Spek et al. emphasise that quantitative methods can be limited by the availability of independent validation data and may underrepresent uncertainty when probability distributions are poorly supported, while also providing limited insight into model-structure and knowledge-base (epistemic/methodological) uncertainty [114].

Pedigree analysis codes structured expert judgement into an ordinal scoring matrix with predefined criteria and linguistic descriptions for each score level [114]. This thesis adopts the four core pedigree criteria *proxy*, *empirical basis*, *theoretical understanding*, and *methodological rigour* (0–4 scale), using the criterion definitions provided by van der Spek et al. in their supplementary material [114]. The criterion *validation* is not used as a scored column here because independent plant-scale datasets are not available for full external validation within the scope of this screening study; instead, internal consistency is addressed through the closure checks described above and through the sensitivity analysis in Phase 4.

Two separate pedigree matrices are evaluated: a *technical* matrix that aligns with the structure of the steady-state model (process design, process variables, mass balance, and energy/utilities accounting), and an *economic* matrix that evaluates the evidence base of the DCF/MSP framework and the screening-level CAPEX/OPEX and boundary-credit conventions. Two separate pedigree matrices are evaluated: a *technical* matrix that aligns with the structure of the steady-state model (process design, process variables, mass balance, and energy/utilities accounting), and an *economic* matrix that evaluates the evidence base of the DCF/MSP framework and the screening-level CAPEX/OPEX and boundary-credit conventions. To reduce single-author bias, two reviewers score the matrices independently (Reviewer A: author; Reviewer B: supervisor). Because pedigree scores are ordinal, results are summarised using a central-tendency score and an agreement indicator; for the two-reviewer case, this thesis reports the mean score and the absolute deviation between reviewers, while retaining the underlying reviewer scores in the supplementary workbook tables [114]. Consolidated pedigree results are reported in Appendix B and in the submitted Excel workbooks, and are used as an interpretation lens in the discussion chapter, particularly to qualify which conclusions are robust within the modelling scope and which are most contingent on weakly supported assumptions.

Technical performance metrics

From the converged mass and energy balances, a set of TPMs is derived to characterise pathway behaviour. The TPMs are designed to be auditable at the plant boundary, comparable across pathways under a common normalisation, and directly transferable to the economic model. Indicators are grouped into (i) *product and yield performance* and (ii) *resource, utility, and boundary-burden performance*. This TPM set is intentionally limited to indicators that are both interpretable within the gate-to-gate scope and directly relevant for later economic handover and discussion.

- **Product and yield performance (feed basis)**
  These indicators describe how effectively the plastic feed is converted into the target liquid blendstocks and how much material leaves the boundary as non-target outlets:
  - **Target product yields**
    $$Y_i = \frac{m_i}{m_{\text{feed}}}$$
    where i denotes the naphtha-range and jet-fuel-range blendstock products.
  - **Non-target outlet yields (boundary completeness)**
    $$Y_{\text{non-target}} = \frac{m_{\text{non-target outlets}}}{m_{\text{feed}}}$$
    capturing key plant-boundary outlets such as heavy residues, solids, and aqueous discharge (reported explicitly in Chapter 6).

- **Resource, utility, and boundary-burden performance (feed basis)**
  These indicators reflect auxiliary requirements and boundary flows that drive operating costs and interpretation of process burden:
  - **Imported hydrogen intensity**
    $$I_{H_2} = \frac{m_{H_2,\text{import}}}{m_{\text{feed}}}$$
    hydrogen imported to meet upgrading demand, expressed per unit of plastic feed.
  - **Electricity intensity**
    $$I_{\text{el}} = \frac{E_{\text{el}}}{m_{\text{feed}}}$$
    net electricity demand per unit of plastic feed (reported in Chapter 6 as kWh/t feed).
  - **Exported byproduct fuel-gas indicator**
    $$I_{\text{fuelgas}} = \frac{m_{\text{fuelgas}}}{m_{\text{feed}}} \quad \text{and where relevant} \quad I_{\text{fuelgas,energy}} = \frac{m_{\text{fuelgas}} \cdot LHV}{m_{\text{feed}}}$$
    describing the magnitude of exported fuel-gas byproduct at battery limits (Chapter 6) and its role as an economic credit basis (Chapter 7).
  - **Vent/purge and discharge indicators**
    $$I_{\text{vent/purge}} = \frac{m_{\text{vent/purge}}}{m_{\text{feed}}}, \qquad I_{\text{water}} = \frac{m_{\text{water discharge}}}{m_{\text{feed}}}$$
    capturing plant-boundary gas and aqueous discharge flows that affect boundary completeness and interpretation.

Together, these TPMs provide a transparent characterisation of each pathway that links technical behaviour to economic consequences. They establish consistent performance profiles that are used as direct inputs to the economic model (Phase 3) and as interpretation anchors for sensitivity outcomes (Phase 4), without implying that TPMs alone determine feasibility.

Environmental scope and reported indicators

This thesis does not perform a full life-cycle assessment. The study scope is a screening-level, gate-to-gate TEA, and consistent upstream and downstream inventory data (e.g., for the waste supply chain, electricity and hydrogen production routes, and end-use combustion) is not available at the fidelity required for robust LCA conclusions within this project. Instead, the assessment reports a limited set of plant-boundary proxy indicators to support interpretation of pathway trade-offs within the defined boundary.

Reported indicators include utility and resource intensities (e.g., electricity and imported hydrogen), boundary byproduct export potential (exported fuel gas), and boundary waste/discharge flows (e.g., solids/residues and aqueous discharge). Where a CO_2 metric is reported later in the thesis, it is restricted to direct on-site combustion only as explicitly modelled; no flare combustion is modelled and no flare emissions are claimed under the baseline scope.

4.3.3. Phase 3: Economic Assessment

This phase addresses the third sub-research question:

> *What are the economic performance outcomes of the naphtha pathway and jet-fuel pathway, and what do these imply for their feasibility under a consistent assessment basis?*

The objective of Phase 3 is to evaluate the economic performance of each pathway by quantifying capital expenditure (CAPEX), operating expenditure (OPEX), revenues, and DCF-based break-even metrics on a basis consistent with the gate-to-gate system definition. Each pathway is assessed using its own technical outputs from Phase 2, while maintaining a harmonised financial basis so that differences in outcomes can be attributed to pathway performance and product definition rather than inconsistent economic conventions.

This phase is formulated as a screening-level TEA rather than as an investment-grade project appraisal. The purpose is to translate the plant-boundary quantities derived in Phase 2 into a transparent and pathway-consistent economic comparison that identifies the dominant cost drivers and break-even requirements under a common financial basis. In methodological terms, the TEA therefore functions as a decision-oriented interpretation layer on top of the technical model: it does not claim to predict a bankable project valuation, but it does provide a structured way to compare how the two pathway intents perform when subjected to the same accounting boundary, cost-year basis, and DCF logic.

Cost basis, boundary alignment, and MSP definition

The economic model uses the same gate-to-gate boundary as the technical model and treats upstream waste management activities as exogenous scenario inputs (e.g., feedstock gate fee versus procurement cost). All costs and prices are expressed on a consistent cost-year basis and financial convention, as specified in the economic assumptions table in Chapter 7 (cost year 2024; construction and operating horizon assumptions; real discounting and end-of-year convention).

The primary economic response metric in this thesis is the minimum selling price, defined as the focal product price that satisfies the DCF break-even condition:

$$NPV = 0$$

under the specified project life, discount rate, tax assumptions, and capital structure. For pathways with co-products, the closure condition is applied in a pathway-consistent manner (Chapter 7), ensuring that MSP reflects the break-even price of the focal product under the chosen product slate. Exported

byproduct fuel gas at battery limits may be monetised as an operating income offset as defined in Chapter 7; vent/purge gas to battery limits is not treated as a saleable export unless explicitly stated.

MSP is used as the primary comparison metric because the thesis compares two pathway intents that differ in product slate and in the designation of the focal product. Under these conditions, MSP provides the most direct pathway-consistent indicator of the economic burden that must be recovered through the designated main product, while preserving traceability to the shared DCF basis. Conventional indicators such as NPV and IRR remain informative and are reported in Chapter 7, but their interpretation depends more directly on assumed selling prices. By contrast, MSP states the break-even price requirement itself and is therefore the most suitable metric for comparing pathway feasibility under the adopted closure convention.

CAPEX and OPEX estimation approach (screening-level)

CAPEX is estimated at screening level using literature-based equipment cost proxies combined with study-level installation and investment factors. Equipment-level purchased-cost proxies are scaled to the relevant design basis (where applicable) using standard power-law relationships and escalated to the analysis cost year using a cost index approach. Installed equipment costs are approximated using a factor method, and total plant investment is obtained through an investment roll-up consistent with standard TEA practice, recognising the uncertainty inherent to screening-level costing.

This costing approach is appropriate for the present study because the system is defined at conceptual level and the available evidence base does not support detailed bottom-up equipment design for all units within the integrated A100–A400 boundary. The aim is not to produce a class-grade estimate for procurement or financing, but to derive a consistent economic magnitude and cost structure that can be compared across pathways under the same assumptions. Screening-level CAPEX estimation therefore matches the level of technical definition developed in Phases 1–2 and avoids introducing an artificial degree of precision that would not be justified by the available data.

OPEX is separated into variable and fixed components. Variable OPEX is computed directly from Phase 2 consumptions and annualised flowrates (feedstock, imported hydrogen, utilities, and waste/discharge handling where applicable) multiplied by scenario unit prices. Fixed OPEX is estimated using factor-based relationships (e.g., maintenance, labour/overhead proxies) consistent with a screening TEA, with all factors and unit prices stated explicitly in Chapter 7 to preserve auditability.

This separation between variable and fixed OPEX is methodologically useful because it makes visible which parts of the annual cost structure are directly driven by the plant-boundary quantities computed in Phase 2 and which are inherited from the chosen screening TEA conventions. In later chapters, this distinction supports interpretation of why some sensitivity levers act primarily through throughput-linked operating terms while others act through the burden of capital-linked and fixed annual charges.

DCF framework and performance indicators

A DCF model is used to translate annual revenues and costs into free cash flows over the project lifetime. Net present value is computed as:

$$NPV = \sum_{t=0}^{T} \frac{FCF_t}{(1+r)^t},$$

where FCF_t is the free cash flow in year t, r is the real discount rate, and T is the project lifetime (as specified in Chapter 7). The internal rate of return (IRR) is the discount rate that satisfies $NPV = 0$, and payback period (PBP) is reported where informative as the time to recover initial investment from cumulative net cash flow. While these indicators provide complementary perspectives, pathway feasibility in this thesis is primarily interpreted through MSP under the consistent economic basis.

The DCF framework is adopted because it provides a coherent way to combine capital investment, operating costs, utilisation assumptions, and pathway-specific revenue structure within a single break-

even logic. This is particularly important in the present thesis because the pathways are not compared as identical end products with a shared selling price assumption, but as alternative outlet intents under a common plant boundary and common financial basis. The DCF structure therefore links the technical handover quantities from Phase 2 to an economically interpretable break-even requirement, while preserving comparability across pathways and supporting the sensitivity analysis in Phase 4.

4.3.4. Phase 4: Sensitivity Analysis

This phase addresses the fourth sub-research question:

> *How sensitive are the economic outcomes of each pathway to variations in key assumptions, and which parameters are the primary drivers of feasibility?*

The objective of Phase 4 is to test the robustness of the baseline economic outcomes by varying a limited set of high-leverage parameters and quantifying their impact on MSP under the same DCF basis. A OAT sensitivity design is adopted: one parameter is perturbed while all other assumptions remain at their baseline values, and MSP is re-solved to satisfy the DCF break-even condition.

The use of an OAT design is deliberate and appropriate for the present study. The purpose of Phase 4 is not to generate a full probabilistic uncertainty distribution for pathway feasibility, but to identify which assumptions exert the strongest control over the break-even selling price within the screening-level model structure. At the thesis scope, the available evidence base does not support well-founded joint probability distributions for many of the economically consequential inputs, particularly commercially contingent parameters such as feedstock contracting conditions and boundary-export monetisation. Under these conditions, an OAT design provides the clearest and most transparent way to isolate parameter influence, preserve interpretability, and rank the dominant feasibility levers without overstating the statistical meaning of the results.

The sensitivity set is intentionally compact to preserve interpretability and to reflect drivers that are not uniquely determined at screening level. The sensitivity set is also informed by the pedigree analysis in Appendix B, prioritising parameters that are not uniquely determined at screening level or that rely on commercially contingent coefficients and boundary-credit conventions [114]. The executed parameters include (i) plant capacity (project scale choice), (ii) plastic feedstock gate price at battery limits (contracting condition), (iii) imported hydrogen price (market uncertainty), and (iv) monetisation of exported byproduct fuel gas (credit basis). These parameters are selected because they are both decision-relevant and sufficiently separable to allow clear interpretation of how each one propagates through the MSP calculation under the fixed system design established in Phase 1.

For coefficient-only variations (feedstock price, hydrogen price, and fuel-gas crediting), technical performance is held invariant: the Phase 2 mass and energy balances and TPM values remain fixed, and only the perturbed economic coefficient changes. Capacity variations are implemented using the consistent scaling conventions described in Chapter 8. This distinction is important for interpretation, because it ensures that the sensitivity results are read correctly as either (i) pure coefficient effects applied to a fixed technical basis, or (ii) throughput-linked scaling effects under the same pathway configuration, rather than as alternative process designs.

The outcomes of Phase 4 complement the baseline TEA by clarifying which assumptions most strongly control MSP, where the pathways are most exposed to uncertainty, and which improvement levers are most impactful within the screening-level modelling scope of this thesis. In this way, the sensitivity analysis functions as a structured robustness layer on top of the baseline TEA: it translates the fixed technical and economic basis into a ranked set of decision-relevant levers, while remaining consistent with the gate-to-gate scope and claim-strength framing used throughout the thesis.

5

System Design

This chapter defines the *fixed system configuration* evaluated in the steady-state modelling (Chapter 6) and TEA (Chapter 7). Building on the literature review and methodological foundation established in the preceding chapters, it translates the process understanding developed in Chapter 2 and Chapter 3 into a coherent gate-to-gate plant definition: system boundary, feedstock specification, area structure (A100–A400), and the pathway-defining design choices that are held constant during the modelling and costing phases. By making these choices explicit, the chapter provides the conceptual basis needed to evaluate technical performance and economic feasibility in line with the research questions introduced in Chapter 4.

This chapter implements *Phase 1* of the research framework introduced in Chapter 4 and addresses *Sub-Research Question 1* by defining the gate-to-gate boundary, feedstock context, and pathway-specific design choices that together constitute the fixed system configuration assessed in the subsequent technical and economic phases.

The system design encompasses the full gate-to-gate configuration of the upgrading plant, beginning with the arrival of a pretreated, polyolefin-rich DKR 350 feedstock and ending with the production of specification-relevant liquid blendstocks. Two upgrading pathways are evaluated on a single shared flowsheet topology: (i) the *naphtha pathway* and (ii) the *jet-fuel pathway*. Both share the same underlying architecture but differ only in (a) the HTU/HCU operating severities and (b) the product cut logic in final fractionation. A small heavy purge is applied in both pathways to prevent accumulation of refractory material and preserve steady-state realism.

The emphasis in this chapter is on conceptual definition and traceable design basis rather than detailed mass and energy balances. Quantitative mass and energy balances and the steady-state modelling framework are presented in Chapter 6, where the system design defined here is transformed into a converged process model. The economic basis (cost year 2024 in real terms and discounted-cash-flow conventions including a 25-year operating horizon) is defined in Chapter 7; this chapter uses the same operating basis and boundary conventions and avoids restating economic assumptions except where needed to prevent cross-chapter inconsistencies.

5.1. System Scope

This section defines the scope and operating context of the reference facility. It establishes the gate-to-gate system boundary applied throughout the technical and economic assessment, outlines the plant scale and location, and introduces the technological configuration that underpins both upgrading pathways. The integrated flowsheet overview and walk-through is provided later in the chapter (Section 5.6), once the design basis has been established.

5.1.1. System Boundaries

A gate-to-gate system boundary is adopted, beginning at the point where the pretreated, polyolefin-rich DKR 350 feedstock arrives at the conversion facility and ending at the plant battery limits where liquid products and boundary outlet streams leave the system. Within this boundary, the facility is represented by four functional areas: the thermal pyrolysis block (A100), the hydrotreating and impurity-removal block (A200), the hydrocracking and fractionation block (A300), and the utilities and energy-integration block (A400). A simplified block-flow representation of this area structure and the principal gate-to-gate inlets and outlets is provided in Figure 5.1.

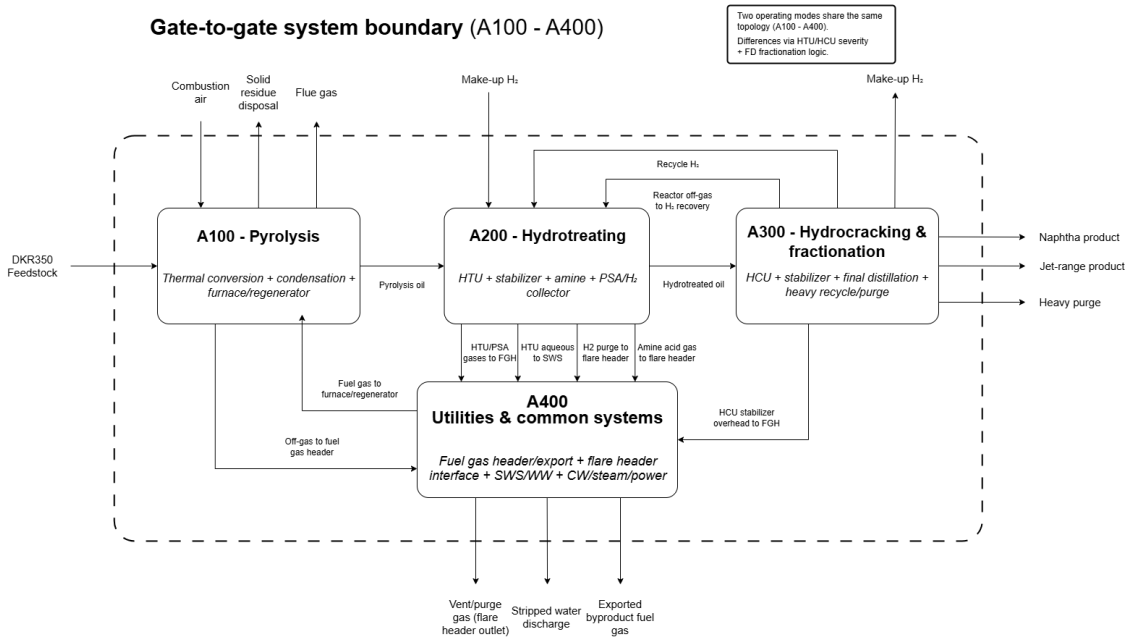

Figure 5.1: Simplified block-flow diagram of the gate-to-gate conversion facility (Areas A100–A400) evaluated in this thesis. The dashed boundary indicates the modelled battery limits. The two pathways share a single topology; differences arise only from HTU/HCU severity parameters and fractionation cut logic.

Included within this gate-to-gate boundary are all steps associated with receiving, converting, upgrading, and internally managing the DKR 350 feedstock. This includes intake and handling of the densified material, its thermal conversion in A100, and separation of the resulting liquid, gaseous, and solid fractions. The upgrading sequence in A200 and A300, which converts the condensable fraction into specification-relevant blendstocks, is likewise contained within the boundary. Utility provision and energy integration in A400 are included because heat supply, fuel-gas routing, electricity use, cooling, and waste handling influence both the technical and economic outcomes.

Hydrogen management is part of the system as well and is treated as a process reactant circulating through the hydrotreating and hydrocracking reactors. The hydrogen purification and recycle interface (amine treating, PSA, H_2 collector, and recycle splits) is treated as an upgrading interface associated with Area A200 and couples Areas A200 and A300. This coupling is made explicit by routing the HCU high-pressure separator return gas (Stream 321) back to the PSA feed header, while recycle hydrogen is distributed back to both reactors as HTU recycle hydrogen (Stream 205) and HCU recycle hydrogen (Stream 305). Make-up hydrogen enters at battery limits as separate feeds to A200 as HTU make-up hydrogen (Stream 206) and to A300 as HCU make-up hydrogen (Stream 306). Area A400 provides shared utilities and boundary-handling interfaces, including the plant fuel-gas header/export interface, sour-water stripping and wastewater handling, and the vent/purge header interface.

Activities that occur prior to delivery of the pretreated feedstock are excluded from the quantitative model. These upstream steps include PMD collection, primary sorting, polyolefin enrichment, dry washing, densification, and transport to the conversion site. As described in Chapter 2, these oper-

ations take place at specialised facilities and enter the analysis only through the assumed gate price for DKR 350. Downstream refining, blending, and product use are likewise excluded. The aim of this study is to evaluate the performance of the conversion facility itself rather than its position within the wider waste-plastic value chain.

These boundary choices reflect both the organisation of the Dutch recycling system and the technical evidence reviewed earlier. As discussed in Chapter 2, PMD sorting and DKR category separation occur at centralised facilities rather than at chemical conversion sites. Pilot-scale studies on DKR 350 pyrolysis adopt the same division of responsibilities, evaluating the conversion step independently of upstream preprocessing [79], [80], [81]. The techno-economic literature reviewed in Chapter 3 likewise focuses on the conversion system rather than on upstream or downstream segments of the waste-plastic value chain. The gate-to-gate boundary adopted here is therefore consistent with the methodological framework introduced in Chapter 4 and applies identically to both upgrading pathways, which operate on the same physical configuration and differ only in operating conditions and product definitions.

A critical boundary convention used consistently in Chapters 5–8 is the treatment of plant fuel-gas streams. Exported byproduct fuel gas at battery limits (Stream 423) is defined as a saleable boundary export and is monetised as a credit in Chapter 7. A separate vent/purge stream leaves the system as *vent/purge gas to battery limits (flare header)* for offsite handling; baseline modelling does not include on-site flare combustion or destruction. The flare system remains part of the conceptual topology as a safety and handling interface, but its function in this thesis is boundary completeness rather than on-site emissions accounting.

CO_2 may be present as a component in exported or vented gas streams. Emissions reporting in this thesis is restricted to *direct on-site combustion only, as explicitly modelled* (e.g., furnace firing); downstream combustion of exported fuel gas and offsite handling of vent/purge streams lie outside the gate-to-gate boundary.

Plant-boundary outlet categories used throughout Chapters 6–8 include: liquid products (naphtha product, Stream 340, and in the jet-fuel pathway the jet-fuel-range blendstock, Stream 344), exported byproduct fuel gas (Stream 423), vent/purge gas to battery limits (flare header outlet), heavy purge from the hydrocracker recycle loop (Stream 342), stripped water discharge (Stream 411), flue gas from on-site combustion after heat recovery (Stream 150), and solid residue (char/inerts/ash) requiring disposal. This explicit outlet slate supports technical auditability in Chapter 6 and later economic traceability in Chapter 7.

5.1.2. Plant Scale, Location, and Operating Basis

The reference facility processes 40 $\mathrm{kt\,yr^{-1}}$ of pretreated, polyolefin-rich DKR 350. This scale reflects both the availability of plastic packaging waste within the Dutch PMD system and the levels at which pyrolysis technologies are currently being deployed. As noted in Chapter 2, DKR 350 represents approximately 195 $\mathrm{kt\,yr^{-1}}$ of sorted plastic packaging waste in the Netherlands [15]. Recent industrial developments reinforce that a 40 $\mathrm{kt\,yr^{-1}}$ reference case aligns with near-term practice: BlueAlp installations operate at approximately 70 $\mathrm{kt\,yr^{-1}}$ [115], Itero's demonstration plant at the Brightlands Chemelot Campus is designed for 27 $\mathrm{kt\,yr^{-1}}$ [116], Xycle's Rotterdam facility targets 21 $\mathrm{kt\,yr^{-1}}$ [117], and the SABIC–Plastic Energy SPEAR project begins at around 20 $\mathrm{kt\,yr^{-1}}$ [118]. Together, these examples illustrate that facilities between 20 and 70 $\mathrm{kt\,yr^{-1}}$ currently represent the technological maturity of thermal pyrolysis in the Netherlands.

A similar level of technological maturity underpins the upgrading steps required to refine pyrolysis liquids into naphtha- or jet-fuel-range blendstocks. Hydrotreating and hydrocracking are long-established refinery operations, applied commercially for desulphurisation, saturation, and molecular restructuring of petroleum fractions. Recent European and international projects have also demonstrated or targeted their application to plastic-derived pyrolysis oils, indicating that these units can be deployed beyond laboratory or pilot scale. The upgrading configuration adopted in this thesis therefore draws on

commercially proven technologies rather than emerging or experimental systems.

The facility is assumed to operate for 8,000 $\mathrm{h\,yr^{-1}}$, a representative utilisation level for continuously operated thermochemical conversion systems where maintenance outages reduce theoretical annual availability. This assumption is consistent with techno-economic studies in the literature [17], [40]. The facility is situated in the Rotterdam–Moerdijk industrial cluster, which hosts several large PMD sorting and post-separation facilities [119], [120] and major petrochemical users such as the Shell Moerdijk steam cracker and the Shell Pernis refinery [121], [122]. While downstream processing falls outside the system boundary, the presence of nearby hydrotreating, hydrocracking, and steam-cracking capacity indicates that the region already provides the industrial infrastructure relevant for both pyrolysis and upgrading operations.

5.1.3. Technological Configuration and Design Intent

Both pathways begin with thermal, non-catalytic pyrolysis of DKR 350 in Area A100. A continuously operated fluidised-bed concept is adopted because it aligns with the Dutch pilot evidence base for enriched, dry-washed DKR 350 and with the maturity of non-catalytic thermochemical conversion for heterogeneous plastic feedstocks [80], [81], [82]. Downstream of pyrolysis, both pathways share a unified upgrading architecture: hydrotreating/impurity removal (A200) followed by hydrocracking and fractionation (A300). Supporting systems in A400 provide shared utilities and boundary-handling interfaces, including plant-wide fuel-gas routing and export, sour-water stripping, and the vent/purge header interface.

At design level, the two pathways should therefore be read as *alternative outlet intents on one fixed plant configuration*, not as different plants. The naphtha pathway is defined to maximise recovery of a cracker-relevant naphtha-range blendstock, while the jet-fuel pathway applies a different upgrading and fractionation intent to recover an additional jet-fuel-range blendstock cut. This distinction becomes technically visible primarily in A300 through heavy-pool conversion and final cut logic and is later translated into plant-boundary performance in Chapter 6 and pathway-specific MSP closure in Chapter 7.

5.2. Feedstock Definition and Pretreatment

The material entering the pyrolysis reactor defines the initial conditions for the conversion process and strongly influences the severity of the downstream upgrading steps. Within the gate-to-gate system boundary established in Section 5.1.1, the feedstock is taken to be a pretreated, polyolefin-rich fraction derived from DKR 350. This section outlines the origin of this material in the Dutch PMD system, describes its untreated composition, and summarises the sorting and cleaning steps that produce the feedstock supplied to Area A100.

5.2.1. Origin of the Feedstock in the Dutch PMD System

Plastic packaging waste in the Netherlands is collected as PMD and processed at specialised sorting installations. Streams with established mechanical-recycling markets, such as mono PE, mono PP, and PET bottles, are removed, and the remaining mixture of heterogeneous packaging types is classified as DKR 350.

Pilot-scale studies reviewed in Chapter 3 have used DKR 350 as input to thermal conversion experiments and show that the fraction contains multiple polymer types and non-plastic impurities. These characteristics limit its suitability for direct use as a pyrolysis feedstock. Following the approach taken in those studies, the present work therefore treats the feedstock as a pretreated, polyolefin-rich derivative of DKR 350. The next subsections describe the untreated composition, the effect of polyolefin enrichment, and the role of dry washing in reducing surface contaminants.

5.2.2. Composition of Untreated DKR 350

Untreated DKR 350 reflects its origin as a residual output of Dutch PMD sorting. It contains a heterogeneous mixture of polymers, including polyethylene, polypropylene, PET, polystyrene, multilayer laminates, and minor plastics [82]. Non-plastic contaminants such as fines, paper-based laminates, aluminium layers, food residues, and other impurities are also typically present.

From a process-design perspective, this heterogeneity introduces several constraints. PET and PVC contribute oxygen and chlorine, which increase the severity of downstream hydrotreating and elevate corrosion risks. Multilayers and fillers contribute inorganic components that promote char formation, while pigments and surface residues add ash and trace metals. These effects were evident in the pilot-scale studies discussed in Chapter 3, where untreated DKR 350 produced pyrolysis oils with higher heteroatom concentrations and more challenging impurity profiles than pretreated material.

These characteristics motivate the need for intermediate sorting and cleaning before pyrolysis. The next subsection quantifies how polyolefin enrichment modifies the polymer distribution and reduces the non-polyolefin and contaminant load.

5.2.3. Sorting and Polyolefin Enrichment

Polyolefin enrichment concentrates the hydrocarbon fraction of DKR 350 and removes most materials that introduce heteroatoms or inorganic residues. Negative-mode NIR sorting, as applied in recent Dutch pilot campaigns, selectively rejects PET, PS, PVC, paper laminates, fines, and other non-polyolefin objects, yielding a stream dominated by PE and PP [80], [81], [82]. Table 5.1 summarises the resulting shift in composition.

Table 5.1: Material composition of DKR 350 before and after polyolefin enrichment, based on data reported by van Akker (2025).

Material	Untreated (wt.%)	PO-rich stream (wt.%)
PE (films and rigids)	46.2	59.0
PP (films and rigids)	22.7	29.6
PS	3.1	0.2
PET	11.5	1.3
Multilayers	13.6	17.8
Other plastics	1.1	0.9
Paper, textiles, organics	6.1	4.2
Fines and inerts	6.0	1.4
Metals	1.1	1.2

Polyethylene and polypropylene together increase from roughly 69 wt.% to nearly 89 wt.% after enrichment, consistent with the feedstocks used in the Dutch pilot campaigns summarised in Chapter 3. PET and PS, both sources of oxygenates and aromatics, are largely removed. Paper-based residues and fines decrease as well, reducing ash formation and char residues during pyrolysis.

Multilayer films remain present because optical sorting cannot always distinguish them from polyolefin films. Although present at lower levels than in the untreated fraction, multilayers remain relevant for downstream upgrading because adhesives and barrier coatings can introduce oxygen, nitrogen, or trace metals.

5.2.4. Dry Washing and Surface Contaminant Removal

NIR-based sorting increases the polyolefin content of the feedstock, but the enriched fraction still contains surface-bound contaminants such as dirt, fines, and residues originating from the use phase and earlier sorting steps. These contaminants increase ash formation and contribute heteroatoms and metals to the pyrolysis oil. To address this, Dutch pilot campaigns applied a dry-washing step to further clean the polyolefin-rich stream before thermal conversion [80]. The treatment mechanically detaches surface residues without the use of water and reduces moisture content.

As summarised in Table 5.2, the treatment lowers the concentrations of chlorine, sulfur, and a range of inorganic elements by factors of two to five. These reductions decrease ash and char formation in the pyrolysis bed, lessen the transfer of heteroatoms into the liquid product, and reduce the dehalogenation and hydrotreating burden in Area A200. Lower metal levels also mitigate catalyst poisoning risks in both the hydrotreating and hydrocracking reactors.

Beyond chemical improvements, the treatment increases the physical consistency of the feed. Reduced fines content improves flowability and limits entrainment in the fluidised bed, supporting more stable feeding conditions in Area A100.

Table 5.2: Effect of dry washing on contaminant levels in the PO-rich DKR 350 stream, based on [80].

Element	Unit	Unwashed	Dry-washed
Cl	wt.%	0.151	0.066
S	wt.%	0.174	0.027
P	wt.%	0.317	0.129
Na	wt.%	0.718	0.213
K	wt.%	0.149	0.065
Ca	wt.%	0.924	0.335
Fe	wt.%	0.085	0.059
Ni	ppm	4512	1890
Cu	ppm	44248	23968
Zn	ppm	4222	2091
Pb	ppm	7712	3202
Cr	ppm	21546	4924

5.2.5. Final Feedstock Specification

The combined effect of NIR-based enrichment and dry washing is a polyolefin-rich, comparatively clean, and physically consistent feedstock that forms the input to Area A100 in the system model. The resulting material is dominated by polyethylene and polypropylene, with approximately 89 wt.% PO content after enrichment [81]. Residual multilayers, paper-based residues, and fines remain present but at much lower levels than in untreated DKR 350. Dry washing reduces chlorine, sulfur, and inorganic elements by factors of two to five [80], limiting ash formation in Area A100 and reducing heteroatom loads entering the upgrading block (Areas A200–A300). Lower metal concentrations mitigate catalyst-deactivation risks in both hydrotreating and hydrocracking.

Before delivery to the facility, the material is densified into millimetre-scale granules through agglomeration or pelletisation [80], [81]. This physical form provides predictable flow behaviour, improves bulk density, and supports continuous feeding into the fluidised-bed reactor.

Table 5.3: Final feedstock specification used in the system model, derived from [80], [81].

Component or property	Value	Source
PE + PP (wt.%)	approx. 89	[81]
Residual non-polyolefins (wt.%)	remainder, mainly multilayers	[81]
Fines and inerts (wt.%)	approx. 1–2	[81]
Cl (wt.%)	0.066	[80]
S (wt.%)	0.027	[80]
P (wt.%)	0.129	[80]
Transition metals	reduced relative to untreated	[80]
Physical form	densified granules, few mm diameter	[80], [81]
Moisture	reduced through dry washing	[80]

5.3. Plastic Pyrolysis Block Design (A100)

The pyrolysis block (Area A100) converts the pretreated, polyolefin-rich DKR 350 feedstock into three product categories: a condensable liquid, a non-condensable gas, and a solid residue (char/inerts).

These categories determine the loads imposed on upgrading (A200/A300) and on the shared systems (A400). This section defines the reference configuration and operating conditions of A100, describes product handling and separation, and summarises the yield basis and key product properties used as design-basis inputs to Chapter 6.

5.3.1. Selection of Pyrolysis Configuration

A thermal, non-catalytic fluidised-bed reactor concept is selected as the reference configuration for Area A100. Pilot-scale studies on enriched and dry-washed DKR 350 [80], [81], [82] report stable operation, reproducible liquid and gas yields, and controllable severity under these conditions. Catalytic alternatives are not adopted as the baseline because they remain less mature for heterogeneous mixed-plastic feedstocks and are not widely deployed in near-term commercial demonstrations.

5.3.2. Operating Conditions and Reactor Operation

The reactor is operated in continuous mode at approximately 460 °C, consistent with the window typically used to maximise liquid formation from polyolefins and with the conditions applied in the Dutch pilot studies [80], [81], [82]. At a nominal capacity of 40 kt yr^{-1} and an operating window of 8,000 h yr^{-1}, the reactor processes roughly 5,000 kg h^{-1} of densified feedstock. The reactor operates near atmospheric pressure in an inert environment established by recycling a portion of the non-condensable gas produced in A100, avoiding imported nitrogen.

5.3.3. Pyrolysis Products Handling and Separation

The product stream leaving the reactor contains condensable hydrocarbons, light non-condensable gases, and entrained solids. Entrained char and bed material are removed in a primary solids-separation step (conceptually represented by a cyclone) to prevent erosion, fouling, and uncontrolled solids transfer into the upgrading block. After solids removal, the vapour–gas mixture is cooled to recover the condensable fraction as a single liquid stream. Residual droplets are removed from the gas to enable reliable routing as recycle gas and/or net fuel gas to the plant-wide header.

5.3.4. Product Yields and Mass-Balance Basis

The distribution of liquid, gas, char, and inerts formed during pyrolysis provides the quantitative basis for the behaviour of Area A100 and determines the loads imposed on upgrading and shared systems. Because the reactor processes pretreated, polyolefin-rich DKR 350, the yield structure applied here is derived from recent Dutch pilot campaigns that used comparable enriched and dry-washed materials [80], [81], [82]. The most complete dataset is reported by van Akker [81].

In the present system design, the unrecovered fraction is assigned to the liquid phase, and the following yield set is used as design-basis input to the steady-state model:

$$y_{\text{liq}} = 0.619, \qquad y_{\text{gas}} = 0.260, \qquad y_{\text{char}} = 0.052, \qquad y_{\text{inerts}} = 0.069.$$

These yields define how the feedstock mass is partitioned among the three product phases and the inert solids carried through the reactor. In Chapter 6, they drive the plant-level distribution between (i) upgrading feed, (ii) internal energy supply and potential exported fuel gas, and (iii) residue disposal.

5.3.5. Key Properties of the Pyrolysis Products

The pyrolysis oil spans a broad boiling range (roughly C_5 to C_{40}) with substantial material in both naphtha- and jet-fuel-range carbon numbers. This motivates the upgrading structure: hydrotreating to stabilise and remove heteroatoms and hydrocracking/fractionation to reshape the heavy tail and recover pathway-defined cuts.

Comprehensive two-dimensional gas chromatography performed by van Strien et al. [80] provides the best available PIONA distribution for this feedstock. Paraffins and iso-paraffins together account

for roughly half of the mass; olefins and naphthenes each contribute about one fifth; and aromatics represent approximately one tenth (Table 5.4). The olefin fraction is a principal driver for high olefin saturation intent in A200.

Table 5.4: PIONA class distribution of pyrolysis oil from dry-washed DKR 350, based on [80].

Class	wt.%
Paraffins	32.4
Iso-paraffins	17.7
Olefins	19.0
Naphthenes	19.4
Aromatics	11.5

Elemental analyses show measurable heteroatom concentrations, with nitrogen near 7000 ppmw, oxygen around 6000 ppmw, and lower levels of chlorine, sulfur, and phosphorus [81], [82] (Table 5.5). These impurities directly influence HTU severity intent, hydrogen consumption, sour-gas production, and aqueous handling loads to A400.

Table 5.5: Elemental impurities in pyrolysis oil from dry-washed PO-rich DKR 350 used as design-basis inputs for upgrading. Heteroatoms are reported in ppmw; silicon is reported in $\mathrm{mg\,kg^{-1}}$ (numerically equivalent to ppmw at these dilute levels).

Species / group	Value	Unit / note
Heteroatoms (whole-oil basis)		
Nitrogen	7000	ppmw
Oxygen	6000	ppmw
Chlorine	155	ppmw
Sulfur	75	ppmw
Phosphorus	9	ppmw
Metals and metalloids (whole-oil basis)		
Silicon	23	$\mathrm{mg\,kg^{-1}}$ (detected)
Other metals	below detection limit	reported assay

Note: “Other metals” were reported as below detection limit in the analytical campaigns; silicon was consistently detected at around 23 $\mathrm{mg\,kg^{-1}}$ [81].

Most metals were reported as below detection limit in the analytical campaigns, while silicon was consistently detected at around 23 $\mathrm{mg\,kg^{-1}}$ [81]. These dilute levels are not modelled explicitly as catalyst deactivation mechanisms within the steady-state scope, but they provide a plausibility check that the assumed upgrading configuration and catalyst protection concept are not obviously inconsistent with trace impurity levels (Table 5.5).

Non-condensable gas accounts for roughly one quarter of the feed on a mass basis and is dominated by light C_2–C_5 hydrocarbons (Table 5.6). This composition underpins its role as internal fuel and potential exported fuel gas at battery limits (exported byproduct fuel gas, Stream 423), once internal firing demand is met.

5.4. Pyrolysis Oil Upgrading: A200 Hydrotreating and A300 Hydrocracking

This section defines the upgrading *design basis* that differentiates the two pathways introduced earlier in this chapter: the *naphtha pathway* and the *jet-fuel pathway*. The intent is to translate the specification-framed discussion in section 3.5 into a model-ready set of outcome-based indicators, without introducing mechanistic detail that cannot be constrained by the available datasets. Upgrading is framed by specification intent rather than boiling range alone, and pathway differences are implemented through reactor-severity parameters and product cut-definition logic while keeping the flowsheet topology identical.

Table 5.6: Gas product yields from thermal pyrolysis of dry-washed, polyolefin-rich DKR 350 at 460 °C, based on van Akker (2025).

Component	Yield (wt.% of feed)
H_2	0.17
Methane	1.33
CO	0.31
CO_2	1.90
Ethylene	2.64
Ethane	1.99
Propylene	5.66
Propane	0.88
C_4 hydrocarbons	5.46
C_5 hydrocarbons	3.87
C_6 hydrocarbons	1.10

Numeric values are stated in the tables in this section as the design basis for the steady-state model. The spreadsheet model implements these values and performs the associated closure and stoichiometric bookkeeping (e.g., hydrogen consumption and product/by-product allocations). Where a literature source does not report a single case-consistent scalar for a parameter, the value is fixed explicitly, and the selected assumption is documented with its citation anchor and rationale to preserve transparency and auditability.

5.4.1. Upgrading Intent and Product Definitions

Two upgrading intents are adopted. The first is a cracker-relevant naphtha blendstock intent recovered as naphtha product (Stream 340). The second is a jet-motivated blendstock intent recovered as jet-fuel-range blendstock (Stream 344), framed against jet-driven specification categories without implying certification or drop-in compliance.

For the naphtha blendstock intent, representative binding indicators include ppm-level limits on heteroatoms and halogens, combined with low olefinicity to avoid fouling and coke formation in downstream processing [26]. For the jet-motivated intent, representative categories include freezing-point and viscosity constraints, a final boiling point cap, and related property windows that can be yield-limiting even when a jet-range fraction exists [100], [102]. Within the gate-to-gate scope of this thesis, these indicators are not treated as compliance claims; they motivate relative severity choices and the cut-definition logic in final fractionation [102], [103].

5.4.2. Common Upgrading Topology and Interfaces

Both pathways employ the same upgrading topology and the same interfaces to Area A400. The upgrading block produces two shared interface categories that determine utility and waste-handling loads: (i) hydrogen-rich and hydrocarbon-rich gases that enter the PSA feed header and the plant fuel-gas header and (ii) aqueous by-products that enter the sour-water system.

Gas streams leaving the high-pressure separators in Area A200 are routed via amine treating to a PSA feed header associated with the A200 upgrading interface. The coupling to Area A300 is made explicit by routing the HCU high-pressure separator return gas (Stream 321) back to this PSA feed header. The PSA produces recycle hydrogen that is redistributed to both reactors as HTU recycle hydrogen (Stream 205) and HCU recycle hydrogen (Stream 305), while purge from the H_2 collector (Stream 233) is routed to the plant vent/purge header interface in Area A400 and leaves the system boundary as vent/purge gas to battery limits for offsite handling (no on-site flare combustion is modelled). Make-up hydrogen enters at battery limits as HTU make-up hydrogen (Stream 206) and HCU make-up hydrogen (Stream 306).

Stabiliser overheads and PSA tail gas join the plant-wide fuel-gas header that supplies furnace duty in Area A100. Surplus fuel gas beyond internal firing demand is treated as exported byproduct fuel gas

at battery limits (Stream 423). Aqueous phases generated by heteroatom removal are routed to the sour-water stripper in Area A400 for stripping and discharge as stripped water discharge (Stream 411).

5.4.3. Area A200 Hydrotreating Design Basis (HTU)

The HTU stabilises the pyrolysis liquid matrix and reduces impurity loads that govern downstream operability. In the TEA-oriented model, this unit function is captured through outcome-based indicators that represent (i) saturation of reactive unsaturates and (ii) conversion of heteroatom- and halogen-containing species into separable products (H_2S, NH_3, HCl, H_2O, CO and CO_2). The magnitude of impurity conversion reported in hydrotreating literature motivates the severity level required for compatibility-oriented upgrading. For example, Sun and Yoon report large reductions in whole-oil nitrogen and chlorine during hydrotreatment of waste plastic pyrolysis oil over sulfided NiMo/γ-Al_2O_3 at 350 °C [106].

The design basis adopted here is also consistent with the impurity burden measured for the DKR 350-derived pyrolysis oil used as feed in this thesis (Table 5.5). This profile implies that hydrotreating must remove heteroatoms and halogens to mitigate corrosion and catalyst disruption and stabilise the olefin-rich fraction indicated by Table 5.4. These outcomes determine hydrogen demand and the generation of sour gas and sour water streams that must be handled by the shared systems in Area A400.

Table 5.7: HTU severity parameters implemented for the two upgrading pathways. Values are direct steady-state model inputs and are documented in the spreadsheet model.

Parameter	Naphtha	Jet-fuel	Anchor
Olefin saturation fraction, $f_{O,\mathrm{sat}}$	0.983	0.980	A1
Aromatic saturation fraction, $f_{A,\mathrm{sat}}$	0.240	0.146	A2
Sulfur removal fraction, $f_{S,\mathrm{rem}}$	0.830	0.869	A3
Nitrogen removal fraction, $f_{N,\mathrm{rem}}$	0.962	0.973	A4
Chlorine removal fraction, $f_{Cl,\mathrm{rem}}$	0.977	0.977	FIX
Oxygen removal fraction, $f_{O,\mathrm{rem}}$	1.000	0.667	A5
Hydrogenated-olefin mapping, $\alpha_{O\to I}$	0.614	0.614	A6
Hydrogenated-olefin mapping, $\alpha_{O\to P}$	0.386	0.386	A6
O fate to H_2O/CO/CO_2	1/0/0	1/0/0	CC

Anchor key:
A1 Sun & Yoon (olefin drop) and Luo (near-zero olefins plausibility) [106], [107].
A2 Sun & Yoon (^{13}C NMR proxy) and Sajdak (aromatics example) [106], [111].
A3 Lim (sulfur reduction proxy) and Sajdak (later-stage example) [111], [123].
A4 Sun & Yoon (whole-oil N) and Sajdak (example) [106], [111].
A5 Sun & Yoon (oxygenates proxy) and Sajdak (CHNSO by-difference) [106], [111].
A6 Kim (paraffin split template) [110].
FIX Fixed assumption for both pathways; Sun & Yoon as plausibility anchor [106].
CC Fixed closure convention documented in the spreadsheet model.
Note: The oxygen-fate entry is a closure convention used to allocate removed oxygen among reaction water and light-gas products. It primarily affects aqueous and light-gas generation and the associated hydrogen balance; it is stated explicitly to preserve traceability.

5.4.4. Area A300 Hydrocracking and Fractionation Design Basis (HCU)

The HCU provides the primary boiling-range reshaping step and governs the final product slate. In the present system, the HCU is coupled to a heavy recycle loop that stabilises reactor feed quality and provides a control handle on heavy-tail behaviour. A small heavy purge is applied in both pathways to prevent accumulation of refractory material and to preserve steady-state realism.

The need for reshaping follows directly from the properties of the DKR 350-derived pyrolysis oil described in Section 5.3: the oil spans a wide boiling range and retains a non-trivial heavy fraction. Hydrocracking therefore acts as the main design handle for reducing that heavy fraction and redistributing carbon toward the pathway-defined liquid products. Within the shared upgrading topology, the pathways differ not by reactor presence or flowsheet architecture, but by the extent to which heavy material is cracked and by how the resulting liquid pool is partitioned in final fractionation. At process level, this difference is expressed most clearly in the final fractionator FD 340: the naphtha pathway targets maximal recovery of the naphtha product (Stream 340), whereas the jet-fuel pathway retains

more middle-distillate material and applies an additional cut to recover the jet-fuel-range blendstock (Stream 344), with naphtha treated as co-product in the later economic interpretation. Although the jet-fuel pathway represents a stricter outlet intent, the present design basis does not assume that pathway differentiation must translate into disproportionately larger make-up hydrogen demand; instead, the principal design distinction is implemented through heavy-pool conversion and cut logic under one shared topology.

Table 5.8: HCU severity parameters and fractionation logic implemented for the two upgrading pathways. Values are direct steady-state design-basis inputs and are traceable to the spreadsheet model and appendix documentation.

Parameter or logic item	Naphtha	Jet-fuel	Anchor
Cracking severity, S_{crack}	0.867	0.636	B1
Gas make fraction, f_{gas} (per cracked mass)	0.10	0.10	FIX
Cracked-liquid LN share	0.653	0.348	B2
Cracked-gas composition split	fixed (SS)	fixed (SS)	B3
Fractionation products	naphtha + heavy	naphtha + kerosene + heavy	DEF
Heavy handling	recycle + purge	recycle + purge	SYN

Anchor key:
B1 Lim Table 4 (Case 3 vs Case 2 via heavy-pool mapping) [123].
B2 Lim Table 4: LN/(LN+HN) for selected cases [123].
B3 Palos indicates predominantly paraffinic C_1–C_4 cracked-gas identity [109].
FIX Fixed steady-state assumption implemented in the spreadsheet model; explicit composition values and workbook traceability are provided in Appendix A. The fixed cracked-gas split is used consistently across pathways and checked qualitatively against the trends reported by Palos [109].
DEF Pathway definition in subsection 5.4.1.
SYN Process synthesis logic.
Interpretation: The naphtha pathway applies higher heavy-pool conversion to maximise naphtha recovery, whereas the jet-fuel pathway retains more middle-distillate material to enable kerosene-range cut recovery through fractionation logic. Pathway differentiation in A300 should therefore be read primarily as a product-reshaping and cut-recovery choice within a shared topology, not as a fundamentally different upgrading train.

5.4.5. Consolidated Upgrading Parameter Set and Modelling Handover

Tables 5.7 and 5.8 provide the compact pathway definitions required for traceability between specification intent, design basis, and steady-state model implementation. For clarity of handover to the modelling framework in Chapter 6, Table 5.9 consolidates the HTU and HCU severity parameters used as direct model inputs for both pathways.

Table 5.9: Consolidated HTU and HCU severity parameter set used as direct steady-state model inputs for both pathways.

Parameter (symbol and meaning)	Naphtha	Jet-fuel
HTU severity parameters		
$f_{O,\mathrm{sat}}$ (olefin saturation fraction)	0.983	0.980
$f_{A,\mathrm{sat}}$ (aromatic saturation fraction)	0.240	0.146
$f_{S,\mathrm{rem}}$ (sulfur removal fraction)	0.830	0.869
$f_{N,\mathrm{rem}}$ (nitrogen removal fraction)	0.962	0.973
$f_{Cl,\mathrm{rem}}$ (chlorine removal fraction)	0.977	0.977
$f_{O,\mathrm{rem}}$ (oxygen removal fraction)	1.000	0.667
$\alpha_{O\to I}$ (hydrogenated-olefin mapping to isoparaffins)	0.614	0.614
$\alpha_{O\to P}$ (hydrogenated-olefin mapping to n-paraffins)	0.386	0.386
O fate to H_2O/CO/CO_2 (closure split)	1/0/0	1/0/0
HCU severity parameters		
S_{crack} (cracking severity)	0.867	0.636
f_{gas} (gas make fraction per cracked mass)	0.10	0.10
Cracked-liquid LN share (light-naphtha share of cracked liquid)	0.653	0.348

Note: Detailed definitions, anchors, and fractionation logic are provided in Tables 5.7 and 5.8. This table consolidates the final scalar inputs used for model handover to Chapter 6.

5.5. Utilities and Energy Integration

The utilities block (Area A400) provides the thermal, electrical, and cooling services that enable continuous operation of the pyrolysis and upgrading blocks defined in Areas A100–A300. These supporting functions determine how internal energy contained in non-condensable gases and char is converted into useful process heat and how the temperature, pressure, and circulation requirements of upgrading reactors and separation units are maintained.

Hydrogen is handled differently from conventional utilities: although some hydrogen-related handling functions interface with Area A400 boundary systems, the hydrogen purification and recycle interface (amine treating, PSA, H_2 collector, and recycle splits) is treated as part of the upgrading system associated with Area A200 and coupled to Area A300 via HCU high-pressure separator return gas (Stream 321).

5.5.1. Heat Supply and Furnace Integration

Heat required in the pyrolysis block and selected preheaters in the upgrading block is supplied by on-site firing. The furnace uses internal fuels generated in Area A100, primarily non-condensable gases and, to a lesser extent, char withdrawn with bed material. When internal fuels are insufficient to meet overall heat demand, additional firing draws from the plant fuel-gas header. On-site combustion produces flue gas (Stream 150) that leaves the system boundary after heat recovery. This combustion interface underpins the “direct on-site combustion only” CO_2 scope used later in the thesis.

5.5.2. Fuel-Gas Management, Export, and Unmodelled Valorisation Options

The integrated plant generates fuel gas beyond that required for internal firing under many operating conditions. In this thesis, surplus is treated as exported byproduct fuel gas at battery limits (Stream 423) and monetised as an energy credit in Chapter 7 on an LHV basis. Alternative valorisation options exist in practice, including CHP/steam-turbine power generation, district heat export, electricity export, or steam export. These options are not modelled in the baseline because they require additional site-specific design choices (power island configuration, export infrastructure, operating regimes) that fall outside the screening scope of this work; their potential impact is instead captured indirectly through the fuel-gas credit treatment and discussed as an opportunity/limitation alongside sensitivity results in Chapter 8.

This boundary split is important for the later techno-economic interpretation. Exported byproduct fuel gas at battery limits (Stream 423) is treated in Chapter 7 as the monetisable plant-gas export, whereas vent/purge gas to battery limits and stripped water discharge are treated as boundary handling or treatment loads rather than as saleable products. In other words, the baseline design distinguishes clearly between technically generated plant-gas value and non-saleable boundary discharges whose costs remain visible in the later economic accounting.

5.5.3. Electricity Demand

Electrical power supports material handling, compression, pumping, and cooling throughout the integrated facility. In Area A100, electrical demand arises primarily from feeding and from circulation and cooling systems associated with condensation. In Areas A200–A300, additional electrical requirements arise from hydrogen circulation, liquid pumping, and cooling duties connected to stabilisation, fractionation, and reactor-effluent heat removal. Across the facility, cooling-water pumps form a substantial share of the steady electrical load.

5.5.4. Hydrogen Circulation and Recycle Management

Hydrogen is a process reactant required for heteroatom removal, olefin saturation, and molecular reshaping in the HTU and HCU. Reactor effluent vapours are conditioned via amine treating and a PSA associated with the upgrading interface in Area A200. The PSA feed header combines the sweet

gas from A200 as sweet gas to PSA feed (Stream 230) with HCU high-pressure separator return gas (Stream 321). Recovered hydrogen is redistributed as HTU recycle hydrogen (Stream 205) and HCU recycle hydrogen (Stream 305). A controlled purge from the H_2 collector as H_2 purge (Stream 233) is routed to the plant vent/purge header interface in Area A400 and leaves the boundary as vent/purge gas to battery limits for offsite handling; no on-site flare combustion is modelled. Make-up hydrogen enters at battery limits as HTU make-up hydrogen (Stream 206) and HCU make-up hydrogen (Stream 306).

5.5.5. Cooling and Condensation Utilities

Cooling duties arise across the pyrolysis and upgrading blocks and are provided by a combination of cooling-water loops and air-cooled heat exchangers within Area A400. In Area A100, cooling condenses hot vapours leaving the reactor after solids removal. In Areas A200–A300, cooling prepares reactor effluents for separation and conditions recycle-gas streams for compression and PSA feed. No chilled-water service is assumed because none of the process steps downstream of condensation operate at sub-ambient conditions.

5.6. Integrated Flowsheet and Process Synthesis

This section provides an integrated overview of the flowsheet that forms the structural basis of the steady-state model presented in Chapter 6. The four process areas A100 to A400 are arranged into a single integrated system that converts a DKR 350 feed into liquid hydrocarbon products while supplying much of its thermal and hydrogen requirements through internal recycles. The narrative below describes the structure and connectivity of each area and highlights the recycles that couple them. At this point in the chapter, the reader has already seen the design-basis choices that motivate the integrated structure (feedstock, A100 configuration/yields, upgrading severities/cut logic, and A400 shared systems).

5.6.1. Area A100 Pyrolysis

Area A100 receives the plastic feed and converts it into condensable vapours, non-condensable gases, and solid residue. The core of the block is the circulating fluidised-bed reactor R 110, which operates at fixed temperature and pressure and is fluidised by recycled non-condensable gas. Plastic feed (Stream 101) contacts recycled gas and hot circulating bed material supplied from the furnace. Together, these streams establish the reaction environment, supply the required heat, and generate the reactor effluent represented in the integrated flowsheet.

The reactor effluent first passes through primary solids removal to separate char and inerts from the vapour-rich stream. The vapour-rich fraction is then condensed to produce the liquid pyrolysis-oil stream that leaves A100 toward upgrading. The remaining net gas is split between internal recycle, furnace use, and transfer to the plant fuel-gas header. In structural terms, A100 therefore determines three plant-wide burdens at once: the liquid feed to upgrading, the available internal fuel-gas pool, and the solids/residue load that must be handled at boundary.

5.6.2. Area A200 Hydrotreating

Area A200 receives condensed pyrolysis liquid from A100 and performs stabilisation and impurity removal. The incoming liquid is mixed with hydrogen, preheated, and passed through the HTU reactor, where olefins are saturated and heteroatom-bearing species are converted into separable gas- and water-phase products. Downstream separation produces a stabilised liquid sent forward to A300, while gas and aqueous phases are routed into the plant-wide hydrogen and sour-water systems.

The gas-side interface is central to plant integration. Sweet gas from A200 joins the PSA feed header, where it is processed together with A300 return gas. The aqueous side is likewise important because heteroatom removal in A200 is the main source of sour-water handling demand later closed in A400. In this sense, A200 is not only a liquid-upgrading block but also the principal generator of the gas- and water-side boundary loads associated with impurity removal.

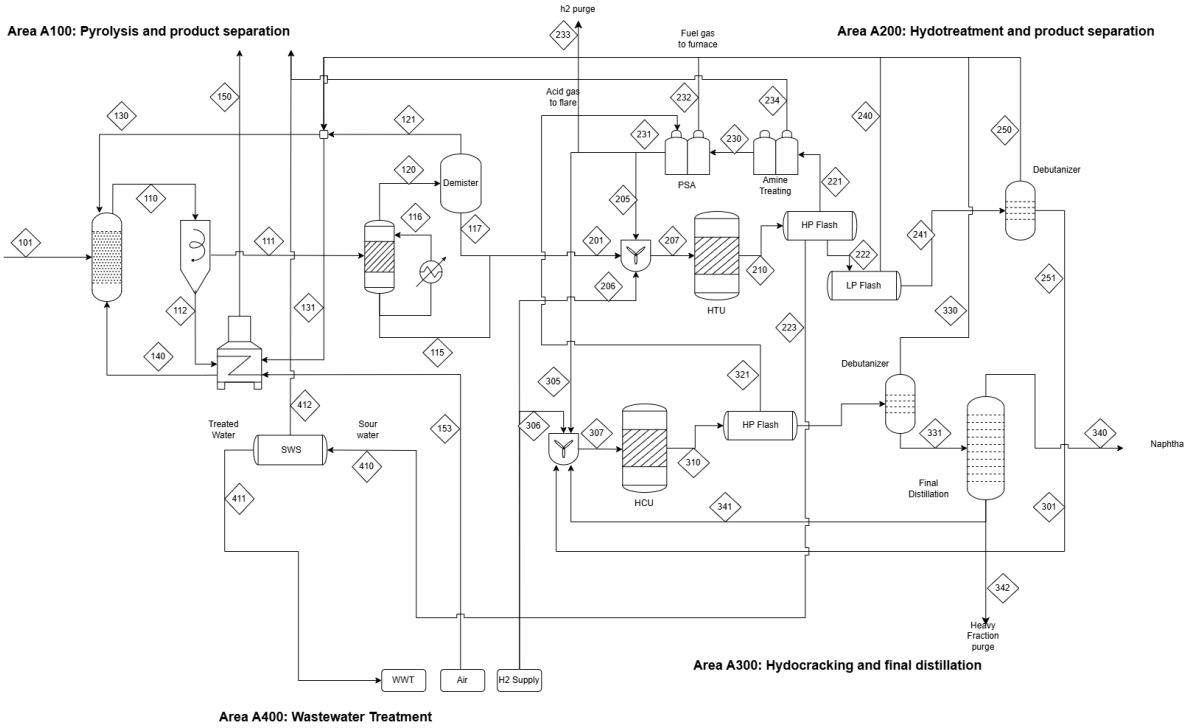

Figure 5.2: Integrated system overview of the gate-to-gate conversion facility (Areas A100–A400). The diagram summarises the main process blocks and their interfaces, including transfer of condensed liquids from A100 to A200, hydrogen recovery and distribution via the A200-centred PSA/H_2 system coupled to A300 via HCU high-pressure separator return gas (Stream 321), fuel-gas collection to the plant-wide header and furnace, and aqueous handling via sour-water stripping. Plant-boundary outlet categories include the liquid products (naphtha product, Stream 340, and for the jet-fuel pathway the jet-fuel-range blendstock, Stream 344), heavy purge (Stream 342), stripped water discharge (Stream 411), flue gas after heat recovery (Stream 150), exported byproduct fuel gas (Stream 423), vent/purge gas to battery limits (flare header outlet), and solid residue (char/inerts/ash) for disposal.

5.6.3. Area A300 Hydrocracking

Area A300 upgrades stabilised liquid from the hydrotreating unit into lighter products through cracking of the heavy fraction. Stabilised liquid to A300 (Stream 251) is pressurised and mixed with the heavy recycle stream and hydrogen. After preheating, the combined feed enters the hydrocracking reactor R 310, where part of the C_{13+} material is cracked into lighter gas and liquid products, consistent with the modelling framework formalised in Chapter 6 (Figure 5.2).

The reactor effluent passes through heat recovery and cooling steps before entering the HCU high-pressure separator V 321, which produces a hydrogen-rich return gas routed back to the PSA feed header and a liquid stream that enters the HCU stabiliser T 330. Light hydrocarbons are removed overhead and routed to the plant fuel-gas header. The stabilised liquid is then distilled in the final fractionator FD 340, which produces naphtha product (Stream 340) and a heavy fraction. The heavy fraction is divided into heavy recycle, which maintains reactor performance, and heavy purge (Stream 342), which prevents accumulation of very heavy material and leaves the system boundary without further upgrading. In the jet-fuel pathway, FD 340 applies an additional cut to produce the jet-fuel-range blendstock (Stream 344) as a second product, with naphtha as co-product.

5.6.4. Area A400 Utilities and Shared Systems

Area A400 provides shared utilities and boundary-handling interfaces that support the process areas. It contains the plant fuel-gas header and export interface, sour-water stripping and wastewater handling, and the plant vent/purge (flare) header interface that together close the gas-side and aqueous-side boundary accounting of the plant.

The plant fuel-gas header FGH 001 receives contributions from the pyrolysis section, the hydrotreating unit, the HCU stabiliser, and PSA tail gas. These gases are mixed and supplied to the furnace in Area A100 as fuel-gas header stream to furnace duty. Surplus fuel gas beyond internal demand is treated as exported byproduct fuel gas at battery limits (Stream 423), consistent with the boundary convention used in Chapter 7. This exported stream is the boundary gas stream later monetised in the base-case TEA.

The plant vent/purge header interface receives H_2 collector purge (Stream 233), acid gas from the amine system (Stream 401), and sour-water stripper overhead (Stream 412). These streams leave the system boundary as vent/purge gas to battery limits for offsite handling; baseline modelling does not include on-site flare combustion or destruction. Together with stripped water discharge (Stream 411) and flue gas from Area A100 (Stream 150), these flows define the environmental and waste/discharge interface of the process within the scope of this thesis. In later economic treatment, these streams are therefore not interpreted as saleable exports, but as part of the boundary handling or treatment burden associated with the fixed system configuration.

5.6.5. Integrated System Implications for Modelling

The four areas A100 to A400 form a single integrated process in which material, energy, and hydrogen move through tightly coupled pathways (Figure 5.2). Two plant-wide couplings dominate the technical behaviour and therefore the modelling approach in Chapter 6: (i) the A200-centred hydrogen loop that couples A200 and A300 via HCU high-pressure separator return gas (Stream 321) and redistributes recycle hydrogen to both reactors as HTU recycle hydrogen (Stream 205) and HCU recycle hydrogen (Stream 305), and (ii) the fuel-gas/heat loop (net gases $\rightarrow$ header $\rightarrow$ furnace and export). Changes in upgrading severity therefore propagate beyond A200/A300 into hydrogen make-up, net utilities, and boundary outlet rates, which are reported as TPMs in Chapter 6 and monetised in Chapter 7.

A second modelling implication is that boundary-stream treatment is fixed at design stage rather than assigned case-by-case later. Exported byproduct fuel gas (Stream 423), vent/purge gas to battery limits, stripped water discharge (Stream 411), heavy purge (Stream 342), and flue gas (Stream 150) are already distinct design-basis outputs here. This preserves consistency between the technical results,

the TEA boundary-credit and waste-handling terms, and the sensitivity analysis of fuel-gas monetisation reported in Chapters 7 and 8.

5.7. Chapter summary and transition to Chapter 6

5.7.1. Answer to Sub-Research Question 1

Sub-Research Question 1: What are the system boundaries, process configurations, and input–output relationships for producing naphtha-range and jet-fuel-range blendstocks from pyrolysis of polyolefin-rich plastic waste?

This chapter answers the question by defining a single, internally consistent gate-to-gate system configuration for a plastic-to-liquids conversion facility spanning A100–A400, expressed as a fixed flowsheet topology with a fixed plant boundary at battery limits. Within this boundary, the system converts pretreated, polyolefin-rich DKR 350 into specification-relevant liquid blendstocks through a sequence of conversion, upgrading, separation, and supporting utilities and handling systems. Two operating pathways are defined on this common configuration. Importantly, the pathways do not represent different plants; they are alternative operating intents applied to the same hardware and boundary accounting rules. The naphtha pathway targets a naphtha-range product slate, while the jet-fuel pathway targets a jet-fuel-range blendstock alongside naphtha-range material. As a result, both pathways recover naphtha product (Stream 340), while the jet-fuel pathway additionally recovers jet-fuel-range blendstock (Stream 344) through pathway-specific upgrading severity and fractionation cut logic.

A key output of the system definition is the set of input–output relationships that are treated consistently across the thesis. The design fixes the principal material interfaces at battery limits, including the plastic feed input, imported utilities and make-up hydrogen, the saleable liquid product streams, and the boundary exports and discharges. In particular, the boundary convention for plant gas and waste handling is established here in a way that remains economically consequential in later chapters. Exported byproduct fuel gas at battery limits (Stream 423) is the monetised boundary export used in the base-case TEA, while vent/purge gas to battery limits and stripped water discharge are treated as separate handling/treatment loads rather than as saleable outputs. By locking this convention at the design stage, later comparisons between pathways remain traceable to pathway intent rather than to changing accounting treatment at the boundary.

5.7.2. Handover to Chapters 6--8

Chapter 5 fixes the design basis that is held constant in the steady-state modelling and techno-economic phases, including the plant boundary and accounting conventions at battery limits, the common throughput basis, the feedstock specification and pretreatment framing, the A100 yield basis that anchors conversion performance, and the pathway definitions expressed through A200/A300 severity parameters and fractionation cut logic. On this fixed basis, Chapter 6 implements Phase 2 by translating the conceptual configuration into converged steady-state mass and energy balances for both pathways. Chapter 7 then implements Phase 3 by monetising the resulting plant-boundary quantities under a consistent DCF basis and MSP closure convention, and Chapter 8 implements Phase 4 by testing how strongly the resulting MSP outcomes depend on a limited set of high-leverage assumptions.

The principal function of the present chapter is therefore to lock the study basis before technical and economic interpretation begins. Read together with the revised methodology in Chapter 4, the chapter establishes that later pathway differences should be interpreted against one shared reference system: the pathways differ by downstream upgrading severity and product-recovery intent, not by a changing plant boundary or a different overall process architecture.

6

Technical Assessment

Building on the system definition and upgrading intent established in Chapter 5, this chapter quantifies the steady-state technical performance of the integrated A100–A400 configuration. Whereas Chapter 5 defined the conceptual design choices, including the plant boundary, feedstock context, and pathway-specific upgrading intent, the purpose here is to translate that design into a coherent set of mass, energy, utility, and boundary-stream indicators. These indicators characterise the technical behaviour of the conversion system across Areas A100–A400 and provide the quantitative handover inputs required for the TEA in Chapter 7.

This chapter implements *Phase 2* of the research framework introduced in Chapter 4 and addresses *Sub-Research Question 2* by converting the Phase 1 system definition into converged steady-state mass, energy, utility, and boundary-stream indicators for both pathways. Consistent with Chapter 5, two pathways are evaluated: (i) the *naphtha pathway* and (ii) the *jet-fuel pathway*, in which a jet-fuel-range fraction is recovered as an additional saleable cut. Both pathways share the same gate-to-gate boundary definition and plastic throughput basis. Differences in outcomes are therefore interpreted as consequences of downstream upgrading and product recovery objectives (severity and cut definition) rather than changes in feed rate. To keep the technical narrative aligned with the fixed-system logic established in Chapter 5, results are first introduced area by area and only then consolidated at plant level. This ordering is intentional: it allows the reader to see where pathway differences arise within the shared flowsheet before encountering the overall comparison and TPM summary.

6.1. Reporting basis and operating cases

The technical assessment is performed on the gate-to-gate boundary defined in Chapter 5, spanning from the arrival of the pretreated, polyolefin-rich plastic feed (Stream 101) to the export of saleable liquid products and the discharge of residual boundary streams. The upstream feed context and specification assumptions follow the DKR 350-derived basis described in Chapter 5, while the system topology and upgrading design bases are consistent with section 5.4 and subsection 5.4.2. Steady-state results are reported as absolute flowrates and duties, and as intensities normalised to the plastic feed rate (Stream 101), to support comparison between pathways and direct transfer into the economic accounting of Chapter 7.

Two gas outlets at battery limits are distinguished in this chapter. First, Stream 423 is treated as exported byproduct fuel gas at the battery limits under the baseline steady-state convention. Second, a combined vent/purge gas routed to the flare header is treated as leaving the system boundary at battery limits for offsite handling. The flare system is therefore represented as a continuous vent/purge routing header in the steady-state accounting; no flare combustion is modelled and no flare CO_2 calculations

Table 6.1: Reporting basis and normalisation (common to both pathways).

Metric	Naphtha pathway	Jet-fuel pathway
Annual plastic throughput [t/y]	40 000	40 000
Annual operating hours [h/y]	8 000	8 000
Steady-state plastic feed rate, Stream 101 [kg/h]	5 000	5 000
Normalisation denominator [kg/h]	5 000	5 000

are claimed within the gate-to-gate boundary.

CO_2 may appear as a component in process gas streams, including exported fuel gas and vent/purge gas. In this chapter, CO_2 is reported as an emission metric only insofar as it represents direct on-site combustion sources that are explicitly modelled within the gate-to-gate boundary. CO_2 present in exported or vented gas streams is not treated as an emitted combustion product within the system boundary. This convention is consistent with the battery-limits treatment fixed in Chapter 5 and is important for interpreting later differences in reported direct CO_2 between pathways: only explicitly modelled on-site combustion is included here.

The two pathways are defined as follows:

- *Naphtha pathway:* the upgraded liquid product is recovered as a single naphtha-range product stream (Stream 340), consistent with a naphtha-oriented product slate (subsection 5.4.1).
- *Jet-fuel pathway:* the upgraded liquid is separated into a naphtha-range product stream (Stream 340) and a jet-range product stream (Stream 344), reflecting the co-product intent described in subsection 5.4.1.

These pathways should be read as alternative outlet intents applied to one shared plant configuration rather than as separate plant designs. As the pathway definition primarily affects downstream product recovery and separation objectives, the A100 conversion section is held constant across both cases. Differences between pathways therefore arise predominantly within A200–A300 and propagate to plant-wide utilities and boundary streams aggregated in A400. The role of the present chapter is to quantify those differences on a common throughput and boundary basis before they are later monetised in Chapter 7.

6.2. Steady-state modelling representation and reporting conventions

The results reported in this chapter are generated from a steady-state, spreadsheet-based representation of the A100–A400 flowsheet consistent with the system definition of Chapter 5 and the research-method framing of Chapter 4. Unit operations are represented at screening level using aggregate (black-box) transformations and split assumptions that preserve internal mass consistency across the integrated plant boundary. A single stream numbering and boundary convention is applied throughout Chapters 6–8, such that plant-boundary quantities reported here correspond directly to the technical inputs monetised in Chapter 7. Both pathways share the same flowsheet topology and boundary definition; differences arise only through the downstream upgrading and product-recovery intent (severity and cut definition), while A100 conversion is held constant by construction.

The integrated plant contains recycle interactions, most notably in the hydrogen system and in heavy-end management, and only converged steady-state solutions are reported. Closure indicators in section 6.3 provide an internal consistency check that the plant-level totals are supported by numerically stable area-level balances. These checks confirm algebraic consistency within the adopted bookkeeping framework, but they should not be interpreted as proof of rigorous thermodynamic equilibrium representation, catalyst-ageing behaviour, or dynamic operability. In this sense, the present chapter reports auditable plant-boundary outcomes required for interpretation and economic handover, rather than a

Table 6.2: Model quality and closure indicators for the converged steady-state cases.

Closure indicator	Naphtha pathway [%]	Jet-fuel pathway [%]
A100 boundary mass closure residual/error	≈ 0	≈ 0
A200 relative closure residual/error	0.235	0.364
A300 relative closure residual/error	-0.096	-0.071
A400 relative closure residual/error	≈ 0	≈ 0

detailed design simulation of individual equipment behaviour.

To keep the technical narrative aligned with the fixed-system logic established in Chapter 5, the results are first introduced area by area (A100–A400) and only then consolidated at plant level. This ordering is intentional. It allows the reader to see where pathway differences arise within the shared flowsheet before encountering the overall comparison tables and TPM summary. In particular, because A100 conversion is held constant by construction, the area-level discussion clarifies that the most important pathway differences emerge primarily in downstream upgrading, product recovery, and integrated utility handling rather than in the front-end conversion basis itself.

6.3. Steady-state closure and numerical consistency checks

Only converged steady-state solutions are reported. As a consistency check, Table 6.2 summarises the area-level closure indicators for the two pathways. In this screening-level black-box model, closure residuals are treated as acceptable when they are below approximately 0.5% and do not show systematic bias between pathways. These checks confirm algebraic mass consistency within the adopted modelling framework; they do not imply rigorous thermodynamic equilibrium representation or dynamic operability validation.

These residuals are small relative to the dominant 5,000 kg/h plastic feed basis used for reporting and indicate that the reported pathway differences are not driven by numerical imbalance. However, numerical closure does not by itself indicate how strongly the underlying assumptions are supported by empirical evidence.

The closure indicators in Table 6.2 confirm algebraic consistency within the adopted screening-level bookkeeping framework, but closure alone does not communicate the strength of the evidence base underlying the black-box transformations and aggregation choices used to generate the reported plant-boundary indicators. Therefore, the technical model is also assessed using the pedigree analysis framework introduced in subsection 4.3.2. Consolidated technical pedigree results for both pathways are reported in Appendix Appendix B, including mean scores and reviewer deviation (agreement indicator) across the four criteria (proxy, empirical basis, theoretical understanding, and methodological rigour).

The technical pedigree outcomes are most supportive of the fixed process-design and overall plant-boundary bookkeeping elements inherited from Chapters 5 and 6. This supports relatively strong interpretation of the plant-boundary outlet structure, the shared A100–A400 topology, and the conclusion that pathway differentiation is concentrated downstream rather than in the common front-end conversion basis. In practical terms, the strongest technical claim in this thesis is therefore not that every aggregated duty or unit-level burden is mechanistically resolved, but that the pathway comparison is internally coherent at plant boundary and that the headline technical differences are not artefacts of numerical imbalance.

6.4. Area A100 results: pyrolysis and fired heat coupling

As defined in Chapter 5, Area A100 performs the thermal conversion of the polyolefin-rich plastic feed into a condensable liquid fraction, a non-condensable gas (NCG) fraction, and solid residues. The condensed liquid stream provides the primary feed to upgrading (A200), while the NCG fraction interfaces

Table 6.3: Area A100 mass results (pyrolysis yields and key streams).

Metric	Naphtha pathway	Jet-fuel pathway
Inputs to Area A100		
Plastic feed to pyrolysis, Stream 101 [kg/h]	5 000.00	5 000.00
Outputs from Area A100 (to downstream / boundary handling)		
Condensed liquid to upgrading, Stream 201 [kg/h]	3 106.66	3 106.66
NCG export to fuel gas system, Stream 131 [kg/h]	1 236.40	1 236.40
Char/solids production [kg/h]	260.00	260.00
Inerts/solids withdrawal [kg/h]	345.00	345.00

Table 6.4: Area A100 energy and utility indicators (condenser duty, fuel gas routing, and net fuel-gas surplus).

Metric	Naphtha pathway	Jet-fuel pathway
Thermal duties (energy indicators)		
A100 condenser duty [kW]	562.62	562.62
Pyrolysis reactor heat duty [kW]	3 263.89	3 263.89
Cooling utility requirement		
Cooling water flow (condenser) [kg/h]	48 454.91	48 454.91
Fuel gas routing (mass flow indicators)		
Fuel gas header total flow, Stream 420 [kg/h]	1 586.41	1 578.47
Fuel gas to furnace, Stream 421 [kg/h]	192.92	192.55
Fuel gas export (byproduct), Stream 423 [kg/h]	1 393.49	1 385.93
External fuel import [kg/h]	0.00	0.00
Fuel gas quality and net surplus (energy basis)		
Fuel gas mixture LHV [MJ/kg]	48.34	48.43
Net fuel-gas surplus (exportable) [MJ/h]	67 362.52	67 126.28

with the plant fuel-gas system and thereby couples conversion to fired heat supply. Solid residues are withdrawn at the plant boundary and form part of the disposal accounting.

6.4.1. Mass results

6.4.2. Energy and utilities results

For consistency with the plant-level reporting, condenser and reactor duties are expressed in kW. Fuel gas availability is summarised via the header flowrates and LHV. The net fuel-gas surplus is reported as an energy rate (MJ/h), representing the excess internally available fuel-gas energy after meeting the furnace duty associated with the pyrolysis heat requirement.

A100 is identical across pathways by construction. It converts 5,000 kg/h of plastic feed into 3,106.66 kg/h of condensed liquid forwarded to upgrading (Stream 201) and produces 1,236.40 kg/h of NCG routed into the fuel-gas system (Stream 131), alongside solid residues withdrawn at the boundary (Table 6.3). These fixed conversion outputs mean that pathway-to-pathway differences observed later in the chapter cannot originate in the pyrolysis yield structure itself, but must arise from downstream upgrading, separation, and recycle interactions.

On the energy side, the furnace duty is met by a small fraction of the fuel gas header flow (Stream 421), while most of the header is exported at battery limits as exported byproduct fuel gas (Stream 423) (Table 6.4). The large net fuel-gas surplus indicates that the integrated plant is energy-self-sufficient for fired heat under the adopted coupling, with an exportable byproduct stream that later becomes an economic credit in Chapter 7. The small difference in fuel gas header total and export between pathways is therefore not an A100 effect. Rather, it is consistent with additional gas contributions entering the header from the upgrading block, notably PSA tail gas and stabiliser offgas routing, while the pyrolysis front end itself remains fixed.

Table 6.5: Area A200 mass results (stabilised liquid, water and gas interfaces).

Metric	Naphtha pathway	Jet-fuel pathway
Inputs to Area A200		
Feed to A200, Stream 201 [kg/h]	3 106.66	3 106.66
Outputs from Area A200 (to downstream / headers / boundary)		
Stabilised liquid to A300, Stream 251 [kg/h]	3 007.38	3 005.52
Sour water to SWS, Stream 223 [kg/h]	40.62	35.41
Acid gas to vent/purge system (via flare header), Stream 401 [kg/h]	0.186	0.195
Sweet gas to PSA feed, Stream 230 [kg/h]	266.17	273.48
A200 gas export to fuel gas system (240+250+232) [kg/h]	337.92	329.94
Stabiliser overhead to fuel gas header, Stream 250 [kg/h]	5.35	5.35

Table 6.6: Hydrogen recovery and purge indicators (PSA and header interface).

Metric	Naphtha pathway	Jet-fuel pathway
Inputs to hydrogen loop / PSA		
HTU make-up H_2 to loop, Stream 206 [kg/h]	0.00	0.00
Outputs from PSA / loop (to headers / purge)		
PSA H_2 product to header, Stream 231 [kg/h]	494.81	506.26
PSA tail gas to fuel gas header, Stream 232 [kg/h]	308.58	300.18
H_2 purge from header, Stream 233 [kg/h]	2.47	2.53
Performance indicators		
PSA H_2 recovery [-]	0.85	0.85
H_2 purge fraction [-]	0.00498	0.00498

6.5. Area A200 results: hydrotreating and treating systems

As defined in Chapter 5, Area A200 stabilises and treats the condensed pyrolysis liquid prior to the main upgrading and fractionation section (A300). It produces the stabilised liquid feed to A300 (Stream 251), removes an aqueous phase routed to sour water stripping (Stream 223), and manages gas-phase impurities via an acid-gas interface (Stream 401). In parallel, A200 interfaces with hydrogen recovery through sweet gas to PSA feed (Stream 230), produces a high-purity hydrogen stream to the recycle header (Stream 231), and exports PSA tail gas to the plant fuel-gas header (Stream 232).

6.5.1. Mass results

6.5.2. Hydrogen loop indicators (A200/PSA interface)

6.5.3. Energy and utilities results

A200 delivers a stable liquid handover to A300, with stabilised liquid to A300 (Stream 251) remaining approximately 3.0 t/h in both pathways (Table 6.5). This indicates that pathway differentiation is not implemented by materially changing the overall liquid throughput through the hydrotreating and stabilisation block, but instead by downstream recovery and severity choices. The stabiliser overhead to the fuel gas header (Stream 250) is identical across pathways, reinforcing that the most visible pathway differences in A200 arise through gas and aqueous interface behaviour rather than through gross stabilised liquid yield.

Table 6.7: Area A200 energy and utility indicators.

Metric	Naphtha pathway	Jet-fuel pathway
A200 total cooling duty [kW]	807.97	681.41
A200 stabiliser reboiler duty [kW]	1 137.91	1 137.28
A200 net heating duty (to utilities) [kW]	1 137.99	1 137.36

The pathway-specific differences in the PSA interface provide a useful diagnostic of how upgrading intent propagates into the hydrogen recovery system. The jet-fuel pathway routes slightly more sweet gas to PSA feed (Stream 230) and produces a higher PSA hydrogen product rate (Stream 231), while the PSA tail gas routed to the fuel gas header (Stream 232) is slightly lower, with PSA recovery held constant (Table 6.6). In the adopted screening representation, this combination is consistent with a modest shift in the flow and composition of the treated gas stream entering the PSA header, driven by pathway-dependent gas formation and routing in the upgrading and separation system. Operationally, such a shift can occur when downstream severity and product recovery logic change the amount of light gases and hydrogen-rich recycle gas entering the treating and recovery network, even if the net external hydrogen requirement remains similar at plant level.

Differences in aqueous streams show a comparable pattern. The jet-fuel pathway produces a lower sour-water flow to stripping (Stream 223) and a lower stripped water discharge at plant level (Table 6.5 and, later, Table 6.11). Within the screening model, sour water generation reflects the combined outcome of separator phase-split assumptions and impurity-handling bookkeeping, including allocation of treated species and condensed water to an aqueous phase. Small pathway-to-pathway differences can therefore arise when the upgrading intent changes the distribution of gases and light ends through separation and treating, which in turn affects how much material is assigned to the aqueous stream. This should be interpreted as a pathway-driven shift in separation and routing behaviour within the adopted representation rather than as a direct mechanistic statement about water chemistry.

The A200 utility profile supports this interpretation. Heating duties, dominated by stabiliser reboiler duty, are essentially unchanged, while cooling duty is lower in the jet-fuel pathway (Table 6.7). A plausible engineering explanation is that pathway-dependent shifts in gas and light-end routing alter the cooling load associated with condensing and stabilising light components, even when reboiler duty is fixed by the chosen stabilisation representation. For Chapter 7, A200 therefore contributes to variable operating costs through purchased utilities and through its role in shaping the hydrogen recovery and fuel-gas systems, which later influence plant-wide fuel-gas export and purge behaviour.

6.6. Area A300 results: upgrading, fractionation, purge and products

Area role and interfaces

As defined in Chapter 5, Area A300 is the primary upgrading and product recovery section of the integrated plant. It receives stabilised liquid from A200, performs upgrading and separation, and exports saleable liquid products at the battery limits. The key distinction between pathways is implemented in A300 through the product recovery objective: either a single naphtha-range product (naphtha pathway) or a split into naphtha and jet-range fractions (jet-fuel pathway). In both cases, a small heavy purge stream is maintained to avoid accumulation of refractory heavy material in the heavy-end management structure.

6.6.1. Products and purge (mass results)

6.6.2. Energy and utilities results

A300 implements the pathway-specific product recovery objective and is therefore the principal source of differences in the saleable liquid slate. The naphtha pathway recovers the saleable pool entirely as naphtha product (Stream 340), whereas the jet-fuel pathway recovers an additional jet-range blendstock (Stream 344) at the expense of the naphtha fraction while maintaining a comparable overall saleable liquid yield on a plastic-feed basis (Table 6.8). Under the adopted intent framing, this indicates that the pathway change is primarily a product redistribution and recovery shift within a shared conversion basis rather than an overall yield expansion.

The heavy purge remains small relative to the saleable products, but it is technically meaningful be-

Table 6.8: Area A300 product slate and purge stream (mass results).

Metric	Naphtha pathway	Jet-fuel pathway
Saleable products and purge (outputs from Area A300)		
Naphtha product, Stream 340 [kg/h]	2 808.00	1 900.00
Jet-range product, Stream 344 [kg/h]	0.00	916.11
Heavy purge, Stream 342 [kg/h]	5.86	6.46
Aggregates (reporting)		
Total saleable liquid products [kg/h]	2 807.73	2 816.11
Total saleable liquid yield [kg/kg feed]	0.5615	0.5632

Table 6.9: Area A300 aggregated energy and utility indicators.

Metric	Naphtha pathway	Jet-fuel pathway
A300 total cooling duty (aggregated) [kW]	1 965.12	1 851.72
A300 total heating duty (aggregated) [kW]	1 750.92	1 452.73

cause it represents deliberate withdrawal to stabilise the heavy-end management structure and prevent accumulation of refractory material. The slightly higher heavy purge rate in the jet-fuel pathway is consistent with the possibility that different cut definitions and upgrading severity settings alter the partitioning of heavy material between recycle and product pools, requiring a marginally different purge to maintain stability in the screening recycle logic.

The aggregated heating and cooling duties in A300 are lower in the jet-fuel pathway (Table 6.9). Since these duties are aggregated at area level, the interpretation is that the chosen jet-fuel-pathway recovery logic shifts the internal separation load such that less total reboiler-equivalent and condenser-equivalent duty is attributed to A300 in the screening representation. This does not imply that the jet-fuel pathway is intrinsically less separation-intensive in a rigorous sense. Rather, it shows that the additional technical burden of recovering a second product cut is not expressed primarily as a dominant increase in A300 thermal duties in the present model. Instead, as the later plant-level synthesis will show, the clearest additional burden appears in aggregated electricity demand and associated auxiliary handling.

6.7. Area A400 results: shared utilities and boundary streams

As defined in Chapter 5, Area A400 aggregates shared utility totals and boundary handling systems, including wastewater handling (sour water stripping discharge), vent/purge routing to battery limits via the flare header, and plant-wide reporting totals. These functions collect contributions from A100–A300 and express them as plant-level discharge and utility indicators at the battery limits.

A400 expresses plant-level utility totals and boundary handling loads at battery limits. The vent/purge stream provides an integrated indicator of gas routed out of the process networks to battery limits for offsite handling, while stripped water discharge (Stream 411) represents the final aqueous effluent

Table 6.10: A400 and plant-wide utilities summary (supporting systems and boundary discharges).

Metric	Naphtha pathway	Jet-fuel pathway
Boundary discharges / exports (outputs from plant)		
Vent/purge gas to battery limits (flare header) [kg/h]	26.05	26.37
Stripped water discharge, Stream 411 [kg/h]	17.23	11.76
Direct CO_2 (on-site combustion only) [kg/h]	1 396.41	1 394.36
Plant-wide utilities (totals)		
Total electricity demand (plant) [kW]	112.40	219.92
Total cooling duty (plant) [kW]	3 335.70	3 095.74
Total steam-type heating duty (plant) [kW]	2 888.91	2 590.09

exported from the plant (Table 6.10). The slightly higher vent/purge flow in the jet-fuel pathway is small relative to the exported fuel-gas byproduct and is interpreted as a minor consequence of the different gas-routing and hydrogen-recovery flows discussed in A200 rather than as a change in purge strategy.

Plant-wide electricity demand increases materially in the jet-fuel pathway, while plant-wide cooling and heating duties decrease modestly (Table 6.10). Because electricity is aggregated, the most defensible interpretation is that the jet-fuel pathway introduces additional auxiliary load associated with separation and routing required to recover and handle an additional product cut, together with the slightly increased PSA handling and hydrogen-recovery load indicated in Table 6.6. The reduction in aggregated thermal duties is consistent with the A200 and A300 duty tables and indicates that the pathway change does not create a dominant increase in reboiler-equivalent or condenser-equivalent duty in the screening representation. This is precisely why the later interpretation should remain at the level of plant function and interfaces rather than be forced into a single-equipment explanation.

The direct CO_2 metric is similar between pathways, which is consistent with A100 being fixed and with furnace duty being governed primarily by the same pyrolysis heat requirement and by internal fuel-gas availability. Under the scope definition of section 6.1, CO_2 in exported fuel gas and vent/purge streams is not treated as an on-site emission, and no flare combustion is modelled. The remaining difference is therefore very small and should not be overinterpreted as evidence of a meaningful pathway-level change in combustion demand.

Taken together, the A100–A400 results show that the pathways share a common front-end conversion basis and diverge primarily through downstream recovery intent and its plant-wide utility consequences. The next sections therefore consolidate these area-level outcomes at plant boundary, so that the net pathway shifts can be read as the integrated consequence of one shared system rather than as isolated section-level differences.

6.8. Plant-level results overview

After the area-level results have been established, Table 6.11 consolidates the principal plant-boundary inlet and outlet streams together with the aggregated utility indicators for each pathway. The purpose of this section is therefore not to introduce the pathway differences for the first time, but to synthesise the area-level findings into a single plant-level technical handover basis for Chapter 7. Read in this position, the overall comparison clarifies the net consequence of the pathway intent after the reader has already seen where the relevant differences arise within A200–A400.

At plant boundary, the most important observation is that total saleable liquid production remains essentially unchanged between pathways, while the saleable liquid pool is redistributed by design from a single naphtha-range product to a split slate that includes an additional jet-fuel-range cut. At the same time, imported hydrogen remains nearly unchanged, whereas electricity demand increases materially in the jet-fuel pathway and plant-wide thermal duties shift more moderately. These consolidated outcomes should therefore be interpreted as the integrated result of downstream upgrading, product recovery, and shared utility interactions within one fixed A100–A400 system, rather than as evidence of a different front-end conversion basis.

In Chapter 7, product flowrates and the exported fuel-gas stream define the monetised output quantities, while imported hydrogen and utilities define the principal variable operating cost drivers; remaining boundary streams define the handling quantities required for consistent battery-limits accounting under the stated gate-to-gate scope. Within these limits, the boundary slate provides the compact technical handover basis for later economic and sensitivity interpretation.

6.9. Technical performance metrics by pathway

To consolidate the main steady-state performance indicators in a format suitable for interpretation and transfer to the TEA, Table 6.12 reports a TPM dashboard by pathway. These TPMs are derived from

Table 6.11: Plant-boundary major process mass slate (plastic + H_2 basis) and aggregated utilities (by pathway).

Boundary metric	Naphtha pathway	Jet-fuel pathway
Inputs to plant (major inlets)		
Plastic feed to plant, Stream 101 [kg/h]	5 000.00	5 000.00
Total imported H_2 to plant (Streams 206 + 306) [kg/h]	112.57	112.67
Saleable products from plant		
Naphtha product from plant, Stream 340 [kg/h]	2 808.00	1 900.00
Jet-range product from plant, Stream 344 [kg/h]	0.00	916.11
Heavy purge from plant, Stream 342 [kg/h]	5.86	6.46
Solids and aqueous outputs (to boundary handling)		
Pyrolysis char/solids to disposal [kg/h]	260.00	260.00
Inerts/solids withdrawal to disposal [kg/h]	345.00	345.00
Stripped water discharge to battery limits, Stream 411 [kg/h]	17.23	11.76
Gas exports and boundary losses (from plant)		
Fuel gas export (byproduct) from plant, Stream 423 [kg/h]	1 393.49	1 385.93
Vent/purge gas to battery limits (flare header) [kg/h]	26.05	26.37
Aggregated utilities (plant total)		
Total cooling duty (plant) [kW]	3 335.70	3 095.74
Total steam-type heating duty (plant) [kW]	2 888.91	2 590.09
Total electricity demand (plant) [kW]	112.40	219.92
Direct emissions metric (scope-defined)		
Direct CO_2 (on-site combustion only) [kg/h]	1 396.41	1 394.36

Notes: This table reports major process mass flows on a plastic + H_2 basis; combustion air and total flue gas flows are excluded from the mass slate. Stream 423 is treated as exported byproduct fuel gas at battery limits and is not combusted within the gate-to-gate boundary. The vent/purge stream routed to the flare header is treated as leaving the boundary at battery limits for off-site handling; no on-site flare combustion is modelled. Direct CO_2 is reported as an on-site combustion metric only; CO_2 present in exported or vented gases is not treated as an emitted combustion product within the system boundary.

the plant-boundary quantities of Table 6.11 using the reporting basis of Table 6.1. Values should be interpreted in the context of each pathway's intended product slate and recovery objective, as defined in subsection 5.4.1.

The TPMs show that the overall saleable liquid yield is comparable between pathways, while the composition of that yield differs by design. Figure 6.1 summarises the most decision-relevant plant-boundary TPMs and shows that the naphtha pathway concentrates the saleable pool into a single naphtha product stream, whereas the jet-fuel pathway distributes the saleable pool between naphtha and jet-range products. At the same time, imported H_2 intensity and net fuel-gas surplus remain nearly unchanged, while electricity demand increases materially in the jet-fuel pathway. This provides a pathway-consistent basis for economic evaluation in which the main difference lies in product distribution and associated revenue structure rather than in total recovered liquid.

Table 6.12: TPM dashboard by pathway.

TPM	Naphtha pathway	Jet-fuel pathway
Naphtha yield [kg/kg feed]	0.5615	0.3800
Jet-range yield [kg/kg feed]	0.0000	0.1832
Total saleable liquid yield [kg/kg feed]	0.5615	0.5632
Heavy purge yield [kg/kg feed]	0.00117	0.00129
Imported H_2 intensity [kg/kg feed]	0.02251	0.02253
Net fuel-gas surplus intensity (exportable) [MJ/kg feed]	13.47	13.43
Electricity intensity [kWh/t feed]	22.48	43.98
Direct CO_2 intensity (on-site combustion only) [kg/kg feed]	0.2793	0.2789
Vent/purge intensity (battery limits) [kg/kg feed]	0.00521	0.00527
Stripped water intensity [kg/kg feed]	0.00345	0.00235

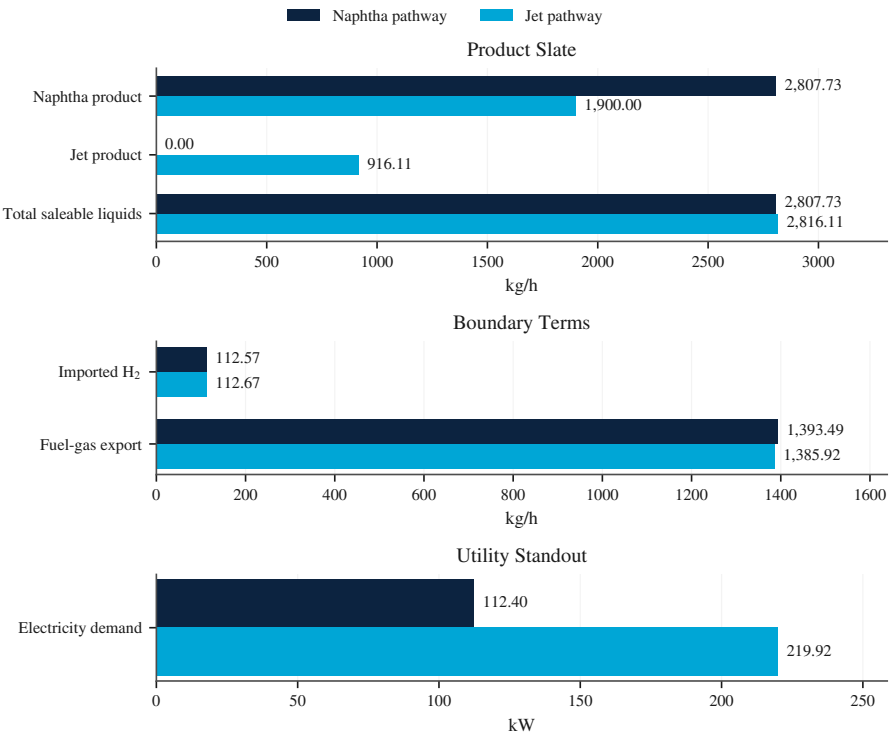

Figure 6.1: Comparative plant-boundary technical performance summary for the naphtha and jet-fuel pathways at the common 40 kt/y, 8,000 h/y basis. The figure highlights the principal Chapter 6 findings: total saleable liquid yield remains nearly unchanged between pathways, the saleable liquid pool is redistributed by design between naphtha-range and jet-range products, imported H_2 remains nearly unchanged, fuel-gas export remains substantial in both pathways, and electricity demand increases materially in the jet-fuel pathway.

The imported hydrogen intensity differs only marginally. Within the screening model and at the selected severities, this indicates that pathway differentiation does not appear as a large change in net external hydrogen requirement. At the same time, A200 results show that internal hydrogen recovery and gas routing through the PSA system differ modestly, which indicates that pathway intent can still alter the internal hydrogen network even when total imported hydrogen remains similar.

Electricity intensity increases materially in the jet-fuel pathway (22.48 versus 43.98 kWh/t feed). The most defensible interpretation is that recovering and handling an additional saleable cut requires additional auxiliary work associated with separation and product routing, and that modest changes in gas handling and hydrogen recovery, specifically PSA feed and product flows, can contribute to increased compression and circulation loads in an integrated plant. Because electricity is aggregated at plant level, this interpretation is stated at the level of system function and interfaces rather than attributed to a single unit. The net fuel-gas surplus intensity remains similar, reinforcing that the pathway shift primarily changes product recovery and auxiliary load rather than the fundamental energy self-sufficiency of the conversion front-end under the adopted fired-heat coupling. To make the relative magnitude and direction of these pathway differences more explicit, Figure 6.2 reports the percentage change in selected plant-boundary indicators for the jet-fuel pathway relative to the naphtha pathway.

6.10. Technical implications of pathway intent

The two pathways serve different end-markets, cracker-relevant naphtha versus jet-fuel-range blendstock, and are not compared as like-for-like products. The side-by-side reporting in this section is therefore used to show how changing the product recovery intent reshapes plant-boundary yields, utilities, and boundary handling loads on a common feed basis, and to clarify which technical quantities are most sensitive to pathway choice within the adopted steady-state representation.

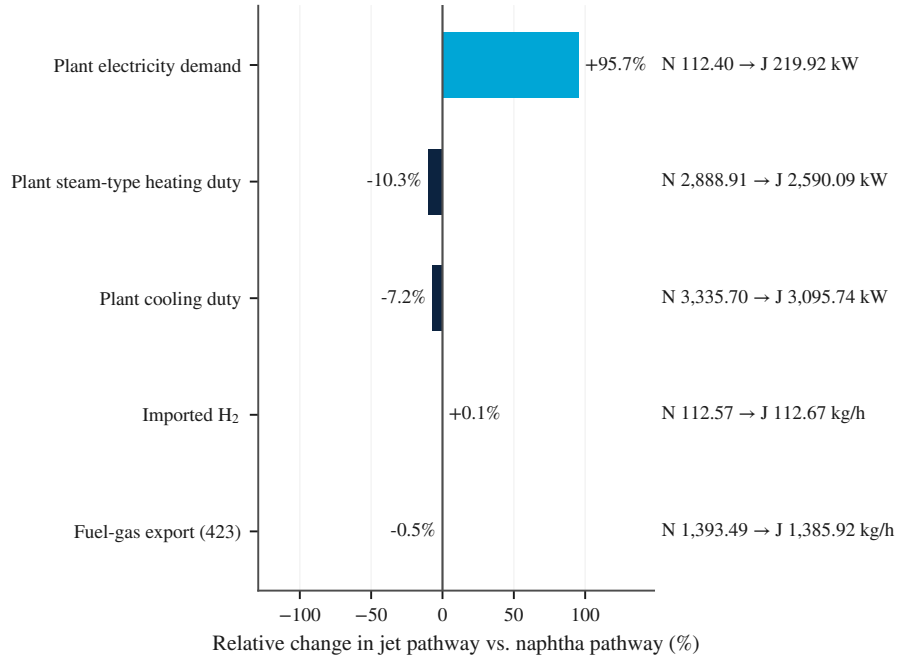

Figure 6.2: Relative change in selected plant-boundary indicators for the jet-fuel pathway compared with the naphtha pathway. Electricity demand shows the clearest increase, whereas imported H_2 intensity and net fuel-gas surplus remain nearly unchanged and plant-wide thermal duties shift more moderately. The figure is intended as a comparative steady-state summary of pathway effects at plant level and should not be interpreted as evidence of equipment-level causality.

A reader might intuitively expect the jet-fuel pathway to require much more imported hydrogen and substantially larger plant-wide thermal duties, because the outlet intent is more restrictive and an additional saleable cut is recovered. Under the present screening representation, however, that is not the dominant pattern. The defining change is in A300: the jet-fuel pathway recovers a jet-range product at the expense of the naphtha fraction while maintaining comparable total saleable liquid yield. The A200 and A400 results then show secondary consequences of this intent shift in gas routing, hydrogen recovery, aqueous handling, and utilities.

This interpretation helps resolve the most important expectation gap in the final results. Imported hydrogen remains nearly unchanged at plant boundary, even though internal hydrogen routing shifts slightly through the PSA system. This means that, for the selected severities and recycle settings, pathway differentiation does not express itself primarily as a step-change in net external hydrogen requirement. Instead, the stronger signal appears in electricity demand and in the integrated handling of gas and liquid side streams.

Utilities complete the picture. Plant-wide heating and cooling duties remain of similar order across pathways, while electricity demand increases materially in the jet-fuel pathway. Interpreted together with the A200 gas-routing differences and the A300 recovery structure, this suggests that the pathway shift manifests primarily as additional auxiliary work and handling complexity rather than as a dominant increase in thermal duties. The direct CO_2 metric remains effectively unchanged and should not be overinterpreted: because A100 is fixed and only direct on-site combustion is counted, the small residual difference reflects the integrated utility bookkeeping of the screening model rather than a meaningful change in combustion demand.

A final interpretive point concerns plant gas. The exported byproduct fuel-gas stream remains large in both pathways and only marginally different between them. Because A100 conversion is fixed, this difference should be read as an integrated gas-balance effect arising from the combined contributions of pyrolysis gas, PSA tail gas, stabiliser offgas, and related routing through the shared fuel-gas header, not as evidence that one pathway fundamentally “produces much more gas” than the other.

Taken together, the results indicate that the pathway shift is best understood as a downstream product-recovery and utility-allocation effect within one fixed A100–A400 plant. The technical implications for Chapter 7 are therefore straightforward: pathway differences in revenue structure and variable operating cost contributions can be traced back directly to the plant-boundary quantities reported here, especially product rates, electricity demand, imported hydrogen, exported fuel gas, and the small but explicit boundary handling streams.

6.11. Chapter synthesis and TEA handover

6.11.1. Answer to Sub-Research Question 2

Sub-Research Question 2: What are the technical characteristics of producing naphtha-range and jet-fuel-range blendstocks from pyrolysis of polyolefin-rich plastic waste?

This chapter answers the question by translating the conceptual system definition of Chapter 5 into converged steady-state mass and energy balances for the integrated A100–A400 configuration, evaluated consistently for two operating pathways within a common gate-to-gate boundary. The results show that, at equal plastic throughput and under a shared flowsheet topology, the principal technical effect of pathway intent is to redistribute the saleable liquid slate through upgrading severity and fractionation cut definition, rather than to change the overall conversion scale. This is most clearly reflected at the product boundary: the naphtha pathway yields a single naphtha-range product stream, whereas the jet-fuel pathway yields a split between naphtha-range and jet-range blendstock streams, while maintaining a comparable total saleable liquid yield (Table 6.8 and Table 6.12).

Beyond the liquid slate, pathway intent produces secondary but non-negligible shifts in the integrated plant interfaces that matter for downstream interpretation. In the jet-fuel pathway, slightly more sweet gas is routed to PSA feed, leading to a marginal increase in recovered hydrogen and a corresponding reduction in PSA tail gas returned to the fuel-gas system, indicating a modest change in gas circulation through the hydrogen-recovery network. Aqueous boundary streams are lower in the jet-fuel pathway within the present screening representation, consistent with pathway-dependent separation and phase-allocation behaviour. Utility requirements remain dominated by steam-type heating and cooling duties in both pathways, while the total plant electricity demand is higher in the jet-fuel pathway, consistent with additional auxiliary load associated with recovering and handling an additional product cut and the associated separation and gas-system interactions. Imported hydrogen and direct on-site combustion CO_2 remain effectively unchanged at plant boundary, indicating that the main pathway shift is downstream and integration-linked rather than front-end conversion-driven.

6.11.2. Implications and handover to the TEA

The steady-state plant-boundary quantities derived in this chapter provide the direct quantitative basis for Phase 3 of the framework defined in Chapter 4, in which the technical performance is monetised under a discounted-cash-flow structure and MSP closure conventions. To preserve traceability, the specific rates and duties that enter revenue, variable operating cost, and boundary handling calculations are transferred without modification into the TEA in Chapter 7. These handover quantities are summarised in Table 6.13.

In Chapter 7, product flowrates and the exported fuel-gas stream define the monetised output quantities, while imported hydrogen and utilities define the principal variable operating cost drivers; remaining boundary streams define the handling quantities required for consistent battery-limits accounting under the stated gate-to-gate scope. Finally, the interpretation of the results throughout Chapters 7 and 8 should remain anchored to the modelling limits of the present work: the balances represent converged steady-state, screening-level performance and do not capture dynamic operability, start-up and shut-down behaviour, catalyst deactivation, long-term fouling, or full fuel certification. In particular, the jet-range stream is treated as a jet-fuel-range blendstock under a specification-intent framing rather than as an ASTM-certified finished fuel. Within these limits, the handover set provides a transparent and

Table 6.13: Handover quantities from the technical assessment to the TEA.

Handover quantity	Naphtha pathway	Jet-fuel pathway
Inputs to plant (economic model basis)		
Plastic feed to plant, Stream 101 [kg/h]	5 000.00	5 000.00
Imported H_2 to plant (Streams 206 + 306) [kg/h]	112.57	112.67
Saleable products and byproducts from plant		
Naphtha product rate, Stream 340 [kg/h]	2 808.00	1 900.00
Jet-range product rate, Stream 344 [kg/h]	0.00	916.11
Heavy purge rate, Stream 342 [kg/h]	5.86	6.46
Fuel gas export (byproduct), Stream 423 [kg/h]	1 393.49	1 385.93
Utilities (plant totals)		
Total electricity demand (plant) [kW]	112.40	219.92
Total steam-type heating duty (plant) [kW]	2 888.91	2 590.09
Total cooling duty (plant) [kW]	3 335.70	3 095.74
Boundary discharges / outputs relevant to TEA treatment		
Vent/purge gas to battery limits (flare header) [kg/h]	26.05	26.37
Stripped water discharge, Stream 411 [kg/h]	17.23	11.76
Direct CO_2 (on-site combustion only) [kg/h]	1 396.41	1 394.36

Notes: Quantities are reported on the common 40 kt/y, 8,000 h/y basis and are transferred directly to the Chapter 7 economic accounting. Fuel gas export (Stream 423) is treated as an exported byproduct at battery limits. Vent/purge gas is treated as leaving the system boundary for offsite handling; no flare combustion is modelled in the baseline.

internally consistent bridge from the technical outcomes quantified here to the economic assessment that follows.

7

Economic Assessment

Building on the fixed system definition established in Chapter 5 and the steady-state plant-boundary performance quantified in Chapter 6, this chapter evaluates the economic implications of two operating *pathways*. The purpose is to translate plant-boundary mass and energy balances into (i) annual operating expenditures and operating income offsets, (ii) capital investment requirements, and (iii) DCF indicators. In the logic of the research framework introduced in Chapter 4, this chapter provides the Phase 3 economic translation of the Phase 2 technical handover under one consistent financial and bookkeeping basis.

This chapter therefore implements *Phase 3* of the research framework introduced in Chapter 4 and answers *Sub-Research Question 3* by monetising the Phase 2 plant-boundary outputs into a screening-level TEA under a shared DCF basis and explicit MSP closure convention. The technical assessment in Chapter 6 showed that both pathways share the same gate-to-gate A100–A400 configuration, the same feed basis, and broadly comparable total saleable liquid yield, while differing mainly in product partitioning and in plant-wide electricity demand. The present chapter carries those same pathways forward into economic terms.

Two pathways are assessed. The first is the *naphtha pathway*, in which the main liquid product is the *naphtha-range blendstock* exported as Stream 340. The second is the *jet-fuel pathway*, in which the *jet-fuel-range blendstock* (Stream 344) is treated as the main product while the naphtha fraction is treated as a fixed-price co-product revenue stream. This accounting convention determines which selling price is solved for when calculating the MSP in the DCF model and is applied consistently in the operating statement, DCF indicators, and MSP contribution analysis. As in Chapter 6, the pathways are not interpreted as like-for-like finished-fuel alternatives. They are alternative outlet intents applied to one shared plant basis, and their economic comparison must therefore be read together with the pathway-specific closure convention.

The system-boundary conventions follow the thesis-safe stream definitions used throughout Chapter 6 to Chapter 8. In particular, Stream 423 is treated as an exported byproduct fuel-gas stream at battery limits and is monetised as a variable operating income offset. Any continuous vent/purge gas is treated as *vent/purge gas to battery limits (flare header), offsite handling*. No flare combustion is modelled and no flare emissions are claimed. These boundary conventions matter economically, because a meaningful part of the annual revenue bridge depends on whether plant-boundary exports are credited inside the TEA.

The chapter proceeds from the baseline economic roll-up to the supporting TEA basis and finally to the break-even interpretation. Table 7.1 first presents the baseline economic results in compact form. The remainder of the chapter then documents the financial basis and input coefficients, explains the CAPEX,

OpEx, and DCF structure used to generate those results, and interprets the resulting MSP outcomes using two complementary figures: an absolute MSP decomposition (Figure 7.1) and a normalised MSP contribution view (Figure 7.2). Together, these elements show not only what the baseline results are, but also why they take the form they do.

7.1. Economic basis and modelling scope

The economic basis used in this chapter fixes the timeline, reporting conventions, and closure definitions against which both pathways are compared. The assessment is conducted in real (constant-price) EUR using a real discount rate, with no explicit inflation in the cash-flow model [124]. All costs and unit-price coefficients are expressed on a **2024** basis, consistent with the CEPCI escalation basis applied in the workbook (section 7.3). The system boundary remains gate-to-gate (A100–A400), consistent with Chapter 5 and Chapter 6, with upstream sorting and downstream refining, blending, and product use excluded. The plant location (Rotterdam–Moerdijk, NL) is used only to guide the price context and interpretation.

The operating basis follows the design utilisation used in the steady-state model: 8,000 h/y, corresponding to a derived capacity factor of 0.913. The DCF model adopts a two-year construction period with a 40/60 capital spending profile and a 25-year operating horizon. Start-up is represented via reduced first-year utilisation (80%), while operating expenses are applied at their full level in the start-up year (Table 7.2) [124]. Cash flows follow an end-of-year convention and are discounted to a reference point at the start of operations (year 0). Concretely, construction spending occurs in years -2 and -1, and operating cash flows begin in year 0, with each year's cash flow realised at the end of that year [124].

Pathway-specific MSP definitions are fixed for the remainder of the chapter. In the naphtha pathway, MSP is defined on Stream 340. In the jet-fuel pathway, MSP is defined on Stream 344 while naphtha is treated as a co-product sold at a fixed assumed naphtha price. This convention is restated in the notes to Table 7.1 and carried consistently through the DCF reporting and the MSP contribution analysis.

Consistent with the research design in Chapter 4, the present chapter is framed as a screening-level TEA rather than an investment-grade appraisal. Capital costs are estimated on a conceptual installed-cost basis using factor methods and a Seider-style investment ladder [125]. Fixed operating costs are represented using Seider-style cost-sheet fractions [125]. Variable operating costs and operating income offsets are tied directly to plant-boundary quantities from Chapter 6. The purpose is not to provide a detailed market forecast or a bankable valuation, but to establish a transparent and internally consistent economic baseline from the fixed technical handover.

The baseline roll-up in Table 7.1 should be read in three steps. First, the annual plant basis remains very similar across pathways: both cases process the same 40 kt/y feed, and the total annual liquid-product slate remains of comparable magnitude, consistent with the technical findings in Chapter 6. Second, the cost architecture is also very similar. Total capital investment differs only modestly (195.08 versus 196.48 M EUR), total OpEx is of similar magnitude (26.05 versus 26.31 M EUR/y), and hydrogen make-up cost is essentially unchanged at about 0.62 M EUR/y in both cases, consistent with the nearly identical imported H_2 intensities reported in Table 6.12. The jet-fuel pathway does carry a somewhat higher utilities burden, in line with the higher electricity intensity reported in Chapter 6, but this is not the dominant explanation for the pathway gap.

Third, and most importantly, similar annual cost totals do *not* imply similar MSP. The much higher jet-pathway MSP does not arise because the plant suddenly becomes much more hydrogen-intensive or because total annual OpEx or TCI increase dramatically. Rather, the remaining annual revenue requirement is recovered over a smaller main-product basis in the jet-fuel pathway: naphtha is credited as a fixed-price co-product, fuel gas is credited in both pathways, and the residual break-even burden is then solved on Stream 344 only. The jet-pathway MSP should therefore be read primarily as a consequence of pathway-specific product partitioning and closure logic, not as evidence of a fundamentally different plant-wide cost structure.

Table 7.1: Baseline economic breakdown for the two operating pathways at 40 kt/y plastic throughput (real 2024 EUR, BASE results pack). OpEx is split into fixed and variable components; variable operating income includes boundary exports (fuel gas) in both cases and naphtha co-product revenue in the jet-fuel pathway. Capital costs are reported via the Seider ladder.

Category	Unit	Naphtha pathway	Jet-fuel pathway
Operating basis and outputs			
Plastic feed (annual)	kt/y	40.00	40.00
Naphtha product (annual)	kt/y	22.46	15.20
Jet-range product (annual)	kt/y	–	7.33
Fuel gas export (annual)	kt/y	11.15	11.09
OpEx per tonne feed (fixed+variable)	EUR/t feed	651.21	657.66
OpEx per tonne liquid products[e]	EUR/t	1,159.67	1,167.68
Operating expenditures (OpEx)			
Fixed operating costs	M EUR/y	**24.55**	**24.73**
Operations labour-related subtotal	M EUR/y	3.58	3.61
Maintenance subtotal	M EUR/y	15.33	15.44
Operating overhead	M EUR/y	2.68	2.70
Property taxes and insurance	M EUR/y	2.96	2.98
Variable operating costs	M EUR/y	**1.50**	**1.58**
Utilities subtotal	M EUR/y	0.65	0.73
Hydrogen make-up (total)	M EUR/y	0.62	0.62
Other variable costs (materials/waste)[a]	M EUR/y	0.23	0.23
Variable operating income (boundary exports; co-products)			
Operating income subtotal	M EUR/y	**5.19**	**17.39**
Fuel gas export revenue (Stream 423)	M EUR/y	5.19	5.17
Naphtha co-product revenue (fixed price)	M EUR/y	–	12.22
Total OpEx (fixed + variable)	M EUR/y	**26.05**	**26.31**
Net annual cost burden before main-product revenue[b]	M EUR/y	-20.86	-8.91
Capital expenditures (CapEx) – Seider ladder			
Total bare-module investment, C_{TBM}	M EUR	109.15	109.93
Direct permanent investment, C_{DPI}	M EUR	125.52	126.42
Total depreciable capital, C_{TDC}	M EUR	148.11	149.18
Total permanent investment, C_{TPI}	M EUR	165.88	167.08
Working capital, C_{WC}	M EUR	29.20	29.41
Total capital investment, C_{TCI}	M EUR	**195.08**	**196.48**
DCF indicators (project-level)			
NPV (PV at year 0, assumed price set)[c]	M EUR	-216.08	-222.97
IRR (project, assumed price set)[c]	%	-3.44	-4.22
MSP (external solve, NPV$=0$)[d]	EUR/t	2,134.09	4,939.76

[a] "Other variable costs" equals (materials & waste incl. H_2) minus the explicit H_2 make-up line; in the BASE case it consists mainly of waste-handling and catalyst-replacement related items.
[b] Net annual cost burden before main-product revenue is defined as (operating income subtotal) $-$ (total OpEx). Main-product revenue is excluded by definition: the main product is the naphtha product in the naphtha pathway and the jet-fuel-range blendstock product in the jet-fuel pathway.
[c] NPV and IRR correspond to the workbook run at its internal assumed price set (naphtha pathway: fixed assumed naphtha price; jet-fuel pathway: fixed assumed jet-fuel-range blendstock price plus fixed assumed naphtha co-product price; Table 7.3).
[d] MSP follows the BASE results-pack convention: **naphtha pathway** solves for the naphtha selling price (Stream 340) at NPV$=0$; **jet-fuel pathway** solves for the jet-fuel-range blendstock selling price (Stream 344) at NPV$=0$ while holding the naphtha co-product selling price fixed.
[e] Defined as total OpEx (fixed + variable) divided by the total exported liquid products (naphtha product in the naphtha pathway; naphtha + jet products in the jet-fuel pathway).

This distinction is central for the rest of the chapter. The naphtha and jet-fuel pathways share the same front-end conversion basis and broadly comparable annual plant-wide cost burden, but they distribute revenue differently and define the MSP denominator differently. As a result, the economic comparison is best understood as a comparison of two accounting closures applied to two outlet intents under one shared gate-to-gate plant basis.

Because the present TEA is screening-level and relies on factor methods and assumed unit-price coefficients, an economic pedigree analysis is used to communicate the relative strength of the evidence base behind the economic model elements, consistent with the methodology introduced in subsection 4.3.2. Consolidated economic pedigree results for both pathways are reported in Appendix Appendix B, including mean scores and reviewer deviation (agreement indicator) across the four criteria (proxy, empirical basis, theoretical understanding, and methodological rigour).

At study scope, the pedigree outcomes indicate strongest support for the *financial model structure* itself, namely the DCF framework, MSP closure logic, and pathway-consistent bookkeeping conventions. By contrast, elements that depend on screening-level cost estimation and commercially contingent accounting assumptions show weaker empirical support. In particular, the empirical basis is comparatively weaker for conceptual CAPEX and fixed-OpEx estimation and for *boundary credits and co-product accounting*, including monetisation of exported fuel gas at battery limits (Stream 423) and the fixed-price co-product treatment of naphtha in the jet-fuel pathway. These pedigree results do not alter the baseline accounting reported here, but they do bound how strongly absolute MSP levels and any pathway differences that depend on price-credit conventions should be interpreted. They also motivate the focused robustness testing in Chapter 8.

7.2. Price basis and economic input coefficients

Plant-boundary material and utility flows from Chapter 6 are monetised using the unit-price coefficients in Table 7.3. Together with the DCF basis in Table 7.2, these coefficients are sufficient to reproduce the variable OpEx and operating income lines reported in Table 7.1. The technical handover quantities used in the TEA are summarised in Table 6.13. Product flowrates and Stream 423 define the principal revenue-side quantities, while imported hydrogen and plant utilities define the main variable-cost drivers. The purpose is to document the economic basis transparently, not to present a full market study.

Three revenue-related coefficients are especially important because they interact directly with the system boundary and the MSP closure rule. First, the process exports a surplus fuel-gas stream at battery limits (Stream 423). This stream is treated as saleable and booked as a variable operating income offset on an energy basis (LHV). In economic terms, it is best understood as an integrated plant-boundary surplus routed via the shared fuel-gas header rather than as an isolated single-unit credit. Second, in the naphtha pathway, the naphtha selling price (Stream 340) is the MSP closure variable. Third, in the jet-fuel pathway, naphtha is treated as a fixed-price co-product revenue stream, while the jet-fuel-range blendstock price (Stream 344) is the MSP closure variable.

A key baseline simplification concerns the plastic feedstock gate price. In the BASE case reported here, the gate price is set to zero, such that feedstock is treated as cost-neutral at battery limits. solates process-internal economic drivers (capital structure, fixed OpEx, utilities, hydrogen, and monetised boundary credits) and avoids embedding an additional exogenous feedstock-price assumption in the baseline pathway comparison. The same zero-price point is then used as the reference for the sensitivity ranges evaluated in Chapter 8.

The monetisation scope follows the screening intent of the thesis. Stream 423 is monetised explicitly as a boundary credit. Heavy purge and sour-water treatment are monetised using explicit unit-cost coefficients. Other boundary streams reported for completeness in Chapter 6 (for example vent/purge gas to battery limits and solid residues) are not assigned separate BASE cash-flow terms unless explicitly represented in the workbook cost sheets. At the reporting precision used here, such effects are either

Table 7.2: Economic basis and financial parameters implemented in the TEA model for the two operating pathways (BASE case). Parameters identical in both pathways are centered across the two value columns.

Parameter	Unit	Value (both pathways)	Reference
System definition and reporting basis			
System boundary	–	Gate-to-gate (A100–A400)	Thesis Ch. 5–6
Plant location (price context)	–	Rotterdam–Moerdijk, NL	Thesis Ch. 5
Cost basis	–	Real terms (constant prices)	[124]
Cost year	–	2024	Study assumption
Currency	–	EUR	Study definition
Annual operating hours	h/y	8,000	Study assumption
Capacity factor $(8{,}000/8{,}760)$	–	0.913	Derived
DCF and timeline assumptions			
Discount rate (real)	%	15.0	[124]
Corporate income tax rate	%	25.8	[126]
Analysis horizon (operating life)	y	25	Study assumption
Construction period	y	2	Study assumption
CAPEX spend profile (year -2 / year -1)	%	40 / 60	Study assumption
Start-up utilisation (first operating year)	%	80	Study assumption
Start-up OPEX factor (first operating year)	%	100	[124]
Cash-flow timing convention	–	End-of-year	[124]
NPV reference year	–	Year 0 (start of operation)	Model convention
Financing structure	–	All-equity (unlevered)	Study assumption
Depreciation			
Depreciation method	–	Straight-line	[124]
Depreciation basis[a]	–	FCI (excl. land, WC)	Model convention
Depreciation period	y	25	Study assumption
Salvage value	% of FCI	0	Study assumption
Fixed OpEx model (Seider-style cost-sheet factors)			
Operations DW&B proxy, f_{opsWB}	% of C_{TDC}	2.0	Model convention
Ops. salaries factor	% of DW&B	15.0	[125]
Ops. supplies & services	% of DW&B	6.0	[125]
Maintenance MW&B, f_{MWB}	% of C_{TDC}	4.5	[125]
Maint. salaries factor	% of MW&B	25.0	[125]
Maint. materials & services	% of MW&B	100.0	[125]
Maint. overhead factor	% of MW&B	5.0	[125]
Operating overhead, f_{OH}	% of (M&O–SW&B)	22.8	[125]
Property taxes & insurance	% of C_{TDC}	2.0	[125]
CAPEX ladder adders and working-capital shortcuts			
Allocated utility-plant CAPEX (utilities purchased)	–	0	Study assumption
Site preparation (integrated addition)	% of C_{TBM}	5.0	[125]
Nonprocess buildings	% of C_{TBM}	5.0	[125]
Other offsite facilities (excl. utility plants)	% of C_{TBM}	5.0	[125]
Contingency + contractor fee	% of C_{DPI}	18.0	[125]
Land	% of C_{TDC}	2.0	[125]
Start-up cost	% of C_{TDC}	10.0	[125]
Working capital	% of C_{TCI}	15.0	[125]

[a] FCI denotes fixed capital investment; the depreciable base excludes non-depreciable land and working capital.
Note: "Study assumption" denotes an author-selected baseline value implemented in the spreadsheet model; "Model convention" denotes a bookkeeping or timing convention used for consistent DCF closure.

Table 7.3: Economic input coefficients used to monetise plant-boundary flows from Chapter 6 (BASE case, real 2024 EUR). Product selling prices listed here correspond to the internal assumed-price set used for the workbook NPV/IRR reporting; MSP values are solved externally as described in section 7.5.

Coefficient	Unit	Value	Note	Reference
Products and boundary credits (assumed-price set; MSP closure differs by pathway)				
Naphtha-range blendstock (Stream 340, assumed selling price)	EUR/t	804.22	Used for NPV/IRR; co-product price in jet-fuel pathway	[127]
Jet-fuel-range blendstock (Stream 344, assumed selling price)	EUR/t	734.00	Used for NPV/IRR in jet-fuel pathway	[128]
Fuel gas export price (Stream 423)	EUR/GJ (LHV)	9.63	Credit applied on LHV basis	[129]
Plastic feedstock gate price	EUR/t feed	0.00	BASE assumption	Study definition
Utilities and consumables				
Hydrogen price	EUR/kg	0.684587	Imported H_2 make-up	[130], [131]
Electricity price	EUR/kWh	0.152	Purchased electricity	[132]
Steam price (selected pressure)	EUR/GJ	5.192337	Purchased steam/heat utility	[131], [133]
Cooling water price	EUR/m^3	0.034202	Purchased cooling water	[131], [134]
Fresh/process water price (if used)	EUR/m^3	0.034202	Optional water input	[131], [134]
Sour water treatment cost	EUR/m^3	0.75	Applied to aqueous waste stream	[135]
Waste handling and catalysts				
Heavy purge disposal cost	EUR/t	150.00	Applied to heavy purge stream	[131], [136]
HTU catalyst price	EUR/kg catalyst	37.7	Replacement cost coefficient	[131], [137]
HTU catalyst lifetime	years	2.0	Replacement interval (model input)	[137]
HCU catalyst price	EUR/kg catalyst	37.7	Replacement cost coefficient	[131], [137]
HCU catalyst lifetime	years	2.0	Replacement interval (model input)	[137]

Notes: Intratec-sourced coefficients reported in USD in the workbook are converted to EUR using ECB FX reference rates.

The fuel-gas export credit is applied on an LHV basis; the workbook derives the coefficient from an annual average TTF price and uses 1 MWh $=$ 3.6 GJ for unit conversion.

captured within aggregated cost lines or excluded as a screening simplification. No carbon price or emissions charge is applied to the direct CO_2 metric in the BASE case; the CO_2 reporting in Chapter 6 is therefore treated as a scope-defined technical indicator rather than as an explicit cost term.

7.3. Capital expenditure estimation

To obtain a screening-level total capital investment consistent with the gate-to-gate boundary, equipment costs are harmonised to the 2024 basis, scaled to the design basis, and converted to installed-cost proxies using factor methods [125]. Plant-level adders are then applied using a Seider-style investment ladder to obtain the total capital investment used in the DCF model (Table 7.1) [125]. Because utilities are purchased in the system definition adopted here, no allocated utility-plant CAPEX is included within the model boundary (Table 7.2); this excludes, for example, on-site boiler/CHP and cooling-tower capital unless explicitly represented.

7.3.1. Equipment-level scaling, escalation and installed-cost proxy

At study level, an installed-cost proxy for equipment item i can be expressed compactly by combining (i) capacity scaling, (ii) cost-index escalation, and (iii) a bare-module installation factor [125]. In Equation 7.1, a purchased-cost proxy $C_{P,\mathrm{ref},i}$ at reference scale $Q_{\mathrm{ref},i}$ and reference cost-index level $I_{\mathrm{ref},i}$ is first scaled and escalated:

$$C_{P,i} = C_{P,\mathrm{ref},i} \left(\frac{Q_i}{Q_{\mathrm{ref},i}} \right)^{n_i} \left(\frac{I}{I_{\mathrm{ref},i}} \right) FX \tag{7.1}$$

where Q_i is the design size variable, n_i is the scaling exponent, I is the cost index in the analysis year (CEPCI), and FX is a currency conversion factor if required. In the implemented workbooks, the escalation term is applied via a common CEPCI ratio,

$$\frac{I}{I_{\mathrm{ref}}} = 1.41 \tag{7.2}$$

consistent across both pathway models [138]. The installed proxy is then obtained via the Guthrie bare-module form:

$$C_{BM,i} = F_{BM,i}\, C_{P,i} \tag{7.3}$$

where $F_{BM,i}$ is selected by equipment class [125]. No additional multiplicative corrections for metallurgy, pressure, or design complexity are applied beyond the selected factor set, consistent with the screening nature of the model.

7.3.2. Plant-level adders and investment roll-up (Seider ladder)

Capital investment is reported using a Seider-style ladder [125]. The ladder begins with total bare-module investment,

$$C_{\mathrm{TBM}} = \sum_i C_{BM,i} \tag{7.4}$$

and adds site preparation, nonprocess buildings, and offsite facilities as screening fractions of C_{TBM} to obtain direct permanent investment C_{DPI}. Contingency and contractor fees are applied as a fraction of C_{DPI} to obtain total depreciable capital C_{TDC}. Land and start-up allowances are then added to obtain total permanent investment C_{TPI}, and working capital is included using the shortcut in Table 7.2 to obtain total capital investment C_{TCI} [125]. The resulting ladder values for each pathway are reported in Table 7.1. As a screening estimate for a conceptual design, the resulting CAPEX carries the uncertainty typical of early-stage factor-method TEA [139].

The key implication for interpretation is that pathway differentiation in CAPEX is modest. The jet-fuel pathway requires somewhat higher total investment, but the difference is small relative to the magnitude of the total capital base. As a result, the economic contrast between pathways is shaped less by a large CAPEX step change than by how that shared capital burden is ultimately recovered in the pathway-specific DCF closure.

7.4. Operating expenditure model and revenue bridge

Operating expenditures (OpEx) are separated into fixed and variable components to support transparent interpretation of economic drivers. Fixed OpEx is estimated using Seider cost-sheet factor rules linked to the depreciable capital basis, while variable OpEx is tied directly to plant-boundary quantities established in Chapter 6 and monetised with the coefficients in Table 7.3. In parallel, byproduct and co-product revenue terms are booked as operating income offsets, reducing the annual revenue requirement that must be recovered by the designated main product under the MSP definition.

7.4.1. Fixed operating costs (Seider cost-sheet structure)

Fixed operating costs include labour-related expenses, maintenance, operating overhead, and property taxes and insurance [125]. In the present model, operations wages and benefits are represented by a

screening proxy fraction of C_{TDC} (Table 7.2); operations salaries and operating supplies are applied as Seider-style fractions of the operations wage base. Maintenance wages and benefits are estimated as a fraction of C_{TDC} and expanded to a maintenance total using Seider factors for maintenance salaries, materials and services, and maintenance overhead. Operating overhead is applied as a fraction of the wage-and-benefit base (M&O–SW&B), and property taxes and insurance are applied as a fraction of C_{TDC} [125].

Under the final baseline, these fixed terms dominate the operating statement in both pathways. This is already visible in Table 7.1, where fixed OpEx is roughly 24.6–24.7 M EUR/y, far exceeding the variable OpEx subtotal. In other words, the baseline TEA is not primarily governed by utility coefficients or other second-order variable terms; it is governed by the annual burden associated with a large conceptual capital base and the fixed-cost structure derived from it.

7.4.2. Variable operating costs and operating income terms

Variable operating costs scale with throughput and are monetised using the coefficients defined in Table 7.3. These costs include purchased utilities (steam/heat utility, cooling water, and electricity), consumables (hydrogen make-up), and waste handling where applicable. The process also exports a surplus fuel-gas stream at the battery limits (Stream 423). Because this stream exits the system boundary and is treated as saleable, it is accounted as a variable operating income offset on an LHV basis using the export credit coefficient in Table 7.3. In the jet-fuel pathway, naphtha is additionally treated as a co-product sold at a fixed assumed price; this co-product revenue is reported explicitly as an operating income term to keep the MSP accounting convention auditable.

Two clarifications are important here. First, the fuel-gas credit is economically material in both pathways, but it remains a *boundary-credit assumption*: its value depends on whether the exported surplus can in fact be placed, used, or contracted on the assumed terms. Second, the variable-cost structure does not support the interpretation that the jet-fuel pathway is “much more hydrogen-driven” than the naphtha pathway. Hydrogen make-up cost is essentially unchanged between pathways, which mirrors the nearly unchanged imported hydrogen intensity at plant boundary. The more visible pathway difference on the variable-cost side is instead the somewhat higher utility burden associated with the jet-fuel pathway, especially electricity, consistent with Chapter 6.

7.5. Discounted cash flow performance and MSP definition

The DCF model converts the annual operating statement and capital investment basis into project-level indicators consistent with the assessment framework in Chapter 4 [124]. Construction spending is allocated over two years using the profile in Table 7.2. Operating cash flows begin after commissioning, with a start-up year represented via reduced utilisation. Corporate tax is applied to taxable income after depreciation [124], and depreciation is implemented using straight-line depreciation over the stated depreciation life on the depreciable capital basis (Table 7.2) [124]. Working capital is invested as a project requirement and recovered at end of life, consistent with screening TEA convention [124].

Project feasibility at the assumed price set is summarised by the NPV and IRR in Table 7.1. MSP is defined as the main-product selling price required for DCF break-even at the selected real discount rate. The break-even condition is expressed as:

$$\mathrm{NPV} = \sum_{t=-2}^{N} \frac{FCF_t}{(1+r)^t} = 0 \tag{7.5}$$

where FCF_t is the free cash flow in year t (including operating cash flow, capital spending, and working-capital movements) and r is the real discount rate [124]. Under the pathway-specific MSP convention, the unknown selling price appears only in the main-product revenue term: naphtha price for the naphtha pathway, and jet-fuel-range blendstock price for the jet-fuel pathway (with naphtha co-product revenue

held fixed).

In the final workbook version used for this thesis, MSP is solved externally from the DCF output using a two-point linearisation around the assumed price point. The DCF model is evaluated at an initial price P_1 (the assumed product price set) and at a perturbed price P_2 while keeping all other coefficients fixed (including fixed co-product pricing in the jet-fuel pathway). With NPVs $\mathrm{NPV}(P_1)$ and $\mathrm{NPV}(P_2)$, the MSP is obtained by linear interpolation:

$$\mathrm{MSP} = P_1 - \mathrm{NPV}(P_1)\left(\frac{P_2 - P_1}{\mathrm{NPV}(P_2) - \mathrm{NPV}(P_1)}\right) \tag{7.6}$$

This reporting-layer solve is accurate when $\mathrm{NPV}(P)$ is approximately linear over the bracket $[P_1, P_2]$; P_2 is selected to provide a well-conditioned local NPV response around P_1 [124]. The resulting MSP values are reported in Table 7.1.

At the assumed internal price set, both pathways remain strongly negative on an NPV basis, and both exhibit negative IRR. The MSP reporting is therefore the more useful comparison metric in this thesis, because it translates the full DCF structure into a single break-even main-product price under pathway-consistent closure rules. However, precisely because MSP is a closure metric, it must be interpreted together with the underlying pathway revenue structure and denominator basis rather than as a simple "cost per tonne" result detached from the accounting convention.

7.6. MSP contribution analysis and interpretation

Table 7.1 provides the baseline economic roll-up in annual terms (M EUR/y) and reports MSP for each pathway on its respective main-product basis. Figure 7.1 complements this tabular view by decomposing MSP into absolute contributions in EUR/t of main product. Each bar is constructed by taking the annual cost and income terms reported in Table 7.1 and normalising them by the annual production of the MSP-denominator product (naphtha-range blendstock in the naphtha pathway; jet-fuel-range blendstock in the jet-fuel pathway). Operating expenditures are shown as positive contributions, boundary credits are shown as negative contributions, and the remaining required revenue is represented as a residual DCF capital charge.

The capital charge term closes the DCF break-even balance. In other words, after accounting for annual operating expenditures and operating income offsets, the remaining portion of MSP must satisfy all project-level DCF requirements beyond OpEx. This includes recovery of the up-front capital investment through the construction spending profile and working-capital timing, as well as tax and depreciation effects and the required return implied by the discount rate. The capital charge is therefore a residual DCF closure term; it is not an accounting depreciation line item [124].

Figure 7.1 should be read as an *allocation of the break-even price on the solved main-product basis*, not as a direct picture of total annual plant cost in isolation. On that basis, MSP is dominated by capital-linked and fixed operating burdens in both pathways. In the naphtha pathway, the largest absolute contributions are the residual capital charge and fixed OpEx, while variable OpEx is comparatively small and the fuel-gas export credit provides only a partial offset. The same overall pattern holds in the jet-fuel pathway, where the capital charge and fixed OpEx remain the largest contributions on a EUR/t main-product basis, despite the presence of both a fuel-gas credit and a substantial fixed-price naphtha co-product credit.

The figure therefore makes two points at once. First, the baseline economics are structurally fixed-cost-heavy in both pathways. Second, the jet-pathway bars are higher not because every annual plant-wide burden is radically larger, but because a similar general annual burden is being recovered over a smaller focal product basis after co-product and byproduct credits are applied. The jet-pathway MSP gap is therefore not primarily a variable-OpEx story; it is a closure-and-denominator story built on top of a fixed-cost-heavy baseline.

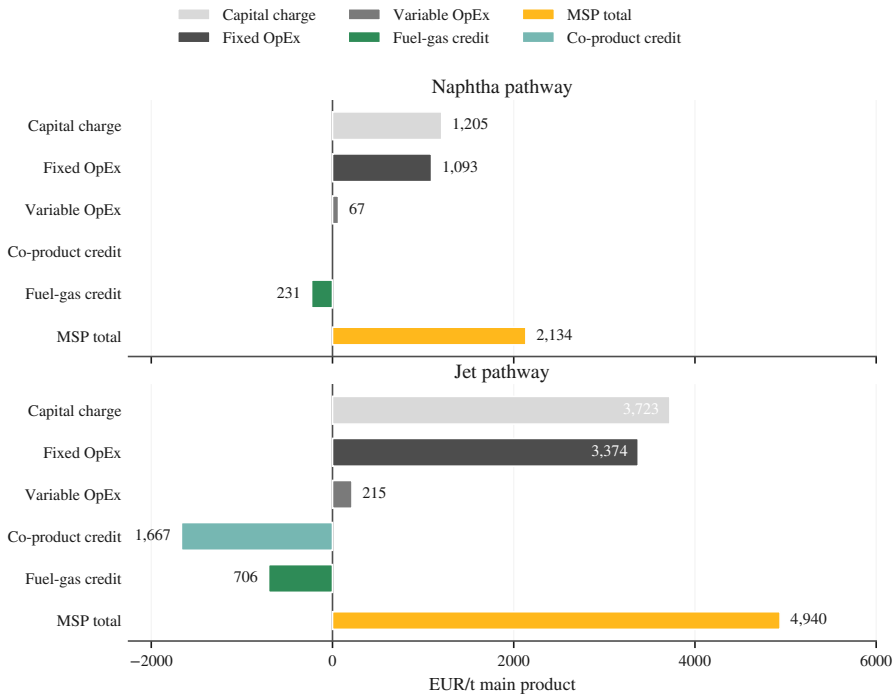

Figure 7.1: Signed decomposition of MSP into major positive burdens and boundary credits for the two operating pathways, reported on each pathway's main-product basis. Rightward bars indicate positive contributions to MSP (capital charge, fixed OpEx, and variable OpEx), while leftward bars indicate credits that reduce the required main-product revenue (fuel-gas export in both pathways and naphtha co-product revenue in the jet-fuel pathway). The final MSP total is shown separately for each pathway.

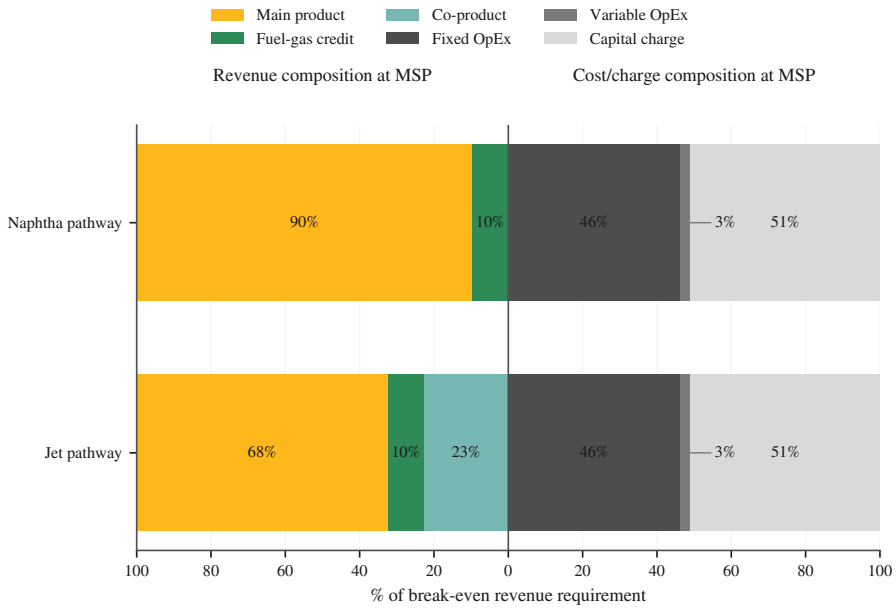

Figure 7.2: Revenue and cost/charge composition at MSP for the two operating pathways. For each pathway, the left side shows the composition of the break-even revenue requirement by revenue source (main product, fuel-gas credit, and where applicable naphtha co-product), while the right side shows the allocation of the same break-even revenue requirement to fixed OpEx, variable OpEx, and the residual capital charge. Shares are normalised to 100% on each side. The capital charge term closes the DCF break-even balance and represents the portion of revenue required to satisfy project-level capital recovery and other non-operating DCF effects beyond reported operating expenditures.

Figure 7.2 provides a complementary structural view of the same break-even condition. On the revenue side, the naphtha pathway recovers most of the required revenue through the main product, with a smaller contribution from fuel-gas export, whereas the jet-fuel pathway recovers a materially larger share through credited co-product revenue and correspondingly a smaller share through the jet-range main product. On the cost/charge side, however, the two pathways are almost identical: fixed OpEx and the residual capital charge together constitute nearly the entire break-even requirement, while variable OpEx remains a minor share.

This figure is useful precisely because it separates *structure* from *magnitude*. Similar share structures on the cost side do *not* mean that the pathways carry the same absolute economic burden on their main-product basis. Rather, they show that the two pathways are governed by a similar fixed-cost-heavy architecture. The large difference in absolute MSP remains, because the revenue requirement is apportioned differently and is closed on a different focal product. In the jet-fuel pathway, a larger fraction of the break-even burden is met through co-product and byproduct credits before the residual requirement is solved on Stream 344, which is a smaller main-product base than Stream 340 in the naphtha pathway.

Taken together, Figure 7.1 and Figure 7.2 show that the baseline MSP outcomes are governed primarily by capital-linked recovery and fixed-cost burden. They also show why the jet-fuel pathway carries a much higher MSP on its main-product basis even though TCI, total OpEx, and hydrogen cost remain broadly similar across pathways.

7.6.1. Contextual competitiveness check

The MSP values in Table 7.1 are reported in real (constant-price) 2024 EUR and represent break-even selling prices under the accounting conventions defined in section 7.1. To provide context only, a snapshot comparison can be made to contemporaneous fossil-derived benchmark indicators. These market quotes are nominal, time- and region-dependent, and not deflated to the thesis cost-year basis.

For naphtha, a representative European benchmark is the European Naphtha Cargoes CIF NWE (Platts) quote, which is on the order of 562 USD/t for Feb 2026 [140]. Using the ECB EUR/USD reference rate for 25 Feb 2026 (1 EUR = 1.1784 USD) [131], this corresponds to approximately 477 EUR/t. For jet fuel, the IATA jet fuel price monitor reports a global average on the order of 95.95 USD/bbl [128]. Using standard conversion ranges for diesel oil and jet kerosene (6.90–7.80 bbl per metric tonne) [141], this corresponds to approximately 562–636 EUR/t on the same FX basis [131]. These indicative benchmarks suggest that the baseline MSP values reported here (2,134 EUR/t for the naphtha pathway and 4,940 EUR/t for the jet-fuel pathway) still exceed conventional fossil benchmarks by multiple factors under current conditions. Within the scope and assumptions of this screening TEA, the assessed configurations are therefore unlikely to be competitive on price alone without additional value mechanisms or substantial improvement in the dominant levers tested in Chapter 8.

7.7. Chapter conclusions

7.7.1. Answer to Sub-Research Question 3

Sub-Research Question 3: What are the economic performance outcomes of the naphtha pathway and jet-fuel pathway, and what do these imply for their feasibility under a consistent assessment basis?

This chapter answers the question by monetising the steady-state plant-boundary quantities established in Chapter 6 into annual operating expenditures, capital investment requirements, and discounted-cash-flow break-even MSP values under a single, consistent financial basis and closure convention. The resulting baseline roll-ups for both pathways are summarised in Table 7.1, while Figure 7.1 and Figure 7.2 provide complementary interpretations of the break-even structure in absolute and normalised terms.

Under the base assumptions adopted in this thesis, both pathways exhibit a strongly capital-linked

and fixed-cost-heavy economic structure. Total capital investment remains of similar magnitude across the two pathways, and the applied cost-sheet method converts this into a large fixed operating-cost burden in both cases. Variable operating costs are smaller in the reported breakdown and are primarily associated with hydrogen make-up, purchased utilities, and remaining materials/waste-related charges. Boundary exports provide meaningful offsets to operating expenditure, most notably the monetised fuel-gas surplus at battery limits (Stream 423). In the jet-fuel pathway, naphtha is additionally treated as a fixed-price co-product, and the remaining revenue requirement is then recovered through the jet-range main product via the MSP closure.

Applying these conventions yields break-even MSP values of 2,134 EUR/t for the naphtha pathway and 4,940 EUR/t for the jet-fuel pathway at the common 40 kt/y basis (Table 7.1). The key interpretation is that the pathway gap in MSP is driven less by large differences in total OpEx, TCI, or hydrogen demand than by the combination of a fixed-cost-heavy baseline and the pathway-specific closure convention. In the jet-fuel pathway, the residual break-even burden is recovered on a smaller main-product basis after co-product and byproduct credits are applied. The resulting MSP values should therefore be read as screening-level indicators of pathway-specific economic burden under the stated conventions, not as like-for-like market prices for interchangeable finished fuels.

A contextual comparison to contemporaneous fossil benchmark indicators is provided in subsection 7.6.1. It indicates that the baseline MSP values remain substantially above conventional fossil benchmarks under current conditions. Within the scope and assumptions of this screening TEA, the assessed configurations are therefore unlikely to be competitive on price alone without additional value mechanisms or substantial improvement in the dominant levers tested in Chapter 8.

7.7.2. Implications and handover to sensitivity analysis

The baseline MSP values reported in this chapter are conditional on four linked components: the economic basis in Table 7.2, the plant-boundary quantities transferred from Chapter 6, the unit-price coefficients in Table 7.3, and the MSP closure convention defined in section 7.1. The BASE feedstock gate price is 0 EUR/t (section 7.2); sensitivity cases in Chapter 8 are therefore stated relative to this baseline.

The baseline structure already suggests which levers are likely to matter most. Because capital-linked recovery and fixed OpEx dominate the break-even requirement, throughput and scale effects are natural candidates for strong MSP sensitivity. Because fuel-gas export provides a material boundary credit, the monetisation of Stream 423 is also likely to be economically important. By contrast, hydrogen price is expected to be a smaller lever at baseline, because hydrogen make-up cost remains modest relative to the fixed annual burden and is nearly unchanged between pathways. Chapter 8 tests these expectations explicitly under a one-at-a-time design while keeping the DCF conventions and pathway-specific MSP closure rules fixed.

This prioritisation also aligns with the economic pedigree analysis in Appendix Appendix B, which identifies screening CAPEX and fixed-OpEx estimation and boundary credit/co-product accounting as comparatively weakly supported elements at the present conceptual stage. The final baseline reported in this chapter therefore serves not only as a reference case, but also as the accounting structure against which the robustness of the dominant economic levers is tested in the sensitivity analysis that follows.

8

Sensitivity Analysis

Building on the baseline techno-economic assessment (TEA) presented in Chapter 7, this chapter tests how robust the minimum selling price (MSP) results are to a limited set of alternative project and market conditions. The analysis is intentionally simple and transparent: one input parameter is varied at a time while all other technical and financial assumptions remain fixed. The resulting MSP response is reported for both pathways and visualised using tornado charts.

This chapter implements *Phase 4* of the research framework introduced in Chapter 4 and addresses *Sub-Research Question 4* by quantifying how the Phase 3 economic outcomes respond to a focused set of high-leverage parameters under the same DCF conventions as the baseline. Read together with Chapter 7, the present chapter functions as a robustness layer on top of the fixed baseline TEA rather than as a new economic model. Its role is to test how strongly the baseline feasibility interpretation depends on a small number of uncertain project and market assumptions.

8.1. Purpose and positioning in the thesis

The baseline TEA in Chapter 7 converts the plant-boundary mass and energy balances from Chapter 6 into operating expenditures, capital investment requirements, and DCF break-even indicators for two operating *pathways*. While the baseline provides a consistent reference point, several economically important inputs are not uniquely determined at the conceptual design stage. Examples include contracting conditions for plastic feedstock at battery limits, the market price of imported hydrogen, and the ability to monetise battery-limit exports such as byproduct fuel gas. In addition, the selected plant scale (40 kt/y) is a project choice rather than a physical constraint.

Sensitivity analysis is therefore used for two related purposes. First, it ranks which assumptions exert the strongest control over MSP within plausible near-term ranges. Second, it translates the dominant sensitivities into practical “levers” relevant to design and project development. In this sense, the chapter provides an interpretive extension of the baseline TEA rather than a full uncertainty quantification exercise.

This distinction matters methodologically. As discussed in Chapter 4, the available evidence base does not support well-founded joint probability distributions for several economically consequential inputs, especially commercially contingent assumptions such as feedstock contracting conditions and battery-limit export monetisation. Under these conditions, a compact OAT design provides the clearest way to isolate parameter influence, preserve interpretability, and rank the dominant feasibility levers without overstating the statistical meaning of the results. The ranges reported in this chapter should therefore be read as *scenario bounds* within the adopted screening model, not as probabilistic confidence intervals.

8.2. Sensitivity framework

8.2.1. Performance metric and MSP definition

MSP is used as the sole performance metric. It is defined consistently with Chapter 7 as the selling price of the designated main product required to satisfy DCF break-even (NPV$= 0$) under the economic basis and timing conventions in Table 7.2 (real 2024 EUR basis as applied in Chapter 7). The closure variable differs by pathway:

- **Naphtha pathway:** MSP is solved for the naphtha product selling price (Stream 340), holding all other cost and revenue coefficients fixed.
- **Jet-fuel pathway:** MSP is solved for the jet-range product selling price (Stream 344), while naphtha is treated as a co-product sold at the fixed naphtha price basis used in Chapter 7.

This convention ensures MSP represents the break-even price of the focal product under a pathway-consistent accounting treatment of co-products and battery-limit exports. It also means that the two pathways should not be interpreted as if they were solved on the same denominator: the jet-fuel pathway recovers the residual break-even burden on Stream 344 after naphtha co-product revenue and the fuel-gas export credit are applied.

8.2.2. OAT design and implementation rules

An OAT design is applied. For each parameter, a low and a high case are evaluated relative to the Chapter 7 baseline, with all remaining inputs held constant. In each case, the spreadsheet TEA model re-solves MSP such that NPV$= 0$ under the same DCF timeline, depreciation, tax rate, and working-capital conventions as the baseline (Table 7.2).

Results are reported as changes relative to baseline:

$$\Delta\mathrm{MSP}_{\mathrm{low}} = \mathrm{MSP}_{\mathrm{low}} - \mathrm{MSP}_{\mathrm{base}}, \qquad \Delta\mathrm{MSP}_{\mathrm{high}} = \mathrm{MSP}_{\mathrm{high}} - \mathrm{MSP}_{\mathrm{base}}.$$

For price-type parameters (feedstock price, hydrogen price, and fuel-gas export credit), only the relevant unit-price coefficient is perturbed; plant-boundary quantities remain fixed at the Phase 2 technical values. For the capacity parameter, capacity is treated as the independent variable and throughput-linked flows and annualised variable costs scale with throughput according to the workbook implementation, while the process topology and operating assumptions remain unchanged.

This distinction is important for interpretation. The feedstock, hydrogen, and fuel-gas cases are *coefficient-only* cases applied to a fixed technical basis. The capacity case is different: it is the only tested lever that materially rescales the plant while keeping the same pathway configuration and DCF conventions.

8.2.3. Consistency with the technical model and boundary conventions

To confirm that the sensitivity analysis isolates economic drivers rather than implicitly changing process performance, steady-state TPMs were cross-checked across scenarios. For coefficient-only cases (feedstock price, hydrogen price, and fuel-gas monetisation), plant-boundary yields and utility intensities remain unchanged; only the selected economic coefficient is perturbed. For capacity cases, plant-boundary mass and energy flows scale with throughput while maintaining the same pathway configuration and operating assumptions defined in Chapter 5 and quantified in Chapter 6.

System boundary conventions follow Chapters 6–7. In particular, Stream 423 is treated as an exported byproduct fuel-gas stream at battery limits and may be monetised as a fuel-gas export credit. Any continuous vent/purge gas is treated as *vent/purge gas to battery limits (flare header), offsite handling*; no flare combustion is modelled and no flare emissions are claimed.

Table 8.1: One-at-a-time (OAT) sensitivity parameters and variation ranges applied in Chapter 8. The baseline corresponds to the Chapter 7 BASE case (Table 7.2 and Table 7.1); in the OAT analysis, only one parameter is changed at a time while all others remain at baseline.

Parameter	Unit	Low	Baseline	High
Plant capacity (annual throughput)	kt/y	20	40	80
Feedstock price at battery limits	EUR/t	-100	0	$+100$
Hydrogen price multiplier	–	0.5×	1.0×	1.5×
Fuel-gas export monetisation (Stream 423 credit)	%	0%	100%	150%

Notes:
Plant capacity is treated as the independent variable; throughput-linked flows and variable OpEx scale with throughput and CAPEX follows the workbook capacity-scaling rule.

Feedstock price is applied to the plastic feedstock price term at battery limits (gate-fee to paid-feed spectrum); the BASE case uses 0 EUR/t.

Hydrogen price multiplier scales the imported H_2 unit price coefficient; consumption is held constant.

Fuel-gas export monetisation scales the baseline Stream 423 export credit (energy basis, LHV); 0% represents no monetisation/offtake and 150% represents improved valorisation relative to the baseline coefficient.

8.3. Sensitivity cases and ranges

The sensitivity parameters are selected to remain minimal and interpretable, while reflecting the dominant terms highlighted by the MSP contribution view in Chapter 7. This selection is also consistent with the pedigree analysis introduced in subsection 4.3.2 and reported in Appendix B, which highlights boundary-credit/co-product accounting and screening-level cost estimation and scaling (including capacity-linked CAPEX and fixed-cost effects) as comparatively weakly supported elements at the conceptual stage. The set includes one project-level scale lever (plant capacity), two market-facing cost levers (feedstock price and hydrogen price), and one boundary/commercial lever (monetisation of exported fuel gas at battery limits). Ranges are scenario ranges intended to bracket plausible near-term uncertainty and commercial variability; they are not treated as probabilistic inputs.

8.4. Baseline interpretation before sensitivity results

Before the OAT results are introduced, it is useful to restate the baseline economic structure established in Chapter 7, because that structure largely determines how the sensitivity ranking should be interpreted. At the common 40 kt/y basis, the baseline MSP is 2,134.09 EUR/t for the naphtha pathway and 4,939.76 EUR/t for the jet-fuel pathway. As shown in Chapter 7, this large pathway gap is not driven primarily by major differences in total capital investment, total OpEx, or imported hydrogen demand. Rather, it arises from the combination of a fixed-cost-heavy baseline and the pathway-specific MSP closure convention, under which the jet-fuel pathway recovers the residual break-even burden on the smaller Stream 344 main-product basis after naphtha co-product revenue and the fuel-gas export credit are applied.

That same baseline also indicates which sensitivity levers should matter most. Because capital-linked recovery and fixed OpEx dominate the break-even requirement, throughput and scale effects are natural candidates for strong MSP sensitivity. Because Stream 423 provides a meaningful battery-limit credit in the baseline operating statement, fuel-gas monetisation is also expected to be economically important. Feedstock price should remain meaningful because it propagates directly into variable cost, whereas hydrogen price is expected to remain smaller at baseline because hydrogen make-up cost is modest relative to the fixed annual burden and is nearly unchanged between pathways.

The purpose of the following results section is therefore not only to report which lever ranks first, second, third, and fourth, but also to test whether the observed ranking follows the structural expectations implied by the baseline TEA.

Table 8.2: MSP sensitivity summary for the naphtha pathway (MSP solved on Stream 340). Positive $\triangle$MSP indicates an increased break-even price requirement relative to baseline (MSP_{base} = 2 134.09 EUR/t).

Lever	Setting	MSP	$\triangle$MSP (EUR/t)	$\triangle$ (%)
Capacity				
Capacity	20 kt/y	2 735.89	+601.80	+28.2%
Capacity	80 kt/y	1 655.42	−478.67	−22.4%
Feedstock price				
Feedstock price	-100 EUR/t	1 954.62	−179.47	−8.4%
Feedstock price	$+100$ EUR/t	2 310.78	+176.69	+8.3%
Hydrogen price				
H_2 price	0.5×	2 118.98	−15.11	−0.7%
H_2 price	1.5×	2 146.43	+12.34	+0.6%
Fuel-gas export monetisation				
Fuel-gas export credit (Stream 423)	0%	2 363.74	+229.65	+10.8%
Fuel-gas export credit (Stream 423)	150%	2 017.18	−116.91	−5.5%

Table 8.3: MSP sensitivity summary for the jet-fuel pathway (MSP solved on Stream 344; naphtha treated as a fixed-price co-product). Positive $\triangle$MSP indicates an increased break-even price requirement relative to baseline (MSP_{base} = 4 939.76 EUR/t).

Lever	Setting	MSP	$\triangle$MSP (EUR/t)	$\triangle$ (%)
Capacity				
Capacity	20 kt/y	6 802.35	+1 862.58	+37.7%
Capacity	80 kt/y	3 466.07	−1 473.70	−29.8%
Feedstock price				
Feedstock price	-100 EUR/t	4 393.98	−545.79	−11.0%
Feedstock price	$+100$ EUR/t	5 485.55	+545.79	+11.0%
Hydrogen price				
H_2 price	0.5×	4 897.67	−42.10	−0.9%
H_2 price	1.5×	4 981.86	+42.10	+0.9%
Fuel-gas export monetisation				
Fuel-gas export credit (Stream 423)	0%	5 645.39	+705.62	+14.3%
Fuel-gas export credit (Stream 423)	150%	4 586.95	−352.81	−7.1%

8.5. Results: MSP sensitivity and tornado charts

Table 8.2 and Table 8.3 summarise MSP outcomes for the evaluated low and high cases. Baseline MSP values at 40 kt/y are 2 134.09 EUR/t for the naphtha pathway and 4 939.76 EUR/t for the jet-fuel pathway under the Chapter 7 economic basis. These values serve as the reference point for the reported $\triangle$MSP values and the tornado charts. For clarity, the tornado-chart legend refers to the value of the *input parameter* being varied (low parameter value versus high parameter value), not to the resulting MSP level.

The tables should be read in two ways. First, they report the direct numerical consequence of each low and high case. Second, taken together, they provide the numerical basis for ranking the dominant feasibility levers and for the threshold-style decision translation later in the chapter. The jet-fuel pathway also deserves special attention when reading percentage changes, because MSP is solved on Stream 344 after naphtha co-product revenue and the fuel-gas export credit are applied. As a result, a similar annual economic perturbation can translate into a larger percentage swing in jet MSP than in naphtha MSP.

8.5.1. Naphtha pathway

Figure 8.1 presents the OAT sensitivity of MSP for the naphtha pathway (MSP solved on Stream 340). Parameters are ranked by the maximum absolute MSP impact across the low-parameter-value and high-parameter-value cases. Two drivers clearly dominate within the evaluated ranges. First, plant capacity produces the largest MSP response: reducing throughput from 40 to 20 kt/y increases MSP by 28.2%, while increasing throughput to 80 kt/y decreases MSP by 22.4% (Table 8.2). Second, monetisation of exported fuel gas (Stream 423 at battery limits) materially affects MSP: removing the export credit increases MSP by 10.8%, whereas increasing the credit to 150% reduces MSP by 5.5%. Feedstock price produces a moderate MSP shift (approximately -8.4 to $+8.3$%), and the hydrogen price multiplier produces only a minor change (approximately -0.7 to $+0.6$%) under the present configuration.

This ranking is consistent with the baseline economic structure established in Chapter 7. Capacity dominates because the baseline operating statement is fixed-cost heavy: changing throughput changes how strongly capital recovery and fixed OpEx are diluted on a per-tonne basis. Fuel-gas monetisation is the strongest coefficient-type lever because it directly changes one of the largest operating income offsets in the annual economics. By contrast, the hydrogen result is small because hydrogen make-up cost is only a minor share of the total annual burden in the baseline case.

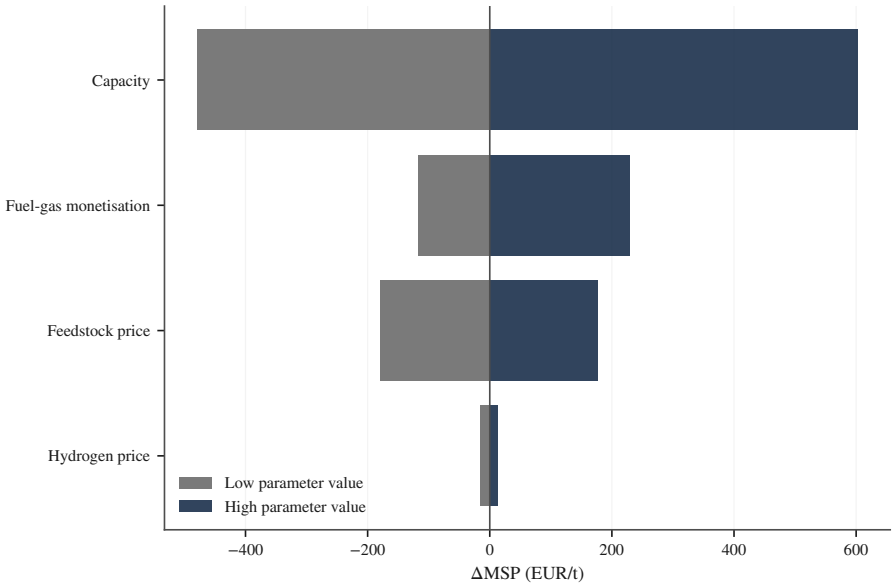

Figure 8.1: One-at-a-time sensitivity of MSP for the naphtha pathway (MSP solved on Stream 340). For each sensitivity lever, the two bars represent the low-parameter-value case and the high-parameter-value case relative to the BASE scenario defined in Table 8.1. Leftward bars indicate a reduction in MSP relative to BASE, while rightward bars indicate an increase. Parameters are ordered by the maximum absolute MSP impact.

8.5.2. Jet-fuel pathway

Figure 8.2 shows the corresponding OAT sensitivity for the jet-fuel pathway, where MSP is solved on jet-range product (Stream 344) and naphtha is treated as a fixed-price co-product revenue stream. As in Figure 8.1, parameters are ranked by the maximum absolute MSP impact across the low-parameter-value and high-parameter-value cases. The qualitative ranking of drivers matches the naphtha pathway but exhibits larger percentage swings. Reducing plant capacity to 20 kt/y increases jet MSP by 37.7% relative to baseline, while increasing capacity to 80 kt/y reduces jet MSP by 29.8%. Removing the fuel-gas export credit increases jet MSP by 14.3%, underscoring the importance of boundary export monetisation when the main-product MSP must recover the residual revenue requirement after co-product credits. Feedstock price remains a mid-level driver ($\pm$11.0%), and hydrogen price has a comparatively small influence ($\pm$0.9%) within the evaluated range.

The larger percentage swings in the jet-fuel pathway should not be read as evidence that the jet-oriented

configuration is categorically “more unstable” in a technical sense. Rather, they follow from the pathway-specific closure convention established in Chapter 7. After naphtha co-product revenue and byproduct credits are applied, the residual break-even burden is recovered on the smaller Stream 344 main-product basis. Economic perturbations that act on that residual burden therefore appear amplified when expressed as percentage changes in jet MSP. The tornado ranking is thus shaped not only by the size of the economic perturbation itself, but also by the pathway-specific denominator on which MSP is solved.

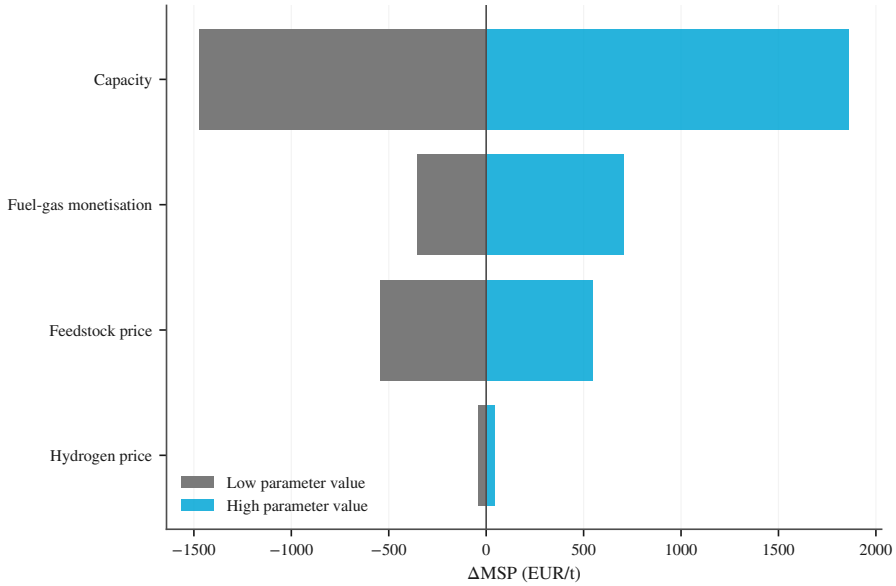

Figure 8.2: One-at-a-time sensitivity of MSP for the jet-fuel pathway (MSP solved on Stream 344; naphtha treated as a fixed-price co-product). For each sensitivity lever, the two bars represent the low-parameter-value case and the high-parameter-value case relative to the BASE scenario defined in Table 8.1. Leftward bars indicate a reduction in MSP relative to BASE, while rightward bars indicate an increase. Parameters are ordered by the maximum absolute MSP impact.

8.6. Decision translation: indicative break-even thresholds

Tornado charts provide a ranked view of influence but do not directly state what a project would need to “do” to improve the economic outcome. To translate sensitivity into more decision-oriented terms without introducing external benchmarks, Table 8.4 reports indicative lever values required to achieve a **10% reduction in MSP** relative to the Chapter 7 baseline in each pathway. The 10% target is used here as an illustrative screening-level improvement benchmark: large enough to be economically meaningful, but still modest enough to compare across levers without implying a specific commercial threshold.

Values are estimated by linear interpolation (or, where necessary, linear extrapolation) between the OAT endpoints in Tables 8.2–8.3. Because capacity scaling is not strictly linear and because some required values fall outside the tested ranges, these thresholds should be interpreted as screening-level decision aids rather than precise design targets.

A practical implication of Table 8.4 is that modest scale-up within the tested range can deliver a 10% MSP reduction in both pathways, while achieving the same improvement purely through improved fuel-gas valorisation would require a multiplier beyond the tested 150% case. For the naphtha pathway, achieving a 10% improvement through feedstock contracting would require a gate-fee magnitude beyond the -100 EUR/t scenario, whereas for the jet-fuel pathway the indicative threshold falls within the tested range.

These observations reinforce the dominant role of capacity selection and boundary export treatment identified by the tornado ranking. They also show why the threshold table should be read as *decision*

Table 8.4: Indicative lever values required to achieve a 10% MSP reduction relative to baseline, estimated by linear interpolation/extrapolation of OAT endpoints. "Out of range" indicates that the required value exceeds the tested high/low range in Table 8.1.

Lever (independent variable)	Naphtha pathway	Jet-fuel pathway
Target MSP (10% below baseline)	$\approx 1{,}921$ EUR/t	$\approx 4{,}446$ EUR/t
Plant capacity (kt/y)	≈ 58 kt/y (within 20–80)	≈ 53 kt/y (within 20–80)
Feedstock price at battery limits (EUR/t)	≈ -119 EUR/t (extrapolation beyond -100)	≈ -91 EUR/t (within tested range)
Fuel-gas export monetisation (Stream 423 credit multiplier)	$\approx 1.91\times$ (out of range; tested to $1.5\times$)	$\approx 1.70\times$ (out of range; tested to $1.5\times$)

translation rather than optimisation advice: it helps identify which levers appear most promising within the current model structure, but it does not replace detailed design, market, or contracting work.

8.7. Interpretation of dominant levers

The sensitivity results separate four parameters into three categories: (i) external contracting and market terms (feedstock price and hydrogen price), (ii) a project-level design choice (capacity), and (iii) a boundary and commercial assumption (Stream 423 export monetisation). This grouping is consistent with the Phase 4 intent in Chapter 4: to distinguish levers that can be influenced by design and commercial integration from those dominated by exogenous markets.

8.7.1. Capacity as the dominant structural lever

Plant capacity is the dominant lever in both pathways. This outcome is consistent with the baseline economic structure in Chapter 7, where capital-linked and fixed-cost components represent a large share of the break-even revenue requirement. Increasing throughput therefore reduces MSP primarily by diluting fixed-capital recovery and fixed operating costs over a larger annual product base. Conversely, reducing throughput sharply increases MSP because the fixed-cost burden remains large while annual product output decreases. Within the tested range, the naphtha pathway shifts by $+28.2\%$ at 20 kt/y and -22.4% at 80 kt/y, while the jet-fuel pathway shifts by $+37.7\%$ and -29.8%, respectively.

The capacity effect is also consistent with the workbook-based scaling behaviour observed across the 20, 40, and 80 kt/y cases. Over that range, total capital investment follows an approximately sub-linear power-law scaling with an exponent of about 0.664 for both pathways. This confirms that the capacity result is not merely a plotting artefact of the tornado chart; it reflects the expected economies of scale of a fixed-cost-heavy screening TEA in which larger throughput reduces the per-ton burden of capital-linked and fixed annual costs.

8.7.2. Fuel-gas monetisation as the strongest operational/commercial lever

The second-most influential lever is monetisation of exported byproduct fuel gas (Stream 423). When the export credit is removed, MSP increases by 10.8% in the naphtha pathway and 14.3% in the jet-fuel pathway (Tables 8.2–8.3). This result highlights that economic conclusions depend not only on purchased inputs but also on how plant-boundary exports are treated.

A conservative assumption (no monetisation or no viable offtake) materially increases the break-even price requirement, while improved valorisation reduces it. Importantly, this lever acts through *boundary accounting and commercial realisation* rather than through a redesign of internal process performance. Stream 423 exists as a technical output in the plant-boundary balances established in Chapter 6; the sensitivity reflects the question of whether, and on what terms, that surplus can actually be placed, used, or contracted outside the battery limits. For that reason, the economic importance of the fuel-gas lever is real within the model logic, but its realised value remains commercially contingent.

8.7.3. Feedstock price as a mid-level contracting lever

Feedstock price produces a clear but moderate MSP response in both pathways. The response remains close to symmetric around the 0 EUR/t baseline and reflects direct propagation of the feedstock-price term into variable operating costs under fixed technical performance. In the final baseline, the naphtha pathway shifts by about -8.4% to $+8.3\%$, while the jet-fuel pathway shifts by $\pm 11.0\%$.

From a project-development perspective, this lever maps to contracting strategy and waste-system context rather than process redesign. In other words, the feedstock result should be read primarily as a statement about gate-fee versus paid-feed conditions at battery limits, not as a statement that the process itself becomes technically different across scenarios. The threshold table reinforces this interpretation: a 10% MSP improvement through feedstock terms alone appears achievable within the tested range for the jet-fuel pathway, but requires extrapolation beyond the tested range for the naphtha pathway.

8.7.4. Hydrogen price as a second-order lever in the current model configuration

Within the evaluated range (0.5$\times$ to 1.5$\times$), hydrogen price has the smallest effect on MSP. This is not a general statement that hydrogen is economically irrelevant for plastic pyrolysis and upgrading. Rather, it reflects the relative weight of hydrogen make-up costs within the overall MSP burden for the present conceptual design and fixed technical basis. In the current configuration, the MSP response is limited to about -0.7% to $+0.6\%$ in the naphtha pathway and -0.9% to $+0.9\%$ in the jet-fuel pathway.

This small response is fully consistent with the baseline interpretation in Chapters 6–7. Imported hydrogen intensity is nearly unchanged between pathways, and hydrogen make-up remains modest relative to the annual fixed-cost burden. Under alternative configurations with higher hydrogen demand, different severity assumptions, or a different boundary treatment of hydrogen supply, this ranking could change. Within the current model, however, hydrogen is clearly not the first-order feasibility lever.

8.7.5. Why the jet-fuel pathway shows larger percentage swings

Finally, the jet-fuel pathway exhibits larger percentage sensitivity to the dominant levers, especially capacity and Stream 423 monetisation. This follows directly from the pathway-specific MSP definition. After co-product credits are applied, the jet-range product carries the residual revenue requirement that closes the DCF break-even condition. The same class of economic perturbation therefore appears amplified when expressed as a percentage change in jet MSP, because the perturbation is propagated onto a smaller main-product denominator.

This point is important for interpretation. The larger percentage swings in the jet-fuel pathway do not imply that the plant is inherently more variable in a technical sense; they reflect how the residual annual burden is allocated under the pathway-specific MSP closure convention.

8.8. Chapter conclusions and implications for the thesis

8.8.1. Answer to Sub-Research Question 4

Sub-Research Question 4: How sensitive are the economic outcomes of each pathway to variations in key assumptions, and which parameters are the primary drivers of feasibility?

This chapter answers the question by re-solving MSP at NPV$= 0$ under a transparent one-at-a-time (OAT) sensitivity design, while holding the Chapter 7 DCF conventions and pathway-specific MSP closure rules fixed. Four parameters were perturbed relative to the BASE case: plant capacity, feedstock price at battery limits (with the BASE gate price set to 0 EUR/t), imported hydrogen price, and the monetisation of exported byproduct fuel gas at battery limits (Stream 423). The resulting MSP responses therefore isolate the influence of each assumption on the break-even selling price, conditional on the fixed system configuration and steady-state performance basis defined in earlier chapters.

Across both pathways, plant capacity is the dominant driver of MSP within the evaluated ranges. This result is a structural consequence of the baseline TEA established in Chapter 7, where capital-linked and fixed operating costs make up the largest share of the annual revenue requirement. The second-most influential lever is the treatment of exported fuel gas. Because Stream 423 represents a monetised boundary export in the BASE case, removing this credit yields a material MSP increase, while improving valorisation reduces the required selling price. Feedstock price at the plant gate produces a moderate MSP response by propagating directly into variable operating cost, whereas hydrogen price is comparatively less influential within the tested range for the present configuration.

Taken together, the sensitivity outcomes show that the feasibility interpretation for both pathways is controlled primarily by assumptions that affect scale-linked cost recovery and by boundary-credit realisation, rather than by modest swings in hydrogen price under the current technical basis. Quantitatively, the dominant responses are largest for capacity ($+28.2\%$ / -22.4% in the naphtha pathway and $+37.7\%$ / -29.8% in the jet-fuel pathway), followed by fuel-gas monetisation and then feedstock price, with hydrogen price remaining a minor lever in the present model configuration.

8.8.2. Implications for project levers and thesis conclusions

The sensitivity ranking provides a clear prioritisation of the practical levers that would most effectively shift MSP under the modelling basis used in this thesis. The threshold analysis presented in Table 8.4 translates relative sensitivity into indicative conditions required to achieve a modest improvement, defined here as a 10% reduction in MSP relative to the baseline. Within the tested ranges, such an improvement is achievable primarily through scale-up, with the results indicating that increasing capacity to approximately 58 kt/y in the naphtha pathway and 53 kt/y in the jet-fuel pathway can deliver an MSP reduction of this magnitude under otherwise unchanged assumptions. Achieving a comparable reduction through enhanced fuel-gas valorisation would require conditions beyond the ranges explored in this chapter in both pathways, while feedstock contracting would need to go beyond the tested range in the naphtha pathway but falls within the tested range for the jet-fuel pathway. These threshold values should therefore be interpreted as screening-level guidance rather than as precise design targets.

In terms of the assessment framework defined in Chapter 4, the chapter completes Phase 4 by identifying which uncertainties most strongly govern the economic outcomes derived in Phase 3. Read in combination with the fixed system definition in Chapter 5 and the steady-state TPM basis in Chapter 6, the results show that the thesis-level feasibility interpretation is most sensitive to (i) scale selection and associated utilisation assumptions implicit in capacity choice, (ii) the commercial ability to monetise battery-limit fuel-gas exports (Stream 423), and (iii) feedstock contracting terms at the plant gate. Conversely, within the tested range and given the present process configuration, hydrogen price is a second-order driver.

These findings provide a focused bridge to the Discussion and Conclusion chapters. The Discussion can use the sensitivity ranking to interpret which parts of the baseline TEA are structurally robust and which remain contingent on a small number of high-leverage assumptions, especially screening-level scale effects and boundary-credit treatment. The Conclusion can then answer the research questions at system level by synthesising the pathway comparison, baseline MSP outcomes, and dominant robustness levers without repeating the detailed parameter-by-parameter results reported here.

9

Discussion

Chapters 1–3 established the motivation for this work: plastic production continues to grow while end-of-life management remains dominated by disposal and energy recovery, and mechanical recycling faces persistent challenges for contaminated and complex polyolefin-rich packaging streams. This motivates advanced recycling routes that can convert polyolefin-rich residual waste into refinery- and petrochemical-relevant intermediates, with pyrolysis frequently proposed as a promising thermochemical option for producing a liquid hydrocarbon intermediate. At the same time, Chapter 3 showed that the available literature remains difficult to interpret in a directly comparative way because feedstock basis, pretreatment quality, upgrading assumptions, product definitions, and system boundaries are often non-aligned. For real residual feeds such as Dutch DKR 350, the literature also indicates that pretreatment can improve the starting point for upgrading, but does not remove the need for impurity-focused downstream treatment [26], [79], [81]..

Against this background, this thesis quantified how a gate-to-gate plastic pyrolysis and upgrading system performs when configured to produce either a naphtha-range blendstock or a jet-range blendstock. The fixed system configuration and modelling scope are defined in Chapter 5, technical plant-boundary performance is reported in Chapter 6, economic performance is evaluated via MSP under a consistent discounted-cash-flow basis in Chapter 7, and robustness is tested via one-at-a-time sensitivity and decision-translation thresholds in Chapter 8. The discussion chapter therefore does not introduce a new model. Its role is to integrate and interpret the results produced by the preceding chapters and to relate them back to the literature and wider system context.

The assessment is explicitly scoped to the A100–A400 gate-to-gate boundary. Reported indicators therefore represent plant-boundary material, utility, and economic bookkeeping within this boundary, without extending to upstream burdens (e.g. hydrogen production or electricity generation), downstream blending and certification, or a market study of offtake feasibility. The thesis also does not perform an LCA, so any environmental relevance is discussed only through plant-boundary proxies and boundary-stream interpretation rather than through cradle-to-grave claims. These scope choices matter for the present chapter, because they determine both what can be interpreted confidently and what must remain outside the strength of claim.

Importantly, the two pathways are not interpreted as a like-for-like comparison of interchangeable end-products. Instead, they are interpreted as the incremental system consequences of targeting a stricter product-recovery intent (recovering an additional jet-range cut) under a shared conversion front-end and a consistent plant boundary. This interpretation is essential for reading the economic results, because pathway comparisons are shaped not only by technical performance but also by the adopted MSP closure conventions in Chapter 7: MSP is solved on Stream 340 for the naphtha pathway and on

Stream 344 for the jet-fuel pathway, while naphtha is treated as a fixed-price co-product in the jet-fuel pathway. More broadly, the two pathways also point toward different external contexts: the naphtha pathway is most naturally aligned with petrochemical circularity and cracker-relevant integration, whereas the jet-fuel pathway points toward a more demanding downstream market shaped by stricter property windows and qualification requirements [26], [100].

A second organising principle for this chapter is *claim strength*. Numerical closure and bookkeeping consistency are necessary but do not, by themselves, communicate how strongly each modelling element is supported by empirical evidence. To address this, the thesis introduced a pedigree analysis in Chapter 4 (subsection 4.3.2) and reported consolidated results in Appendix B. Throughout this discussion, interpretations are therefore framed as (i) robust within the defined boundary and bookkeeping structure, (ii) indicative or directional within the screening representation, or (iii) commercially contingent where results depend on boundary monetisation and co-product conventions. This framing also supports interpreting the sensitivity ranges in Chapter 8 as scenario bounds rather than probability-weighted confidence intervals.

The chapter proceeds in six steps. Section 9.1 summarises the cross-chapter headline findings and positions them against the broader literature on real residual-feed pyrolysis, specification-oriented upgrading, and TEA comparability. Sections 9.2 and 9.3 then interpret the technical and economic outcomes, with explicit attention to product redistribution, downstream utility burden, MSP closure logic, fixed-cost dominance, and the treatment of boundary exports. Section 9.4 translates the sensitivity results into decision-relevant levers and clarifies what the tested ranges do, and do not, imply. Section 9.5 applies the pedigree results to qualify how strongly the thesis conclusions can be generalised and to identify where stronger evidence would most improve interpretation. Finally, Section 9.6 closes with an integrated synthesis that bridges to the separate Conclusion chapter.

9.1. Headline findings

This section synthesises the main outcomes from Chapters 6–8. Together, these findings address the linked sub-research questions posed in Chapter 4 (technical performance, economic feasibility, and robustness; see section 4.1) and establish the discussion points developed in the remainder of this chapter. To support transparent interpretation, each headline finding is tagged with an indicative claim-strength qualifier, consistent with the pedigree framing introduced in subsection 4.3.2 and Appendix B. Read together with Chapter 3, these headline findings also indicate where the present thesis aligns with, sharpens, or helps organise the wider literature on real residual-feed pyrolysis, specification-oriented upgrading, and plastic-pyrolysis TEA comparability.

- **The pathways differ mainly by *product redistribution*, not by total saleable liquid yield.**

  At plant boundary, total saleable liquid yield is essentially unchanged between the naphtha and jet-fuel pathways (0.5615 vs. 0.5632 kg/kg feed), while the jet-fuel pathway partitions the saleable pool into a naphtha-range product (0.3800 kg/kg feed, Stream 340) and a jet-range blendstock (0.1832 kg/kg feed, Stream 344) (Table 6.12). This supports reading the pathway difference primarily as a downstream recovery and product-intent effect rather than as a major change in front-end conversion. In that sense, the result is consistent with the literature reviewed in Chapter 3, which shows that for real mixed-plastic feeds the decisive issue is often not total liquid production alone, but how the liquid pool can be partitioned and upgraded toward specification-relevant blendstocks under realistic impurity constraints [18], [79], [81].

- **Imported hydrogen is not a baseline differentiator, whereas electricity demand is.**

  At plant boundary, imported H_2 intensity is effectively identical across pathways (0.02251 vs. 0.02253 kg/kg feed), while electricity intensity increases from 22.48 to 43.98 kWh/t feed in the jet-fuel pathway (Table 6.12). This indicates that baseline pathway differentiation is expressed more through plant-level utility burdens than through make-up hydrogen demand. Within the adopted screening representation, the electricity result should therefore be read as a system-level conse-

quence of the stricter jet-recovery objective rather than as evidence of a fundamentally different hydrogen requirement or a fully resolved unit-by-unit utility attribution.

- **Baseline MSP outcomes are high, and the jet MSP is higher largely due to MSP closure and main-product basis.**

  The naphtha pathway MSP is 2,134 EUR/t (solved on Stream 340), while the jet-fuel pathway MSP is 4,940 EUR/t (solved on Stream 344, with naphtha treated as a fixed-price co-product) (Table 7.1, section 7.1). The difference is shaped less by large differences in total annual OpEx or TCI than by the pathway-specific closure convention and the smaller main-product denominator in the jet-fuel pathway. This is an important discussion point because Chapter 3 identified non-aligned product definitions, upgrading assumptions, and boundary conventions as a central reason why published plastic-pyrolysis TEAs are difficult to compare directly [17], [18].

- **Boundary exports are economically material and strongly shape MSP under the adopted monetisation assumptions.**

  Both pathways export a substantial fuel-gas surplus (Stream 423) at battery limits (13.47 vs. 13.43 MJ/kg feed, Table 6.12). In the sensitivity analysis, removing the fuel-gas export credit increases MSP by 10.8% (naphtha pathway) and 14.3% (jet-fuel pathway) (Table 8.2–8.3). The implication is that plant-boundary export treatment is not a bookkeeping detail but a major feasibility determinant under the adopted gate-to-gate TEA basis. This aligns with the wider literature, which shows that product routing, upgrading extent, and downstream integration assumptions strongly shape whether pyrolysis-derived streams are interpreted as fuels, blendstocks, or chemical feedstocks [18], [26], [99].

- **Feasibility is dominated by scale, followed by fuel-gas monetisation; other coefficient changes are second-order within the tested ranges.**

  Capacity is the dominant MSP lever in both pathways (Figure 8.1–8.2), consistent with a fixed-cost-heavy cost structure. The decision-translation table shows that a 10% MSP improvement is achievable through modest scale-up within the tested range, whereas achieving the same improvement purely via boundary-credit or feedstock-price changes requires conditions outside the evaluated ranges (Table 8.4). This ranking is also consistent with the limited TEA literature, which repeatedly identifies plant scale and product-rate realisation as decisive economic drivers while highlighting the scarcity of full-scale, directly comparable cases [17], [18].

The remainder of the chapter explains why these patterns arise within the defined A100–A400 boundary and under the adopted MSP conventions, relates them more explicitly to the literature reviewed in Chapter 3, and then qualifies how strongly they can be generalised beyond the present screening assumptions using the pedigree lens (Appendix B).

9.2. Technical interpretation

9.2.1. Product redistribution

Chapters 5 and 6 define a shared system boundary, throughput basis, and front-end conversion configuration for both pathways, with pathway differentiation implemented primarily in Area A300 through the product-recovery objective (subsection 5.4.1, section 6.6). The TPM dashboard confirms that total saleable liquid yield remains comparable between pathways, while the product slate shifts from a single naphtha-range product to a split between naphtha-range and jet-range blendstocks (Table 6.12). This outcome supports two related interpretations.

First, within the model structure, changing the recovery objective reallocates the upgraded liquid pool into different saleable cuts rather than materially changing overall conversion at the plant boundary. The naphtha pathway recovers the saleable pool as naphtha (Stream 340), whereas the jet-fuel pathway recovers an additional jet-range fraction (Stream 344) at the expense of the naphtha fraction, while

maintaining a similar total saleable liquid yield on a plastic-feed basis (Table 6.8, Table 6.12). The pathways therefore represent alternative product intents under a common conversion basis, consistent with the modelling objective of isolating the effect of downstream recovery choices.

This reading is also consistent with the literature reviewed in Chapter 3. For real mixed-plastic feeds, the decisive issue is often not total liquid production alone, but how the liquid pool can be partitioned and upgraded toward specification-relevant blendstocks under realistic impurity constraints [18], [79], [80], [81], [82]. In this sense, the present result should not be read as showing that the two pathways are technically equivalent in product quality terms. Rather, it shows that under a shared conversion front-end, the stricter outlet intent primarily reshapes the distribution of the saleable liquid pool. This is an important distinction because Chapter 3 argued that upgrading for both cracker-relevant naphtha and jet-range blendstocks is driven by specification intent, olefinicity, and trace contaminants, not by boiling range alone [26], [100].

Second, because the heavy purge stream remains small in both pathways (Table 6.12), the pathway distinction is not driven by increased rejection of heavy material at the boundary. Instead, the heavy purge stabilises the heavy-end management structure introduced in Chapter 5 and creates a boundary stream requiring handling assumptions (Chapter 6). This matters economically because even small boundary streams can map to cost terms or disposal assumptions in the operating statement, but it does not change the core conclusion that pathway differentiation is dominated by how the saleable liquid pool is partitioned.

A practical nuance is that slate redistribution also functions as a proxy for product intent and quality constraints. The thesis treats the jet product as a jet-range blendstock recovered by cut logic rather than as a certified SAF or Jet-A fuel, and this distinction should remain explicit when interpreting the technical outcomes in a gate-to-gate screening context. The broader jet-fuel literature reinforces this caution: jet-oriented fractions are governed by property windows, stability requirements, and downstream qualification constraints that can remain limiting even when a jet-range cut exists [100], [103].

9.2.2. Utility burdens

The second prominent technical difference is electricity intensity. It increases from 22.48 to 43.98 kWh/t feed between the naphtha and jet-fuel pathways (Table 6.12). Within the adopted screening representation, this increase is interpreted as a system-level consequence of recovering and conditioning an additional saleable product cut in the jet-fuel pathway. The jet-fuel pathway imposes a stricter recovery objective in Area A300, and this objective is associated with additional separation, handling, and utility demands aggregated at plant level in the reported A300 and A400 totals (Chapter 6). Because utilities are reported as consolidated duties and electricity consumption is not attributed to individual unit operations at a detailed equipment level, the appropriate interpretation is directional: the jet-fuel recovery objective is more utility-intensive under the modelling structure used, and electricity remains a key technical differentiator between pathways.

This directional reading is consistent with the wider upgrading literature, but it should not be overstated. Hydrotreating studies show that upgrading plastic-derived oils is strongly linked to impurity removal and compositional stabilisation, including reductions in chlorine, nitrogen, and olefinicity [26], [106]. Hydrocracking studies likewise show that reshaping the boiling-range distribution toward lighter or more targeted fractions involves trade-offs among naphtha, middle-distillate, gas, and coke production [103], [109]. What these studies support is the general proposition that stricter downstream upgrading and fractionation objectives are likely to increase processing burden and handling complexity. What they do not provide is a directly transferable equipment-level utility coefficient for the Dutch DKR 350-derived system assessed here. For that reason, the electricity result should remain framed as a system-level signal within the adopted screening model rather than as a precise mechanistic claim about a single unit or compressor train.

By contrast, imported H_2 intensity is nearly identical across pathways (0.02251 versus 0.02253 kg/kg

feed, Table 6.12). This indicates that, at the plant boundary and under the fixed upgrading bases, hydrogen make-up does not drive pathway differentiation in the baseline configuration. The implication is that the higher MSP of the jet-fuel pathway cannot be attributed to a substantially higher imported hydrogen requirement at baseline, and should instead be explained through the MSP closure convention, product basis, and fixed-cost structure discussed in section 9.3. This does not mean that hydrogen is unimportant in plastic-oil upgrading more generally; rather, it means that under the present shared-topology comparison its baseline contribution does not emerge as the principal technical differentiator.

9.2.3. Boundary streams

Several plant-boundary streams reported in Chapter 6 are small in mass terms but economically consequential because they map directly to cost or credit coefficients in Chapter 7. The most prominent example is the surplus fuel-gas export (Stream 423), reported as a net fuel-gas surplus intensity of 13.47 and 13.43 MJ/kg feed in the naphtha and jet-fuel pathways, respectively (Table 6.12). In the economic model, this export is monetised as a variable operating income offset on an LHV basis (Chapter 7). The sensitivity analysis further shows that the treatment of this boundary export is among the dominant drivers of MSP outcomes (Figure 8.1–8.2).

This point is especially important in light of the TEA literature reviewed in Chapter 3. Published plastic-pyrolysis TEAs vary widely in how off-gases and other boundary streams are treated: some combust NCG and char internally for process heat, some route gases to CHP systems, and others treat light ends, credits, and utility offsets less transparently [17], [18], [93], [94]. The present thesis therefore does not interpret fuel-gas treatment as a minor bookkeeping detail. Rather, it should be read as one of the central comparability issues in plastic-pyrolysis TEA: under a gate-to-gate basis, the technical existence of a battery-limits gas export is robust, but its economic value depends on downstream handling, integration opportunities, and contractual conditions outside the plant boundary.

A second example is the vent/purge stream discharged at battery limits and the stripped water discharge, both reported in the TPM dashboard (Table 6.12). These streams represent boundary handling quantities that translate into operating costs or boundary accounting assumptions in Chapter 7. Importantly, Chapter 6 limits direct CO_2 reporting to on-site combustion only and does not model flare combustion, preserving consistency between technical reporting and boundary monetisation assumptions. The interpretation is therefore twofold: first, feasibility is sensitive to how boundary streams are treated commercially and operationally, even when their mass contributions are small relative to saleable liquids; second, maintaining one consistent battery-limits convention across Chapters 5–8 is methodologically important precisely because the literature shows that alternative routing assumptions can materially reshape TEA outcomes.

Taken together, the technical results indicate that pathway differentiation is concentrated downstream rather than in the shared conversion front-end. The most important technical consequences of the stricter jet-oriented recovery objective are the redistribution of the saleable liquid pool, the increase in aggregated electricity demand, and the continued importance of boundary-stream treatment as an economic interface. This conclusion provides the immediate bridge to the next section: once the technical differentiation is understood as a downstream product-intent and boundary-accounting problem, the baseline MSP gap can be interpreted more clearly in terms of closure convention, main-product basis, and fixed-cost structure rather than by assuming a fundamentally different plant-wide conversion burden.

9.3. Economic interpretation

9.3.1. MSP closure and main-product basis

The MSP results reported in Chapter 7 are a function of both (i) the operating statement, comprising annualised CAPEX-linked charges, fixed OpEx, variable OpEx, and boundary credits, and (ii) the MSP closure convention, meaning which product stream is solved for at discounted-cash-flow break-even.

These conventions are defined explicitly in section 7.1 and must remain visible when interpreting pathway differences.

In the naphtha pathway, MSP is solved on the naphtha-range product exported as Stream 340. In the jet-fuel pathway, MSP is solved on the jet-range product exported as Stream 344, while naphtha is treated as a fixed-price co-product revenue stream. Under this convention, the jet product recovers the residual annual revenue requirement after co-product naphtha revenue and byproduct fuel-gas credits have already been accounted for. Conceptually, MSP satisfies the break-even condition that discounted revenues equal discounted costs over the project lifetime. At an annualised level, this can be expressed as

$$\underbrace{P_{\mathrm{main}} \cdot M_{\mathrm{main,yr}}}_{\text{main-product revenue}} + \underbrace{\sum_i P_i \cdot M_{i,\mathrm{yr}}}_{\text{co-product revenue}} + \underbrace{\sum_j C_{j,\mathrm{yr}}}_{\text{credits (e.g. fuel gas)}} = \underbrace{\text{Annualised CAPEX} + \mathrm{OpEx}_{\mathrm{yr}}}_{\text{annual requirement}}. \tag{9.1}$$

In the jet-fuel pathway, the main-product term is evaluated on Stream 344 only. Because the total saleable liquid pool is partitioned between Stream 340 and Stream 344, the jet MSP is recovered over a smaller main-product mass basis (baseline jet yield of 0.1832 kg/kg feed, Table 6.12) than the naphtha pathway (baseline naphtha yield of 0.5615 kg/kg feed, Table 6.12). This denominator effect does not imply that the jet-fuel pathway has substantially lower total saleable liquid conversion. Rather, it reflects how the residual annual requirement is allocated under the stated co-product and MSP conventions. This mechanism explains why the jet MSP can be substantially higher even when total saleable liquids are comparable across pathways and imported hydrogen intensity is essentially unchanged.

This interpretation also clarifies what the present thesis adds relative to the literature reviewed in Chapter 3. The TEA literature on plastic pyrolysis is difficult to compare directly because feed basis, upgrading extent, product definitions, and boundary assumptions often vary simultaneously [17], [18]. By contrast, the present thesis fixes feed basis, plant topology, and gate-to-gate accounting conventions across the two pathways. The pathway gap can therefore be interpreted more cleanly as a consequence of product partitioning and MSP closure convention, rather than as the compound effect of multiple non-aligned design changes. In that sense, the higher jet-pathway MSP should be read primarily as an accounting and denominator effect under a stricter outlet intent, not as evidence that the entire plant becomes uniformly more expensive in annual terms.

9.3.2. Fixed-cost structure

Chapter 7 shows that the baseline operating statement is dominated by CAPEX-linked charges and fixed operating costs, while variable operating costs are smaller and are primarily associated with purchased hydrogen and utilities (Table 7.1; Figure 7.2). Within the model logic, this structure is consistent with a conceptual, capital-intensive plant configuration evaluated at a fixed 40 kt/y basis and costed using screening-level methods typical of early-stage TEA. The baseline MSP is therefore shaped mainly by the magnitude of the annual fixed-cost burden that must be recovered through product sales after accounting for byproduct and co-product revenues.

This fixed-cost dominance provides the most direct bridge to Chapter 8. If the largest terms are largely throughput-invariant at baseline, then increasing capacity dilutes these terms on a per-ton basis, while decreasing capacity amplifies them. The fact that capacity is the dominant MSP lever in both tornado charts (Figure 8.1–8.2) is therefore a structural consequence of the fixed-cost-heavy operating statement rather than a pathway-specific anomaly.

The broader TEA literature points in the same direction, although usually under less directly comparable assumptions. Laghezza et al. review a field still dominated by laboratory studies and note the scarcity of full-scale, directly comparable economic cases [18]. Fivga and Dimitriou likewise show strong sensitivity of plastic-pyrolysis economics to throughput and scale, with economies of scale rapidly reducing

production cost as plant capacity increases [17]. The present thesis aligns with that broader pattern, but the contribution here is more controlled: scale sensitivity is demonstrated for two pathway intents under one shared technical basis and one common financial structure. This makes the ranking itself more informative than a simple cross-study comparison of absolute prices.

The strength of this interpretation remains bounded by the pedigree results. Appendix B indicates strongest support for the financial model structure and closure logic, while the empirical basis is weaker for screening-level CAPEX and fixed-OpEx estimation. Consequently, the qualitative conclusion that fixed costs dominate MSP is robust within the adopted accounting framework, but the absolute MSP magnitudes remain screening-level outcomes rather than bankable project estimates.

9.3.3. Boundary credits and co-products

The economic outcomes depend materially on how boundary exports and co-products are treated. In both pathways, the plant exports surplus fuel gas at battery limits (Stream 423) and receives a revenue credit evaluated on an LHV basis (Chapter 7). In the jet-fuel pathway, naphtha revenue is additionally booked as a fixed-price co-product income stream, reducing the residual annual revenue requirement that must be recovered via jet MSP. These credits directly interact with the closure convention discussed in subsection 9.3.1.

The sensitivity analysis underscores this dependence: removing the fuel-gas export credit increases MSP by 10.8% in the naphtha pathway and 14.3% in the jet-fuel pathway (Table 8.2–8.3). The larger swing in the jet-fuel pathway is consistent with the smaller main-product basis and the fact that the remaining burden is recovered on Stream 344 after credits have been booked. This reinforces the interpretation from Sections 9.1 and 9.2.3: boundary treatment is not an incidental accounting detail but one of the central determinants of screening feasibility.

This point is also strongly supported by the literature reviewed in Chapter 3. Published plastic-pyrolysis TEAs vary widely in how light ends, gases, and other boundary streams are routed and valued, and this is one of the main reasons why economic results are difficult to benchmark directly [17], [18]. Likewise, the upgrading literature shows that whether pyrolysis-derived streams are interpreted as fuel substitutes, petrochemical feedstocks, or intermediate blendstocks depends heavily on how much downstream treatment is assumed and where credits are booked [26], [99]. Accordingly, conclusions that depend strongly on monetising exported fuel gas or on assumed co-product pricing should remain framed as commercially contingent: they describe what the model implies under the adopted boundary accounting assumptions, not what any specific offtake contract or market arrangement will guarantee.

9.3.4. Market context

The MSP values reported in Chapter 7 represent break-even prices under the adopted screening basis and boundary conventions. A contextual benchmark comparison to fossil-derived indicators is provided in subsection 7.6.1 and is used here only to situate the screening-level feasibility gap implied by the baseline MSP results, not to present a market forecast. The interpretation remains decision-oriented within the defined A100–A400 boundary: under baseline assumptions, the assessed configurations are unlikely to be competitive on price alone without substantial improvement in the dominant levers identified in Chapter 8, especially scale and boundary-credit realisation.

At the same time, the two pathways should not be read as if they were aimed at the same downstream market. The naphtha pathway is most naturally situated in the logic of petrochemical circularity, where the value of the product lies in its relevance as a cracker-oriented blendstock and its potential integration into existing petrochemical infrastructure. This is consistent with the Rotterdam–Moerdijk location logic adopted earlier in the thesis, where proximity to sorting, refining, and petrochemical assets provides the contextual rationale for a naphtha-oriented upgrading route (Chapter 5). In that setting, the feasibility question is closely tied to whether sufficiently stable, sufficiently clean, and sufficiently integrated feedstock and product interfaces can be established.

The jet-fuel pathway points toward a different external logic. Here, the stricter recovery objective is motivated by the wider decarbonisation challenge of aviation, but that challenge does not by itself remove the technical and commercial barriers associated with jet-oriented fractions. The recent SAF literature continues to emphasise that aviation fuels are governed by demanding property windows, qualification pathways, and blending constraints, and that many alternative jet-fuel routes remain certification- and market-constrained even when a technically plausible jet-range cut exists [100], [103]. The present thesis therefore does not interpret the higher jet-pathway MSP simply as a sign that the jet route is "worse" in a generic sense. Rather, it suggests that under the adopted screening conventions the stricter product intent imposes a larger residual economic burden on a smaller main-product denominator, while also pointing toward a market with more stringent downstream requirements.

Seen this way, the baseline feasibility gap has a different meaning in each pathway. For the naphtha pathway, it indicates a screening-level challenge of closing the loop economically into petrochemical feedstock logic under current scale and boundary assumptions. For the jet-fuel pathway, it indicates not only a break-even price challenge, but also the fact that the route targets a more tightly constrained downstream value chain. This broader context does not overturn the central economic reading of the chapter; instead, it clarifies why pathway comparison must be interpreted alongside closure convention, downstream market role, and specification stringency rather than as a simple comparison of two near-substitutable products.

9.4. Robustness and decision levers

9.4.1. Dominant sensitivity levers

The tornado charts in Chapter 8 rank MSP sensitivity to one-at-a-time parameter variations within predefined ranges (Figure 8.1–8.2). Across both pathways, two levers clearly dominate: plant capacity and the monetisation of exported fuel gas (Stream 423). This ranking follows directly from the baseline economic structure interpreted in Section 9.3: MSP is shaped primarily by a fixed-cost-heavy operating statement and by the treatment of economically meaningful boundary exports.

Capacity dominates because the annual revenue requirement is strongly influenced by annualised CAPEX and fixed OpEx, both of which are large relative to variable-cost terms in the baseline TEA (Chapter 7). Increasing throughput therefore dilutes these large fixed terms on a per-tonne basis, while decreasing throughput amplifies them. The large MSP swings observed for 20–80 kt/y relative to the 40 kt/y baseline (Table 8.2–8.3) are thus interpreted as a structural consequence of the cost-sheet formulation and scaling logic rather than as a pathway-specific anomaly. In that sense, the sensitivity ranking is fully consistent with the fixed-cost reading developed in Section 9.3.2.

This pattern is also consistent with the broader TEA literature, although the available comparison base remains limited. Fivga and Dimitriou report strong cost reductions with scale-up in plastic-waste pyrolysis to fuel, showing that economic feasibility improves rapidly as throughput increases [17]. Laghezza et al. likewise identify the scarcity of directly comparable full-scale TEA studies as one of the key gaps in the field, while still highlighting scale and industrial implementation as central feasibility determinants [18]. The present thesis aligns with that broader pattern, but the comparison here is methodologically tighter: scale sensitivity is demonstrated for two outlet intents under one fixed technical basis, one fixed gate-to-gate boundary, and one shared DCF framework. The ranking is therefore more informative than a simple comparison of absolute selling prices across unrelated studies.

Fuel-gas monetisation is the second dominant lever because it affects one of the largest revenue offsets in the operating statement. When the export credit is removed, MSP increases materially in both pathways (Table 8.2–8.3). Importantly, this lever acts through boundary accounting and commercial offtake conditions rather than through internal process performance: the fuel gas exists as a technical output in the plant-boundary balances (Table 6.12), but its economic value depends on whether it can be exported, at what specification, and at what contractual value. This directly reinforces the argument made earlier in Sections 9.2.3 and 9.3.3: boundary-stream treatment is one of the main

bridges between technical bookkeeping and economic feasibility.

This boundary dependence is also a literature-facing point. Chapter 3 identified non-aligned routing and valuation of light ends, byproducts, and intermediate streams as a major reason why plastic-pyrolysis TEAs are difficult to compare. Kusenberg et al. similarly emphasise that pyrolysis-oil valorisation depends heavily on contaminant levels, upgrading steps, and downstream integration assumptions, all of which affect where value can be booked in the chain [26]. Accordingly, while the sensitivity ranking robustly indicates that fuel-gas treatment matters, the magnitude of its economic benefit remains commercially contingent rather than technically guaranteed.

Other coefficient-only drivers, including feedstock price and hydrogen price, show smaller relative influence within the tested ranges. This should not be interpreted as a general claim that these variables are unimportant for plastic-pyrolysis economics. It is a statement about the present model structure at the 40 kt/y basis: when fixed costs dominate the annual requirement, changes to smaller variable-cost terms yield smaller proportional changes in MSP. In other words, the ranking is model-structural and range-specific, not universal.

9.4.2. Decision thresholds

While tornado charts rank relative influence, Table 8.4 translates sensitivity into indicative conditions required to achieve a modest improvement target, defined here as a 10% MSP reduction relative to the Chapter 7 baseline. This threshold framing is especially useful for discussion because it shifts the interpretation from “which parameter matters most” to “which improvement route is realistically available within the evaluated scenario space”.

Two conclusions follow from Table 8.4. First, a 10% MSP reduction is achievable through modest scale-up within the tested capacity range for both pathways. This reinforces the interpretation that the most direct lever available within the present model structure is an engineering and project-development decision: selecting a sufficiently large plant scale, with associated utilisation, to dilute fixed costs over a larger throughput basis. In practical terms, this means that feasibility improvement in the present thesis is driven more by project configuration than by fine-tuning small variable-cost coefficients.

Second, achieving a 10% reduction purely through improved fuel-gas valorisation requires conditions outside the tested ranges in both pathways and should therefore be treated as a stretch condition rather than as a baseline expectation. This does not make fuel-gas valorisation unimportant; on the contrary, it confirms that the export stream is economically material. But it does show that under the current assumptions, scale-up is the more accessible improvement route within the evaluated design space. For feedstock contracting, the same general reading holds for the naphtha pathway, whereas the indicative threshold for the jet-fuel pathway falls within the tested range. This suggests that the jet-pathway economics are somewhat more exposed to feedstock-price improvement as a screening-level lever, although the broader interpretation remains subordinate to the dominant effects of scale and closure basis.

Read together, the threshold analysis supports a useful distinction between *high-impact* levers and *reachable* levers. Fuel-gas treatment is high-impact, but the required improvement to deliver a 10% MSP reduction lies beyond the evaluated range. Capacity change is both high-impact and reachable within the tested range. This distinction is important for decision interpretation because it clarifies that the most economically consequential variable is not always the most practically available project lever under the current design basis.

9.4.3. Interpretation of sensitivity ranges

The sensitivity outcomes in Chapter 8 should be interpreted as scenario bounds derived from one-at-a-time parameter ranges, not as probability-weighted confidence intervals. This distinction is methodologically important and follows directly from the research design established in Chapter 4: at thesis scope, the available evidence base does not support well-founded joint probability distributions for many

economically consequential inputs, particularly commercially contingent parameters such as feedstock contracting conditions and boundary-export monetisation (section 4.3).

For coefficient-only cases (feedstock price, hydrogen price, and fuel-gas crediting), the underlying technical mass and energy balances are held fixed and only the selected economic coefficient is perturbed (subsection 8.2.3). Capacity is the only tested lever that materially rescales the plant while retaining the same pathway configuration and accounting conventions. The sensitivity analysis therefore isolates influence clearly, but it does not estimate likelihood. The interpretation is decision-oriented rather than statistical: the OAT design identifies which assumptions exert the largest influence on MSP under the present model structure and indicates where further evidence refinement, contracting clarity, or alternative system design work would be most valuable.

This caveat is also important when comparing the thesis to the wider literature. Chapter 3 showed that plastic-pyrolysis TEAs often differ simultaneously in feedstock basis, upgrading extent, coproduct treatment, and system boundary, which already makes direct comparison difficult. Presenting the Chapter 8 ranges as scenario bounds rather than pseudo-probabilistic uncertainty intervals therefore strengthens interpretive honesty. It signals that the thesis contributes a transparent ranking of dominant levers under one internally consistent modelling basis, rather than claiming to predict the full uncertainty distribution of project outcomes.

Taken together, the robustness results indicate that the baseline feasibility reading is structurally stable in one sense and contingent in another. It is structurally stable in that the dominant ranking is clear: scale first, fuel-gas monetisation second, feedstock price third, hydrogen price last. It is contingent in that the magnitude of improvement available from several of these levers depends strongly on external market, contracting, and offtake conditions that sit partly outside the plant boundary. This dual reading provides the immediate bridge to the pedigree section that follows: the sensitivity analysis tells us which levers matter most, while the pedigree analysis helps determine how strongly each of those levers is empirically supported and how confidently the resulting conclusions can be generalised.

9.5. Pedigree lens

The preceding sections interpreted the technical, economic, and robustness results under one internally consistent gate-to-gate modelling basis. The pedigree results now provide a second interpretive layer: they do not ask which result is algebraically or financially consistent, but how strongly the underlying modelling elements are supported by empirical evidence, theoretical understanding, proxy quality, and methodological rigour (Appendix B). In the logic of this thesis, pedigree therefore functions as a qualifier of *claim strength*. It indicates where the discussion can be read as structurally robust within the adopted bookkeeping and where it should instead be treated as indicative, screening-level, or commercially contingent.

This distinction is especially important for Chapter 9 because the present discussion does not only interpret the thesis on its own terms; it also positions the thesis relative to the literature reviewed in Chapter 3. That literature is heterogeneous in feed basis, upgrading representation, product definition, and boundary treatment. The pedigree lens therefore helps in two ways: first, it qualifies how strongly the present thesis findings can be generalised beyond the current screening basis; second, it clarifies why comparison with the wider literature must remain selective and mechanism-focused rather than framed as a simple comparison of absolute values.

9.5.1. Technical pedigree

The technical pedigree outcomes are most supportive of the process-design and mass-balance bookkeeping elements inherited from Chapters 5 and 6. This supports relatively strong interpretation of the plant-boundary outlet structure, the shared A100–A400 topology, and the conclusion that pathway differentiation is concentrated downstream rather than in the common front-end conversion basis. In practical terms, the strongest technical claim in this thesis is therefore not that every aggregated duty

or unit-level burden is mechanistically resolved, but that the pathway comparison is internally coherent at plant boundary and that the headline technical differences are not artefacts of numerical imbalance.

This supports the main reading developed in Section 9.2: the two pathways differ primarily by product redistribution and downstream handling burden, while total saleable liquid yield remains similar and imported hydrogen intensity remains nearly unchanged. The boundary-bookkeeping component of that interpretation is comparatively robust within the adopted representation.

By contrast, the technical pedigree is weaker for process-variable translation and utilities attribution. This is consistent with the modelling rationale in Chapter 4, which explicitly adopts a screening-level black-box representation where more mechanistic detail could not be supported consistently across the full system. Accordingly, the higher electricity demand of the jet-fuel pathway should remain interpreted as a directional, system-level consequence of the stricter recovery objective rather than as a precise equipment-level causal claim. The pedigree lens therefore reinforces the wording already adopted in Sections 9.1 and 9.2.2: electricity is informative as a plant-level differentiator, but not as a high-confidence statement about individually resolved unit duties.

This also helps position the thesis relative to the literature. Recent studies on DKR 350-derived and post-consumer plastic streams show that real-feed pyrolysis and upgrading are strongly shaped by contamination, pretreatment quality, and feed heterogeneity [79], [80], [81], [82]. The present thesis aligns well with that literature in its emphasis on representative feed context and plant-boundary bookkeeping, but it does not claim to reproduce full process-level mechanistic detail. The technical contribution is therefore best read as a controlled, specification-aware comparison under one shared boundary, rather than as a fully resolved process simulation.

9.5.2. Economic pedigree

The economic pedigree outcomes draw a clear distinction between (i) the robustness of the DCF structure and MSP closure logic and (ii) the weaker empirical support for screening-level CAPEX and fixed-OpEx estimation and for the monetisation of boundary credits and co-products.

The strongest economic element is the accounting framework itself. This supports strong interpretation of the MSP definition, break-even logic, and the central conclusion that the jet-pathway MSP is materially shaped by the chosen closure convention and the smaller main-product denominator. In other words, the pedigree results support the *structure* of the economic interpretation developed in Section 9.3: the pathway gap is meaningfully explained through closure basis, fixed-cost-heavy cost structure, and residual burden allocation.

What is weaker is the empirical support for the absolute magnitudes of several large annual cost terms, especially CAPEX and fixed OpEx. This does not undermine the internal consistency of the operating statement, but it limits how strongly the reported baseline MSP values should be generalised as commercial price expectations. The appropriate reading is therefore that the thesis provides screening-level economic magnitudes under a transparent and internally coherent factor-method framework, while its main economic value lies in identifying dominant structural drivers rather than in producing bankable project pricing.

The pedigree results also support the use of “commercially contingent” language for exported fuel-gas credits and co-product treatment. These elements are high-leverage in the sensitivity analysis, but comparatively weak in empirical grounding because their realised value depends on external integration conditions, contractual arrangements, and market interfaces that sit partly outside the A100–A400 plant boundary. This directly reinforces the discussion in Sections 9.3.3 and 9.4.1: the model can show how strongly such terms matter *if* they are realised, but it cannot guarantee that they will be realised in practice.

This distinction is also useful when comparing the thesis to the TEA literature. Chapter 3 showed that many published plastic-pyrolysis TEAs vary simultaneously in product routing, coproduct account-

ing, and system boundary, which already limits direct benchmarking. The present thesis improves interpretability by holding these conventions fixed across pathways, but the pedigree results caution against interpreting this improved comparability as equivalent to high empirical certainty in all economic magnitudes. The comparative structure is stronger than the absolute number confidence.

9.5.3. Pedigree and sensitivity

Sensitivity analysis and pedigree analysis answer different questions and should be read together. The one-at-a-time sensitivity analysis in Chapter 8 ranks which assumptions matter most to MSP within the tested ranges. The pedigree analysis indicates how strongly the corresponding underlying elements are empirically supported. Their combination therefore helps distinguish between three different categories of decision relevance.

First, some results are both high-impact and structurally well supported within the modelling framework. The clearest example is the importance of MSP closure logic and the fixed-cost-heavy baseline structure, which together explain why capacity dominates the sensitivity ranking. Here, pedigree strengthens confidence in the qualitative mechanism even if absolute cost magnitudes remain screening-level.

Second, some results are high-impact but weakly supported empirically. Boundary credit treatment is the clearest example. Fuel-gas monetisation strongly affects MSP, but its realised value depends on conditions outside the plant boundary and is therefore commercially contingent. In such cases, sensitivity identifies leverage, while pedigree identifies caution.

Third, some results are more weakly supported and also more interpretively delicate, such as utilities attribution and process-variable translation. These do not necessarily invalidate the direction of the thesis findings, but they indicate where future work would most improve the explanatory strength of the pathway comparison. In practical terms, the most valuable evidence-improvement priorities are therefore: (i) better empirical grounding for CAPEX and fixed-OpEx estimation, because these dominate the baseline economics; (ii) better documentation and realism of boundary-credit and co-product assumptions, because these are both high-leverage and weakly grounded; and (iii) better evidence for utility attribution and upgrading-variable translation, because these would strengthen the technical interpretation of downstream pathway differentiation.

Read in this way, the pedigree lens does not weaken the thesis; it clarifies how the thesis should be used. The strongest contribution of the work is not that every parameter is equally well evidenced, but that the pathways are compared under one explicit, traceable, and internally consistent framework, and that the discussion remains honest about where the conclusions are robust, where they are directional, and where they depend on commercial conditions beyond the immediate plant boundary. This also provides the bridge to the closing synthesis: the final interpretation of the thesis should retain both parts of the message at once: a clear structural ranking of the dominant levers, together with disciplined qualification of how far those rankings can be generalised beyond the present screening basis.

9.6. Closing synthesis

Taken together, the discussion in this chapter supports a coherent reading of the thesis results across technical performance, economics, robustness, and claim strength. At the technical level, the two pathways are best interpreted not as fundamentally different conversion systems, but as two outlet intents applied to one shared gate-to-gate configuration. The principal technical distinction is downstream: the stricter jet-oriented recovery objective redistributes the saleable liquid pool, increases aggregated electricity demand under the adopted screening representation, and leaves the shared front-end conversion basis largely unchanged. This means that pathway differentiation should be read primarily through product partitioning, downstream handling, and boundary-stream implications rather than through a different front-end conversion regime.

At the economic level, the discussion clarifies that the large MSP gap between pathways is shaped less by large differences in annual plant-wide burden than by how that burden is translated into break-even

product pricing. The baseline operating statement is dominated by capital-linked and fixed operating costs, and the jet-fuel pathway recovers the residual annual requirement on the smaller Stream 344 main-product basis after co-product and byproduct credits are applied. Accordingly, the higher jet-pathway MSP is best understood as the joint outcome of a fixed-cost-heavy baseline, pathway-specific MSP closure, and denominator effect under a stricter product-recovery objective.

At the robustness level, the thesis establishes a clear ranking of the dominant feasibility levers within the tested ranges. Capacity is the strongest lever in both pathways because it changes how fixed annual burdens are distributed over throughput. Fuel-gas monetisation is the second most important lever because it directly affects one of the largest revenue offsets in the operating statement, even though its realised value depends on downstream integration and offtake conditions beyond the immediate plant boundary. Feedstock price remains meaningful but secondary within the tested range, while hydrogen price is a comparatively weak lever in the present configuration. The threshold analysis further refines this reading by showing that some levers are high-impact but difficult to realise within the evaluated range, whereas others, especially scale-up, are both high-impact and reachable.

The pedigree lens then qualifies how these findings should be used. Confidence is strongest in the boundary bookkeeping, DCF structure, and internal closure logic that support the comparative interpretation of the two pathways. Confidence is weaker for screening-level CAPEX and fixed-OpEx estimation, for detailed utility attribution, and for the realised value of commercially contingent boundary credits. The thesis should therefore be read neither as a fully mechanistic process simulation nor as a bankable valuation. Its strongest contribution lies instead in providing a transparent, specification-aware, and internally consistent comparison under one shared technical and economic basis, while remaining explicit about which conclusions are robust within that basis and which remain directional or commercially contingent.

Positioned against the literature reviewed in Chapter 3, this yields a more specific contribution than a generic claim about plastic-pyrolysis feasibility. Much of the literature remains difficult to compare directly because feedstocks, upgrading assumptions, product definitions, and system boundaries are frequently non-aligned [17], [18]. The present thesis reduces several of these comparability problems by holding feed basis, plant topology, gate-to-gate scope, and DCF framework constant across the two pathways. This does not eliminate uncertainty, but it does make the resulting differences more interpretable. In that sense, the thesis contributes a controlled comparison of two specification-oriented outlet intents rather than a universal feasibility verdict on plastic-pyrolysis upgrading routes.

The broader meaning of the results is therefore twofold. On the one hand, they show that under the present screening basis both pathways face a substantial feasibility gap at baseline, with the naphtha pathway more naturally aligned to petrochemical circularity and the jet-fuel pathway pointing toward a more demanding downstream market shaped by stricter property and qualification constraints. On the other hand, they show that the routes are not equally constrained in the same way: some barriers are primarily structural and internal to the model logic, such as fixed-cost dilution through scale, whereas others are external and contingent on integration, contracting, and downstream value recognition.

This synthesis provides the basis for the final chapter. Chapter 10 does not reopen the detailed technical and economic interpretation developed here. Instead, it distils the system-level answer to the main research question, states the integrated conclusions of the thesis more directly, and translates the findings into their final implications for feasibility interpretation, limitations, and next steps.

10

Conclusion

This chapter presents the final thesis-level answer to the main research question. Detailed answers to the four sub-research questions are provided in Chapters 5–8, and the integrated interpretation of those results is developed in Chapter 9. The purpose here is therefore not to reopen the detailed discussion, but to distil what the combined technical, economic, and robustness results establish for the fixed A100–A400 gate-to-gate system assessed, and what that means for final feasibility interpretation.

The main research question posed in Chapter 1 is:

> *What is the techno-economic performance of producing a cracker-relevant naphtha-range blendstock and a jet-fuel-range blendstock through pyrolysis-based recycling of polyolefin-rich plastic waste in the Netherlands under a consistent gate-to-gate screening TEA basis?*

10.1. System-level answer to the main research question

Under the screening-level, gate-to-gate basis adopted in this thesis, the answer is as follows. A shared A100–A400 pyrolysis and upgrading configuration can be represented consistently for two outlet intents, a naphtha pathway and a jet-fuel pathway, and, at the common 40 kt/y basis, the pathways differ mainly in downstream product partitioning and economic closure rather than in total saleable liquid production. On that basis, the naphtha pathway is the less burdensome of the two economically, while the jet-fuel pathway carries a substantially higher MSP under the adopted accounting convention. In both pathways, feasibility interpretation is governed primarily by scale and boundary-integration assumptions rather than by modest changes in secondary variable-cost coefficients.

Technically, the system produces very similar total saleable liquid yields in the two pathways (0.5615 vs. 0.5632 kg/kg feed), while the jet-fuel pathway redistributes that liquid pool into a naphtha stream and an additional jet-range blendstock stream rather than materially increasing total liquids (Table 6.12). Imported hydrogen intensity is effectively unchanged between pathways, whereas total electricity demand increases from 112.40 to 219.92 kW under the present screening representation (Table 6.12). The most robust technical conclusion is therefore that pathway differentiation is concentrated downstream of the shared front-end conversion basis. The electricity result remains informative at plant level, but it should be read as a directional system consequence of the stricter recovery objective rather than as a fully resolved equipment-level causal claim.

Economically, both pathways exhibit high break-even selling prices at the assessed 40 kt/y basis, with MSP values of 2,134 EUR/t for the naphtha pathway and 4,940 EUR/t for the jet-fuel pathway (Table 7.1). This gap should not be interpreted as evidence that the jet-oriented case carries a fundamentally different annual plant burden. Rather, it reflects the combination of a fixed-cost-heavy screening TEA

structure and the pathway-specific MSP closure convention, under which the jet-fuel pathway recovers the residual break-even burden on the smaller Stream 344 main-product basis after co-product naphtha revenue and byproduct credits have been applied. The resulting MSP values should therefore be read as screening-level indicators of relative economic burden under one explicit accounting basis, not as investment-grade price forecasts.

In robustness terms, the thesis shows that feasibility interpretation is dominated by structural and boundary-condition levers rather than by modest changes in smaller coefficients. Across the tested ranges, plant capacity is the dominant MSP lever in both pathways, followed by monetisation of exported byproduct fuel gas at battery limits (Stream 423), then feedstock price, with hydrogen price remaining a secondary driver in the present configuration (Table 8.2–8.3). Within the tested range, modest scale-up delivers larger MSP improvements than coefficient-only adjustments, and removing the fuel-gas export credit increases MSP by 10.8% in the naphtha pathway and 14.3% in the jet-fuel pathway. Taken together, the thesis therefore establishes a transparent screening baseline and a controlled comparison of two specification-oriented outlet intents, rather than a universal feasibility verdict on plastic-pyrolysis upgrading routes.

10.2. Integrated conclusions on pathway meaning and feasibility

The pathway comparison developed in this thesis should be read as a comparison between two *outlet intents* applied to one shared gate-to-gate conversion system, not as a comparison between two fundamentally different plants. Both pathways are evaluated on the same A100–A400 topology, the same Dutch-context feed basis, and the same discounted-cash-flow framework. The most important technical conclusion is therefore that the assessed difference between pathways is concentrated downstream of the shared front-end conversion basis: the jet-fuel pathway primarily redistributes the saleable liquid pool into a jet-range cut and a co-produced naphtha stream, while total saleable liquid yield remains nearly unchanged.

This technical reading matters directly for feasibility interpretation. Within the adopted screening representation, the stricter jet-oriented recovery objective does not establish a meaningfully larger total liquid output than the naphtha pathway, but it does introduce a more demanding downstream product-partitioning logic and a higher aggregated electricity burden. The pathway contrast should therefore be interpreted primarily through downstream recovery, utility handling, and product-definition consequences, rather than through a claim that the two pathways represent materially different front-end conversion performance.

At economic level, the thesis indicates that the large MSP difference between pathways is shaped less by large differences in annual plant-wide burden than by how that burden is translated into break-even pricing. The baseline screening TEA is dominated by capital-linked and fixed operating cost terms, and the jet-fuel pathway recovers the residual break-even requirement on the smaller Stream 344 main-product basis after fixed-price naphtha co-product revenue and byproduct credits have been applied. Accordingly, the higher jet-pathway MSP should be read primarily as the joint outcome of a fixed-cost-heavy baseline, a stricter outlet intent, and the pathway-specific MSP closure convention, rather than as evidence that the jet-oriented case is simply a much more expensive plant in absolute annual terms.

This also means that the two pathways are not constrained in exactly the same way. The naphtha pathway is more naturally aligned with petrochemical circularity logic and cracker-oriented integration, whereas the jet-fuel pathway points toward a more demanding downstream context in which a smaller designated main-product stream must carry the residual economic burden under a stricter product objective. In this sense, the thesis does not show that one pathway is universally preferable in all external contexts; rather, it shows that under the present gate-to-gate screening basis, the naphtha pathway is the less burdensome economic route, while the jet-fuel pathway is more exposed to the consequences of product partitioning, pricing convention, and denominator effect.

The robustness results further refine this conclusion. Across the evaluated ranges, the most impor-

tant feasibility levers are those that change the recovery of fixed annual burdens over throughput and those that determine whether economically material boundary exports can be realised under credible integration and offtake conditions. Capacity is therefore the dominant lever in both pathways, while monetisation of exported byproduct fuel gas at battery limits (Stream 423) is the second most important. Feedstock contracting remains meaningful but secondary within the tested range, and hydrogen price is a comparatively weak driver in the present configuration. Read together, these outcomes show that feasibility improvement in this thesis is governed primarily by project scale, utilisation logic, and boundary integration conditions rather than by fine-tuning smaller variable-cost coefficients in isolation.

Taken together, the integrated conclusion of the thesis is not that pyrolysis-based upgrading is either categorically feasible or categorically unfeasible. Rather, it is that under one explicit Dutch-context, gate-to-gate, screening-level basis, both assessed pathways face a substantial baseline feasibility burden, that this burden is lower for the naphtha pathway than for the jet-fuel pathway, and that the most decision-relevant improvements lie in structural and boundary-condition levers rather than in modest coefficient adjustments. This is the level on which the pathway comparison in this thesis is strongest and most defensible.

10.3. Practical implications and pathway positioning in the Dutch system

The results of this thesis suggest practical implications for stakeholders, but these should be read in proportion to the study scope. They are implications derived from a screening-level, gate-to-gate comparison of two outlet intents under one explicit accounting basis, not validated deployment prescriptions. Within that qualification, the results still indicate where action would matter most if such systems were to be developed in the Dutch context.

For project developers and industrial partners, the main implication is that the strongest feasibility levers are structural rather than marginal. Because fixed annual burdens dominate the baseline TEA and capacity is the strongest MSP lever in both pathways, the first practical question is whether a credible scale, utilisation, and integration case can be established for the assessed configuration. On the same basis, the second major interface is boundary integration: the ability to place, use, or contract the exported byproduct fuel gas at battery limits (Stream 423) is economically material in both pathways and should therefore be treated as a front-end project-development issue rather than as a secondary optimisation detail. In practical terms, this means that site selection, industrial symbiosis, and offtake structure are likely to matter more to screening feasibility than incremental tuning of small variable-cost coefficients in isolation.

The pathway comparison also implies that the two outlet intents are best positioned differently in the Dutch industrial system. The naphtha pathway is the more natural fit with petrochemical circularity logic, because its value proposition lies in producing a cracker-relevant naphtha-range blendstock that can, in principle, connect to existing petrochemical infrastructure. This is consistent with the Rotterdam–Moerdijk location logic adopted elsewhere in the thesis, where proximity to sorting, refining, and petrochemical assets provides the contextual rationale for a naphtha-oriented route. The jet-fuel pathway, by contrast, points toward a more demanding downstream context. Its screening MSP is higher not only because of the stricter outlet objective but also because the residual burden is recovered on a smaller designated main-product stream under the adopted closure convention. The practical implication is not that the jet-oriented pathway is irrelevant, but that it requires more cautious interpretation and is more exposed to downstream qualification, pricing, and market-structure conditions than the naphtha pathway under the present basis.

For waste and feedstock actors, the main implication is that specification discipline remains important even though this thesis is not a feedstock-market study. The analysis is built around a pretreated, polyolefin-rich Dutch residual stream derived from DKR 350, and the literature reviewed in Chapter 3 shows that enrichment and pretreatment can materially reduce impurity burden while still leaving

upgrading-relevant contaminants that propagate into downstream treatment requirements. This means that feed definition, pretreatment consistency, and contracting terms at the plant gate remain practically important, especially because feedstock price is still a meaningful MSP lever within the tested range and because the representativeness of the PO-rich residual basis depends on continued upstream sorting and preparation performance.

For policymakers and system-level actors, the most defensible implication is not that this thesis proves the desirability of one specific policy instrument, but that it clarifies where enabling conditions would matter most if advanced recycling routes of this type are to play a role. Within the present model structure, the dominant barriers are not primarily hydrogen price in isolation, but scale realisation, credible utilisation, and the practical handling and valuation of boundary streams. Policy and infrastructure choices that improve integration conditions, reduce ambiguity around industrial interfaces, and support the placement of residual polyolefin-rich streams in coherent value chains are therefore likely to be more consequential than support focused only on minor variable-cost terms. At the same time, the two pathways serve different broader system logics: the naphtha pathway aligns more naturally with petrochemical circularity, whereas the jet-fuel pathway connects more closely to the wider challenge of aviation decarbonisation, but under a more commercially and qualification-sensitive downstream context.

Finally, the broader valorisation landscape should not be reduced to the two outlet intents modelled here. This thesis deliberately evaluates only a naphtha-range blendstock route and a jet-range blendstock route under one fixed boundary and shared topology. However, complementary literature indicates that plastic-derived pyrolysis intermediates may also be routed toward higher-value chemical products under different process concepts. Recent work from the same broader research ecosystem has, for example, demonstrated pilot-scale conversion of hard-to-recycle mixed plastic waste toward pyrolysis oil and BTX aromatics [81]. This does not alter the conclusions of the present thesis, nor does it demonstrate such performance for the DKR 350-based system assessed here. It does, however, reinforce the broader practical point that product-routing and boundary-integration choices can materially shape the value proposition of advanced recycling systems beyond the two outlet intents compared in this study.

10.4. Validity conditions and limitations

The conclusions of this thesis are bounded by four validity conditions, each of which limits how far the results can be generalised beyond the present study basis.

First, the assessment is steady-state and gate-to-gate. The analysed system is restricted to the fixed A100–A400 plant boundary and to a fixed Dutch-context design basis as defined in Chapter 5. Upstream activities such as collection, sorting, washing, densification, and transport are excluded from the quantitative model, as are downstream refining, blending, certification, and end use. The thesis therefore supports interpretation of plant-boundary material, utility, and economic behaviour for the assessed conversion facility, but it does not provide a full value-chain evaluation. This means, for example, that the results can support comparison of outlet intents under one shared plant basis, but not a cradle-to-grave claim about overall circularity or climate performance.

Second, the technical model is screening-level and outcome-based. As established in Chapter 6, the steady-state representation is designed to preserve internal mass consistency, explicit boundary-stream accounting, and pathway comparability, rather than to provide a rigorous first-principles simulation of every unit operation. The strongest technical conclusions are therefore those tied to plant-boundary bookkeeping: the shared A100–A400 topology, the similar total saleable liquid yield across pathways, and the downstream concentration of pathway differentiation. By contrast, more detailed process-variable attributions, especially utilities attribution and the precise causal interpretation of the higher electricity burden in the jet-fuel pathway, should remain directional within the adopted representation rather than read as fully resolved equipment-level findings.

Third, the techno-economic assessment is a screening TEA, not an investment-grade appraisal. The economic results are built from factor-based cost estimation, screening-level fixed-OpEx treatment, and a discounted-cash-flow closure designed for transparent comparative interpretation in Chapter 7. This gives the thesis a strong basis for comparing the two pathways under one common accounting structure and for identifying which levers dominate MSP within that structure. However, it also means that the absolute magnitudes of MSP, CAPEX-linked burden, and fixed operating cost recovery should be read as screening-level outcomes rather than bankable project estimates. In particular, the conclusion that fixed-cost structure and capacity dominate the baseline economics is robust within the accounting framework, whereas the precise numerical scale of the burden remains contingent on the early-stage costing basis.

Fourth, several important interpretation layers lie outside the validated scope. The thesis does not perform a full life-cycle assessment, does not quantify upstream emissions from electricity or hydrogen production, and does not establish downstream specification compliance or certification readiness for aviation use. The jet-fuel pathway is therefore interpreted strictly as a jet-range blendstock objective under specification intent, not as a certified drop-in aviation fuel claim. Similarly, boundary-stream monetisation, most notably the treatment of exported byproduct fuel gas at battery limits, is economically important in the model but remains commercially contingent on real offtake, infrastructure, and contracting conditions outside the present assessment boundary.

Taken together, these limitations do not invalidate the main contribution of the thesis. Rather, they define the level on which the conclusions are strongest. The thesis is most robust as a transparent, internally consistent, gate-to-gate screening comparison of two outlet intents under one fixed technical and financial basis. Its strongest outputs are the controlled pathway comparison, the explanation of why the jet-fuel pathway carries a higher MSP under the adopted closure convention, and the ranking of the dominant feasibility levers. Generalisation beyond that level should remain cautious and proportional to the evidence base.

10.5. Future work

The most valuable future work is not the addition of more model complexity for its own sake, but targeted evidence improvement in those parts of the pathway comparison that are both high-leverage and comparatively weakly grounded. On that basis, four priorities follow from the present thesis.

First, stronger continuous-operation and feed-representativeness evidence would improve the technical credibility of the assessed system. The present thesis is built on a pretreated, polyolefin-rich DKR 350-derived basis and a steady-state representation of the A100–A400 system. Future work should therefore test how robust the present pathway comparison remains under longer continuous operation, realistic feed variability, and tighter empirical linkage between feed composition, impurity behaviour, and boundary-stream formation. This would strengthen the technical interpretation without changing the basic comparative logic of the thesis.

Second, better downstream upgrading and utility-attribution realism would sharpen the interpretation of pathway differentiation. The most robust technical conclusion of the thesis is that the pathways differ mainly through downstream product partitioning rather than front-end conversion scale. However, the detailed interpretation of electricity burden, internal gas handling, and utility allocation remains directional within the current screening model. Future work should therefore focus on improved evidence for upgrading severity, cut-definition realism, recycle behaviour, and utility attribution, especially in A200–A300 and their integration through A400. In practical terms, this would help clarify how much of the observed jet-pathway burden is a stable consequence of stricter outlet intent and how much is sensitive to the present simplified modelling representation.

Third, stronger economic grounding for CAPEX and fixed operating costs is a high priority because these terms dominate the baseline feasibility burden. The current thesis is strongest in its comparative DCF structure and MSP closure logic, but the absolute magnitudes remain limited by screening-

level cost estimation and fixed-OpEx representation. Future work should therefore prioritise better installed-cost evidence, clearer scaling relationships, and more defensible fixed-cost estimation based on technology-specific and integration-specific analogues. This would not primarily change the value of the current thesis as a controlled comparison; rather, it would improve how confidently the absolute MSP burden can be interpreted beyond the present early-stage basis.

Fourth, improved treatment of boundary interfaces and commercially contingent assumptions would strengthen the practical relevance of the feasibility interpretation. The present results show that monetisation of exported byproduct fuel gas at battery limits (Stream 423) is economically material, while the pedigree framing indicates that boundary-credit and co-product assumptions are among the weaker empirical elements of the assessment. Future work should therefore examine more explicit offtake cases, alternative integration and valorisation options for boundary streams, and clearer commercial scenarios for how exported gas and co-products would actually be placed and valued. The goal would not be to remove uncertainty entirely, but to replace generic credits with more realistic interface cases that better connect the gate-to-gate model to plausible industrial deployment conditions.

A final extension, outside the immediate scope of the present thesis but relevant for system interpretation, is broader route comparison beyond the two outlet intents assessed here. This thesis deliberately compares only a naphtha-range blendstock pathway and a jet-range blendstock pathway under one fixed topology and accounting basis. Future work could examine how these routes compare with alternative valorisation concepts for polyolefin-derived pyrolysis intermediates, including chemical-routing options beyond the present boundary logic. Such work would be most useful once the core technical, costing, and boundary-interface uncertainties identified above have first been reduced.

Taken together, these priorities indicate that the next step is not simply to build a larger model. It is to improve the empirical grounding of those specific elements that most strongly influence feasibility interpretation: downstream upgrading realism, fixed-cost evidence, and commercially contingent boundary treatment. That is the most direct route for turning the present screening comparison into a stronger basis for later-stage decision support.

Nomenclature

Abbreviations

Abbreviation	Definition
A100	Process Area A100 (pyrolysis)
A200	Process Area A200 (hydrotreating unit, HTU)
A300	Process Area A300 (hydrocracking unit, HCU, and final fractionation)
A400	Process Area A400 (utilities and integration)
AACE	The Association for the Advancement of Cost Engineering
ABS	Acrylonitrile butadiene styrene
ASTM	ASTM International (standards organisation; formerly American Society for Testing and Materials)
BTX	Benzene, toluene, and xylene
CAPEX	Capital expenditures
CEPCI	Chemical Engineering Plant Cost Index
CHP	Combined heat and power
CO	Carbon monoxide
CO_2	Carbon dioxide
DCF	Discounted cash flow
DKR	Dutch plastics sorting specification code (e.g., DKR 350)
FCC	Fluid catalytic cracking
FCI	Fixed capital investment
FGH	Fuel-gas header
GHG	Greenhouse gas
H_2	Hydrogen
HCl	Hydrogen chloride
HCU	Hydrocracking unit
HDPE	High-density polyethylene
HTL	Hydrothermal liquefaction
HTU	Hydrotreating unit
IRR	Internal rate of return
LCA	Life-cycle assessment
LDPE	Low-density polyethylene
LHV	Lower heating value
LHSV	Liquid hourly space velocity
LLDPE	Linear low-density polyethylene
MDPE	Medium-density polyethylene
MSP	Minimum selling price
NCG	Non-condensable gas
NIR	Near-infrared
NPV	Net present value
OAT	One-at-a-time (sensitivity analysis)
OPEX	Operating expenditures
PA	Polyamide
PBP	Payback period

Abbreviation	Definition
PC	Polycarbonate
PE	Polyethylene
PET	Polyethylene terephthalate
PFD	Process flow diagram
PIONA	Paraffins, isoparaffins, olefins, naphthenes, and aromatics
PMD	Plastics, metals, and drink cartons (Dutch household collection stream)
PP	Polypropylene
PPW	Plastic packaging waste
PSA	Pressure swing adsorption
PS	Polystyrene
PSW	Plastic solid waste
PVC	Polyvinyl chloride
rPET	Recycled polyethylene terephthalate
SAF	Sustainable aviation fuel
SWS	Sour-water stripping
TEA	Techno-economic assessment
TPM	Technical performance metric
USD	United States dollar

Symbols

Symbol	Definition
C_{DPI}	Direct permanent investment [EUR]
C_{TBM}	Total bare-module investment [EUR]
C_{TCI}	Total capital investment [EUR]
C_{TDC}	Total depreciable capital [EUR]
C_{TPI}	Total permanent investment [EUR]
C_{WC}	Working capital [EUR]
FCF_t	Free cash flow in year t [EUR/y]
FX	Currency conversion factor [–]
I_{fuelgas}	Exported fuel-gas mass indicator [kg/kg feed]
$I_{\text{fuelgas,energy}}$	Exported fuel-gas energy indicator [MJ/kg feed]
$I_{\text{vent/purge}}$	Vent/purge mass indicator [kg/kg feed]
I_{water}	Water-discharge mass indicator [kg/kg feed]
r	Real discount rate [–]
S_{crack}	Cracking severity [–]
T	Project lifetime [y]
$\Delta\mathrm{MSP}_{\mathrm{high}}$	High-case change in MSP relative to baseline [EUR/t]
$\Delta\mathrm{MSP}_{\mathrm{low}}$	Low-case change in MSP relative to baseline [EUR/t]
$\alpha_{O\to I}$	Hydrogenated-olefin mapping to isoparaffins [–]
$\alpha_{O\to P}$	Hydrogenated-olefin mapping to n-paraffins [–]
$f_{A,\mathrm{sat}}$	Aromatic saturation fraction [–]
$f_{Cl,\mathrm{rem}}$	Chlorine removal fraction [–]
$f_{N,\mathrm{rem}}$	Nitrogen removal fraction [–]
$f_{O,\mathrm{rem}}$	Oxygen removal fraction [–]
$f_{O,\mathrm{sat}}$	Olefin saturation fraction [–]
$f_{S,\mathrm{rem}}$	Sulfur removal fraction [–]

Symbol	Definition
f_{gas}	Gas-make fraction per cracked mass [–]
$\mathrm{MSP}_{\mathrm{base}}$	Baseline MSP [EUR/t]
y_{char}	Char yield [–]
y_{gas}	Non-condensable-gas yield [–]
y_{inerts}	Inerts yield [–]
y_{liq}	Liquid yield [–]

References

[1] M. Ilyas, W. Ahmad, H. Khan, S. Yousaf, K. Khan, and S. Nazir, "Plastic waste as a significant threat to environment - a systematic literature review," *Reviews on Environmental Health*, vol. 33, no. 4, pp. 383–406, 2018.

[2] C. J. Rhodes, "Plastic Pollution and Potential Solutions," en, *Science Progress*, vol. 101, no. 3, pp. 207–260, Sep. 2018.

[3] Plastics Europe. "Plastics – the facts 2024," Accessed: May 1, 2025. [Online]. Available: `https://plasticseurope.org/knowledge-hub/plastics-the-fast-facts-2024/`.

[4] M. Dokl et al., "Global projections of plastic use, end-of-life fate and potential changes in consumption, reduction, recycling and replacement with bioplastics to 2050," en, *Sustainable Production and Consumption*, vol. 51, pp. 498–518, Nov. 2024.

[5] R. Geyer, J. R. Jambeck, and K. L. Law, "Production, use, and fate of all plastics ever made," en, *Science Advances*, vol. 3, no. 7, e1700782, Jul. 2017.

[6] D. K. A. Barnes, F. Galgani, R. C. Thompson, and M. Barlaz, "Accumulation and fragmentation of plastic debris in global environments," en, *Philosophical Transactions of the Royal Society B: Biological Sciences*, vol. 364, no. 1526, pp. 1985–1998, Jul. 2009.

[7] I. Napper and R. Thompson, "Plastics and the Environment," en, *Annual Review of Environment and Resources*, vol. 48, no. 1, pp. 55–79, Nov. 2023.

[8] S. R. Nicholson et al., "The Critical Role of Process Analysis in Chemical Recycling and Upcycling of Waste Plastics," en, *Annual Review of Chemical and Biomolecular Engineering*, vol. 13, no. 1, pp. 301–324, Jun. 2022.

[9] P. Pathak, S. Sharma, and S. Ramakrishna, "Circular transformation in plastic management lessens the carbon footprint of the plastic industry," en, *Materials Today Sustainability*, vol. 22, p. 100 365, Jun. 2023.

[10] I. Agenda, "The new plastics economy rethinking the future of plastics," in *World Economic Forum*, vol. 36, 2016.

[11] F. Bauer et al., "Plastics and climate change—Breaking carbon lock-ins through three mitigation pathways," en, *One Earth*, vol. 5, no. 4, pp. 361–376, Apr. 2022.

[12] K. Houssini, J. Li, and Q. Tan, "Complexities of the global plastics supply chain revealed in a trade-linked material flow analysis," en, *Communications Earth & Environment*, vol. 6, no. 1, p. 257, Apr. 2025.

[13] European Commission, "Closing the loop - an eu action plan for the circular economy," European Commission, Brussels, Communication from the Commission to the European Parliament, the Council, the European Economic and Social Committee and the Committee of the Regions COM(2015) 614 final, Dec. 2015.

[14] U. R. Gracida-Alvarez, P. T. Benavides, U. Lee, and M. Wang, "Life-cycle analysis of recycling of post-use plastic to plastic via pyrolysis," en, *Journal of Cleaner Production*, vol. 425, p. 138 867, Nov. 2023.

[15] L. Snijder and S. Nusselder, "Plasticgebruik en verwerking van plastic afval in Nederland," CE Delft, Tech. Rep., 2019.

[16] Plastics Europe. "Plastics – the facts 2022," Accessed: May 4, 2023. [Online]. Available: `https://plasticseurope.org/knowledge-hub/plastics-the-facts-2022/`.

[17] A. Fivga and I. Dimitriou, “Pyrolysis of plastic waste for production of heavy fuel substitute: A techno-economic assessment,” en, *Energy*, vol. 149, pp. 865–874, Apr. 2018.

[18] M. Laghezza, S. Fiore, and F. Berruti, “A review on the pyrolytic conversion of plastic waste into fuels and chemicals,” en, *Journal of Analytical and Applied Pyrolysis*, vol. 179, p. 106 479, May 2024.

[19] S. Yin, R. Tuladhar, F. Shi, R. A. Shanks, M. Combe, and T. Collister, “Mechanical reprocessing of polyolefin waste: A review,” *Polymer Engineering & Science*, vol. 55, no. 12, pp. 2899–2909, 2015.

[20] J. Petrík, H. C. Genuino, G. J. Kramer, and L. Shen, “Pyrolysis of Dutch mixed plastic waste: Lifecycle GHG emissions and carbon recovery efficiency assessment,” en, *Waste Management & Research: The Journal for a Sustainable Circular Economy*, Dec. 2024.

[21] D. Lobelle et al., “Knowns and unknowns of plastic waste flows in the Netherlands,” en, *Waste Management & Research: The Journal for a Sustainable Circular Economy*, vol. 42, no. 1, pp. 27–40, Jan. 2024.

[22] J. Hopewell, R. Dvorak, and E. Kosior, “Plastics recycling: Challenges and opportunities,” en, *Philosophical Transactions of the Royal Society B: Biological Sciences*, vol. 364, no. 1526, pp. 2115–2126, Jul. 2009.

[23] M. Wijngaard et al., “Don’t waste it! solving the dark side of today’s plastic,” TNO, Tech. Rep., Nov. 2020, White Paper.

[24] O. Dogu et al., “The chemistry of chemical recycling of solid plastic waste via pyrolysis and gasification: State-of-the-art, challenges, and future directions,” en, *Progress in Energy and Combustion Science*, vol. 84, p. 100 901, May 2021.

[25] M. Solis and S. Silveira, “Technologies for chemical recycling of household plastics – a technical review and trl assessment,” *Waste Management*, vol. 105, pp. 128–138, 2020.

[26] M. Kusenberg et al., “Towards high-quality petrochemical feedstocks from mixed plastic packaging waste via advanced recycling: The past, present and future,” en, *Fuel Processing Technology*, vol. 238, p. 107 474, Dec. 2022.

[27] Intergovernmental Panel On Climate Change (Ipcc), Ed., *Climate Change 2022 - Mitigation of Climate Change: Working Group III Contribution to the Sixth Assessment Report of the Intergovernmental Panel on Climate Change*, 1st ed. Cambridge University Press, Aug. 2023.

[28] I. Hussain, S. A. Ganiyu, H. Alasiri, and K. Alhooshani, “A state-of-the-art review on waste plastics-derived aviation fuel: Unveiling the heterogeneous catalytic systems and techno-economy feasibility of catalytic pyrolysis,” en, *Energy Conversion and Management*, vol. 274, p. 116 433, Dec. 2022.

[29] P. Nayanathara Thathsarani Pilapitiya and A. S. Ratnayake, “The world of plastic waste: A review,” en, *Cleaner Materials*, vol. 11, p. 100 220, Mar. 2024.

[30] “Copyright,” in *Handbook of Recycling (Second Edition)*, C. Meskers, E. Worrell, and M. A. Reuter, Eds., Second Edition, Elsevier, 2024, p. iv.

[31] A. Frick, C. Stern, and V. Muralidharan, *Practical Testing and Evaluation of Plastics*, en, 1st ed. Wiley, Jan. 2019.

[32] D. J. Da Silva and H. Wiebeck, “Current options for characterizing, sorting, and recycling polymeric waste,” en, *Progress in Rubber, Plastics and Recycling Technology*, vol. 36, no. 4, pp. 284–303, Nov. 2020.

[33] P. Bajpai, *Chapter 18 - Polymer Chemistry*, Third Edition, P. Bajpai, Ed. Elsevier, 2018, pp. 373–380.

[34] A. Shrivastava, *2 - Polymerization* (Plastics Design Library), A. Shrivastava, Ed. William Andrew Publishing, 2018, pp. 17–48.

[35] L. W. McKeen, *1 - Introduction to Plastics and Elastomers* (Plastics Design Library), Second Edition, L. W. McKeen, Ed. Norwich, NY: William Andrew Publishing, 2008, pp. 1–39.

[36] C. A. Harper and E. M. Petrie, *Plastics Materials and Processes: A Concise Encyclopedia*, en, 1st ed. Wiley, Sep. 2003.

[37] E. Butler, G. Devlin, and K. McDonnell, "Waste Polyolefins to Liquid Fuels via Pyrolysis: Review of Commercial State-of-the-Art and Recent Laboratory Research," en, *Waste and Biomass Valorization*, vol. 2, no. 3, pp. 227–255, Aug. 2011.

[38] A. Feil and T. Pretz, "Mechanical recycling of packaging waste," en, in *Plastic Waste and Recycling*, Elsevier, 2020, pp. 283–319.

[39] M. T. Brouwer, E. U. Thoden Van Velzen, A. Augustinus, H. Soethoudt, S. De Meester, and K. Ragaert, "Predictive model for the Dutch post-consumer plastic packaging recycling system and implications for the circular economy," en, *Waste Management*, vol. 71, pp. 62–85, Jan. 2018.

[40] C. Lubongo, T. Congdon, J. McWhinnie, and P. Alexandridis, "Economic feasibility of plastic waste conversion to fuel using pyrolysis," en, *Sustainable Chemistry and Pharmacy*, vol. 27, p. 100 683, Jun. 2022.

[41] S. P. Gundupalli, S. Hait, and A. Thakur, "A review on automated sorting of source-separated municipal solid waste for recycling," en, *Waste Management*, vol. 60, pp. 56–74, Feb. 2017.

[42] S. Al-Salem, P. Lettieri, and J. Baeyens, "Recycling and recovery routes of plastic solid waste (PSW): A review," en, *Waste Management*, vol. 29, no. 10, pp. 2625–2643, Oct. 2009.

[43] J. M. Garcia and M. L. Robertson, "The future of plastics recycling," en, *Science*, vol. 358, no. 6365, pp. 870–872, Nov. 2017.

[44] S. Kumar, A. K. Panda, and R. Singh, "A review on tertiary recycling of high-density polyethylene to fuel," en, *Resources, Conservation and Recycling*, vol. 55, no. 11, pp. 893–910, Sep. 2011.

[45] F. van Eijk, E. Beuken, W. Sederel, J. Groen, M. Perez, and G. Locati, *Chemical Recycling in circular perspective. From vision to action: How Chemical Recycling steers the transition towards a circular and carbon neutral chemical industry*. Aug. 2023.

[46] R. A. Clark and M. P. Shaver, "Depolymerization within a circular plastics system," *Chemical Reviews*, vol. 124, no. 5, pp. 2617–2650, 2024, PMID: 38386877. eprint: `https://doi.org/10.1021/acs.chemrev.3c00739`.

[47] S. D. Anuar Sharuddin, F. Abnisa, W. M. A. Wan Daud, and M. K. Aroua, "A review on pyrolysis of plastic wastes," en, *Energy Conversion and Management*, vol. 115, pp. 308–326, May 2016.

[48] Ministerie van Infrastructuur en Waterstaat, "Landelijk afvalbeheerplan 2017-2029: Slimmer omgaan met grondstoffen (versie tweede wijziging - aanpassing aan omgevingswet)," Ministerie van Infrastructuur en Waterstaat, Den Haag, Tech. Rep., Jan. 2021.

[49] S. Al-Salem, P. Lettieri, and J. Baeyens, "The valorization of plastic solid waste (PSW) by primary to quaternary routes: From re-use to energy and chemicals," en, *Progress in Energy and Combustion Science*, vol. 36, no. 1, pp. 103–129, Feb. 2010.

[50] S. Nanda and F. Berruti, "Thermochemical conversion of plastic waste to fuels: A review," en, *Environmental Chemistry Letters*, vol. 19, no. 1, pp. 123–148, Feb. 2021.

[51] S. Nanda, T. R. Sarker, K. Kang, D. Li, and A. K. Dalai, "Perspectives on Thermochemical Recycling of End-of-Life Plastic Wastes to Alternative Fuels," en, *Materials*, vol. 16, no. 13, p. 4563, Jun. 2023.

[52] R.-X. Yang, K. Jan, C.-T. Chen, W.-T. Chen, and K. C.-W. Wu, "Thermochemical Conversion of Plastic Waste into Fuels, Chemicals, and Value-Added Materials: A Critical Review and Outlooks," en, *ChemSusChem*, vol. 15, no. 11, e202200171, Jun. 2022.

[53] U. Arena, "Process and technological aspects of municipal solid waste gasification. A review," en, *Waste Management*, vol. 32, no. 4, pp. 625–639, Apr. 2012.

[54] S. H. Chang, “Plastic waste as pyrolysis feedstock for plastic oil production: A review,” en, *Science of The Total Environment*, vol. 877, p. 162 719, Jun. 2023.

[55] J.-H. Gong, M.-J. Kim, K.-W. Jeon, S. Back, J.-O. Shim, and W.-J. Jang, *A Concise Review of Plastic Pyrolysis and Upgrading Pyrolysis Oil*, 2024.

[56] L. Dai et al., “Pyrolysis technology for plastic waste recycling: A state-of-the-art review,” en, *Progress in Energy and Combustion Science*, vol. 93, p. 101 021, Nov. 2022.

[57] L. C. Mendes and P. S. d. C. Pereira, “Optical Microscopy as a Tool to Correlate Morphology and Thermal Properties of Extruded PET/PC Reactive Blends,” en, *Materials Sciences and Applications*, vol. 2, no. 8, pp. 1033–1040, Aug. 2011.

[58] Adnan, J. Shah, and M. R. Jan, “Effect of polyethylene terephthalate on the catalytic pyrolysis of polystyrene: Investigation of the liquid products,” *Journal of the Taiwan Institute of Chemical Engineers*, vol. 51, pp. 96–102, 2015.

[59] A. Awad, A. Aly Abd El-Wahab, R. El-Gamsy, and M. H. Abdel-latif, “A study of some thermal and mechanical properties of HDPE blend with marble and granite dust,” en, *Ain Shams Engineering Journal*, vol. 10, no. 2, pp. 353–358, Jun. 2019.

[60] F. Xu, B. Wang, D. Yang, J. Hao, Y. Qiao, and Y. Tian, “Thermal degradation of typical plastics under high heating rate conditions by TG-FTIR: Pyrolysis behaviors and kinetic analysis,” en, *Energy Conversion and Management*, vol. 171, pp. 1106–1115, Sep. 2018.

[61] Y.-T. Pan, M. Castillo-Rodríguez, and D.-Y. Wang, “Mesoporous metal oxide/pyrophosphate hybrid originated from reutilization of water treatment resin as a novel fire hazard suppressant,” en, *Materials Chemistry and Physics*, vol. 203, pp. 49–57, Jan. 2018.

[62] I. Vollmer et al., “Beyond Mechanical Recycling: Giving New Life to Plastic Waste,” en, *Angewandte Chemie International Edition*, vol. 59, no. 36, pp. 15 402–15 423, Sep. 2020.

[63] X. Li et al., “Improving the aromatic production in catalytic fast pyrolysis of cellulose by co-feeding low-density polyethylene,” en, *Applied Catalysis A: General*, vol. 455, pp. 114–121, Mar. 2013.

[64] C. Kassargy, S. Awad, G. Burnens, K. Kahine, and M. Tazerout, “Gasoline and diesel-like fuel production by continuous catalytic pyrolysis of waste polyethylene and polypropylene mixtures over USY zeolite,” en, *Fuel*, vol. 224, pp. 764–773, Jul. 2018.

[65] J. Gersten, V. Fainberg, G. Hetsroni, and Y. Shindler, “Kinetic study of the thermal decomposition of polypropylene, oil shale, and their mixture,” *Fuel*, vol. 79, no. 13, pp. 1679–1686, 2000.

[66] G. Özsin and A. E. Pütün, “Insights into pyrolysis and co-pyrolysis of biomass and polystyrene: Thermochemical behaviors, kinetics and evolved gas analysis,” en, *Energy Conversion and Management*, vol. 149, pp. 675–685, Oct. 2017.

[67] K. Praveen Kumar and S. Srinivas, “Catalytic Co-pyrolysis of Biomass and Plastics (Polypropylene and Polystyrene) Using Spent FCC Catalyst,” en, *Energy & Fuels*, vol. 34, no. 1, pp. 460–473, Jan. 2020.

[68] J. Encinar and J. González, “Pyrolysis of synthetic polymers and plastic wastes. Kinetic study,” en, *Fuel Processing Technology*, vol. 89, no. 7, pp. 678–686, Jul. 2008.

[69] G. Lopez, M. Artetxe, M. Amutio, J. Bilbao, and M. Olazar, “Thermochemical routes for the valorization of waste polyolefinic plastics to produce fuels and chemicals. A review,” en, *Renewable and Sustainable Energy Reviews*, vol. 73, pp. 346–368, Jun. 2017.

[70] M. S. Qureshi et al., “Pyrolysis of plastic waste: Opportunities and challenges,” en, *Journal of Analytical and Applied Pyrolysis*, vol. 152, p. 104 804, Nov. 2020.

[71] S. Al-Salem, A. Antelava, A. Constantinou, G. Manos, and A. Dutta, “A review on thermal and catalytic pyrolysis of plastic solid waste (PSW),” en, *Journal of Environmental Management*, vol. 197, pp. 177–198, Jul. 2017.

[72] G. Martínez-Narro, N. J. Royston, K. L. Billsborough, and A. N. Phan, “Kinetic modelling of mixed plastic waste pyrolysis,” en, *Chemical Thermodynamics and Thermal Analysis*, vol. 9, p. 100 105, Mar. 2023.

[73] Z. A. Hussein, Z. M. Shakor, M. Alzuhairi, and F. Al-Sheikh, “Kinetic and Thermodynamic Study of the Pyrolysis of Plastic Waste,” en, *Environmental Processes*, vol. 10, no. 2, p. 27, May 2023.

[74] S. Mirkarimi, S. Bensaid, and D. Chiaramonti, “Conversion of mixed waste plastic into fuel for diesel engines through pyrolysis process: A review,” en, *Applied Energy*, vol. 327, p. 120 040, Dec. 2022.

[75] T. Xayachak et al., “Pyrolysis for plastic waste management: An engineering perspective,” en, *Journal of Environmental Chemical Engineering*, vol. 10, no. 6, p. 108 865, Dec. 2022.

[76] P. Das and P. Tiwari, “The effect of slow pyrolysis on the conversion of packaging waste plastics (PE and PP) into fuel,” en, *Waste Management*, vol. 79, pp. 615–624, Sep. 2018.

[77] G. Yan, X. Jing, H. Wen, and S. Xiang, “Thermal Cracking of Virgin and Waste Plastics of PP and LDPE in a Semibatch Reactor under Atmospheric Pressure,” en, *Energy & Fuels*, vol. 29, no. 4, pp. 2289–2298, Apr. 2015.

[78] H.-S. Tai and J.-L. Yeh, “Evaluation and verification of the virgin–recycled mixing ratio of polypropylene plastic,” en, *Journal of the Chinese Institute of Engineers*, vol. 41, no. 1, pp. 69–75, Jan. 2018.

[79] H. C. Genuino, M. C. P. Van Eijk, S. R. A. Kersten, and M. P. Ruiz, “Pyrolysis of Real Packaging Plastic Waste Streams in a Fluidized-Bed Pilot Plant,” en, *Energy & Fuels*, vol. 38, no. 3, pp. 2188–2199, Feb. 2024.

[80] J. R. Strien, H. C. Genuino, M. C. Van Eijk, P. J. Deuss, and H. J. Heeres, “Pyrolysis of Polyolefin-Enriched Mixed Plastic Waste Streams: Effects of Pretreatments and Presence of Hydrogen during Pyrolysis,” en, *Energy & Fuels*, vol. 39, no. 1, pp. 686–698, Jan. 2025.

[81] M. Van Akker et al., “Full Utilization of Hard-to-Recycle Mixed Plastic Waste by Conversion toward Pyrolysis Oil and BTX Aromatics on a Pilot Scale,” en, *Energy & Fuels*, vol. 39, no. 13, pp. 6438–6451, Apr. 2025.

[82] H. C. Genuino, M. P. Ruiz, H. J. Heeres, and S. R. Kersten, “Pyrolysis of mixed plastic waste (DKR-350): Effect of washing pre-treatment and fate of chlorine,” en, *Fuel Processing Technology*, vol. 233, p. 107 304, Aug. 2022.

[83] D. Zhao, X. Wang, J. B. Miller, and G. W. Huber, “The Chemistry and Kinetics of Polyethylene Pyrolysis: A Process to Produce Fuels and Chemicals,” en, *ChemSusChem*, vol. 13, no. 7, pp. 1764–1774, Apr. 2020.

[84] S. Al-Salem, “Thermal pyrolysis of high density polyethylene (HDPE) in a novel fixed bed reactor system for the production of high value gasoline range hydrocarbons (HC),” en, *Process Safety and Environmental Protection*, vol. 127, pp. 171–179, Jul. 2019.

[85] E. T. Aisien, I. C. Otuya, and F. A. Aisien, “Thermal and catalytic pyrolysis of waste polypropylene plastic using spent FCC catalyst,” en, *Environmental Technology & Innovation*, vol. 22, p. 101 455, May 2021.

[86] M. Martynis, Mulyazmi, E. Winanda, and A. N. Harahap, “Thermal Pyrolysis of Polypropylene Plastic Waste into Liquid Fuel: Reactor Performance Evaluation,” *IOP Conference Series: Materials Science and Engineering*, vol. 543, no. 1, p. 012 047, Jun. 2019.

[87] Y. Jaafar, L. Abdelouahed, R. E. Hage, A. E. Samrani, and B. Taouk, “Pyrolysis of common plastics and their mixtures to produce valuable petroleum-like products,” en, *Polymer Degradation and Stability*, vol. 195, p. 109 770, Jan. 2022.

[88] Y.-H. Seo, K.-H. Lee, and D.-H. Shin, “Investigation of catalytic degradation of high-density polyethylene by hydrocarbon group type analysis,” en, *Journal of Analytical and Applied Pyrolysis*, vol. 70, no. 2, pp. 383–398, Dec. 2003.

[89] K.-H. Lee, N.-S. Noh, D.-H. Shin, and Y. Seo, “Comparison of plastic types for catalytic degradation of waste plastics into liquid product with spent FCC catalyst,” en, *Polymer Degradation and Stability*, vol. 78, no. 3, pp. 539–544, Jan. 2002.

[90] M. S. Abbas-Abadi, M. N. Haghighi, H. Yeganeh, and A. G. McDonald, “Evaluation of pyrolysis process parameters on polypropylene degradation products,” en, *Journal of Analytical and Applied Pyrolysis*, vol. 109, pp. 272–277, Sep. 2014.

[91] A. López, I. De Marco, B. Caballero, M. Laresgoiti, A. Adrados, and A. Aranzabal, “Catalytic pyrolysis of plastic wastes with two different types of catalysts: ZSM-5 zeolite and Red Mud,” en, *Applied Catalysis B: Environmental*, vol. 104, no. 3-4, pp. 211–219, May 2011.

[92] T. Maqsood, J. Dai, Y. Zhang, M. Guang, and B. Li, “Pyrolysis of plastic species: A review of resources and products,” en, *Journal of Analytical and Applied Pyrolysis*, vol. 159, p. 105 295, Oct. 2021.

[93] M. Larrain et al., “Economic performance of pyrolysis of mixed plastic waste: Open-loop versus closed-loop recycling,” en, *Journal of Cleaner Production*, vol. 270, p. 122 442, Oct. 2020.

[94] G. Yadav et al., “Techno-economic analysis and life cycle assessment for catalytic fast pyrolysis of mixed plastic waste,” en, *Energy & Environmental Science*, vol. 16, no. 9, pp. 3638–3653, 2023.

[95] J. Zheng, M. Arifuzzaman, X. Tang, X. C. Chen, and T. Saito, “Recent development of end-of-life strategies for plastic in industry and academia: Bridging their gap for future deployment,” en, *Materials Horizons*, vol. 10, no. 5, pp. 1608–1624, 2023.

[96] M. A. Martín-Lara, A. Piñar, A. Ligero, G. Blázquez, and M. Calero, “Characterization and Use of Char Produced from Pyrolysis of Post-Consumer Mixed Plastic Waste,” en, *Water*, vol. 13, no. 9, p. 1188, Apr. 2021.

[97] D. A. Wijesekara, P. Sargent, C. J. Ennis, and D. Hughes, “Prospects of using chars derived from mixed post waste plastic pyrolysis in civil engineering applications,” en, *Journal of Cleaner Production*, vol. 317, p. 128 212, Oct. 2021.

[98] S. Belbessai et al., “Recent advances in the decontamination and upgrading of waste plastic pyrolysis products: An overview,” *Processes*, vol. 10, no. 4, p. 733, 2022.

[99] W. Zeb et al., “Purification and characterisation of post-consumer plastic pyrolysis oil fractionated by vacuum distillation,” *Journal of Cleaner Production*, 2023.

[100] H. Jeon et al., “Evaluation of the properties and compositions of blended bio-jet fuel produced from wood-derived pyrolysis bio-oil,” *Korean Journal of Chemical Engineering*, 2024.

[101] Chevron, *Aviation fuel specifications (jet a and jet a-1) – overview*, Industry overview document commonly cited for Jet A / Jet A-1 specification intent, 2007.

[102] N. A. N. Halimi et al., “Waste to biofuel: Process design and optimisation for sustainable aviation fuel production from corn stover,” *Energies*, vol. 18, no. 13, p. 3418, 2025.

[103] Y.-C. Liu and W.-C. Wang, “Process design and evaluations for producing pyrolytic jet fuel,” *Biofuels, Bioproducts and Biorefining*, vol. 14, no. 2, pp. 249–264, 2020.

[104] A. H. H. Tameesh et al., “Gas chromatographic determination of total aromatics in kerosene,” *Journal of Chromatography A*, 1985.

[105] K. Lissitsyna et al., “Piona analysis of kerosene by comprehensive two-dimensional gas chromatography coupled to time-of-flight mass spectrometry,” *Fuel*, vol. 116, pp. 716–722, 2014.

[106] B. S. Yoon, C. Kim, G.-J. Park, S. G. Jeon, and C. H. Ko, “Upgrading waste plastic pyrolysis oil via hydrotreating over sulfur-treated ni-mo/al2o3 catalysts,” *Fuel*, vol. 369, p. 131 688, 2024.

[107] T. Luo et al., “Integrating microwave pyrolysis and hydrotreating for converting low-density polyethylene into jet fuel,” *Renewable Energy*, vol. 236, 2024.

[108] S. Tomasek, Z. Varga, and J. Hancsók, “Production of jet fuel from cracked fractions of waste polypropylene and polyethylene,” *Fuel Processing Technology*, vol. 197, p. 106 197, 2020.

[109] R. Palos et al., “Hydrocracking of plastic pyrolysis oil (ppo) blended with vacuum gas oil (vgo) over pt–pd catalysts supported on usy–asa–al2o3 composites,” *Energy & Fuels*, 2024.

[110] C. Kim et al., “Catalytic hydrocracking of waste plastic pyrolysis oil for production of high-quality naphtha over nimo/mesoporous hzsm-5 catalyst,” *Fuel*, vol. 385, p. 134 036, 2025.

[111] M. Sajdak et al., “Design of experiments method into upgrading pyrolytic oil for sustainable aviation fuel additives by hydrotreating and hydrocracking,” *Waste Management*, 2025.

[112] G. Thomassen, M. Van Dael, S. Van Passel, and F. You, “How to assess the potential of emerging green technologies? Towards a prospective environmental and techno-economic assessment framework,” en, *Green Chemistry*, vol. 21, no. 18, pp. 4868–4886, 2019.

[113] M. Van Dael, T. Kuppens, S. Lizin, and S. Van Passel, “Techno-economic Assessment Methodology for Ultrasonic Production of Biofuels,” en, in *Production of Biofuels and Chemicals with Ultrasound*, Z. Fang, R. L. Smith, and X. Qi, Eds., vol. 4, Dordrecht: Springer Netherlands, 2015, pp. 317–345.

[114] M. van der Spek, A. Ramirez, and A. Faaij, “Improving model uncertainty evaluation by using pedigree matrices: A case study on co2 capture with monoethanolamine,” *Computers & Chemical Engineering*, vol. 85, pp. 1–15, 2016.

[115] BlueAlp. “Bluealp technology — fast and lower-cost scaling.” States scaling from 24.5 kt/y to 70 kt/y input capacity, Accessed: Sep. 12, 2025. [Online]. Available: https://www.bluealp.nl/expertise/technology/.

[116] Itero Technologies. “Itero to build plastic waste recycling plant at brightlands chemelot campus.” Announces demonstration plant sized at ~27,000 t/y, Accessed: Sep. 12, 2025. [Online]. Available: https://www.itero-tech.com/news/itero-brightlands-chemelot-campus.

[117] Xycle. “Xycle will start construction of its first plastic recycling plant in 2024.” Plant designed to process 21,000 t/y of plastic waste in Rotterdam, Accessed: Sep. 12, 2025. [Online]. Available: https://xyclegroup.com/xycle-will-start-construction-of-its-first-plastic-recycling-plant-at-the-end-of-2022/.

[118] Plastic Energy. “Sabic plastic energy advanced recycling (spear).” Geleen advanced recycling plant capacity: 20,000 t/y; JV with SABIC, Accessed: Sep. 12, 2025. [Online]. Available: https://plasticenergy.com/project/spear/.

[119] PreZero. “Prezero sorting facility port of rotterdam.” Capacity of 100–110 kt/yr PMD, Accessed: Sep. 12, 2025. [Online]. Available: https://www.prezero.com/nl-en/news/prezero-opens-new-sorting-facility-in-the-port-of-rotterdam.

[120] AVR. “Avr residual waste sorting rozenburg.” Capacity of 430 kt/yr, extracts plastics and beverage cartons, Accessed: Sep. 12, 2025. [Online]. Available: https://www.avr.nl/en/what-we-do/residual-waste-sorting.

[121] Argus Media. “Shell to replace moerdijk cracker furnaces.” Ethylene capacity 970 kt/yr, propylene 500 kt/yr, Accessed: Sep. 12, 2025. [Online]. Available: https://www.argusmedia.com/en/news-and-insights/latest-market-news/2138648-shell-to-replace-moerdijk-cracker-furnaces.

[122] Shell. “Shell pernis refinery.” Large crude oil refinery producing fuels including aviation kerosene, Accessed: Sep. 12, 2025. [Online]. Available: https://www.shell.com/business-customers/chemicals/manufacturing-locations.html.

[123] S. H. Lim, H. H. Pham, E. H. Kwon, and N. S. Nho, “Optimizing the use of pyrolysis waste oil as a feedstock for the naphtha cracking process by hydrotreating and hydrocracking,” *Resources, Environment and Sustainability*, vol. 22, p. 100 277, 2025.

[124] G. Towler and R. Sinnott, *Chemical Engineering Design: Principles, Practice and Economics of Plant and Process Design*, 2nd ed. Elsevier, 2012.

[125] W. D. Seider, D. R. Lewin, J. D. Seader, S. Widagdo, R. Gani, and K. M. Ng, *Product and Process Design Principles: Synthesis, Analysis, and Evaluation*, 4th ed. Wiley, 2017.

[126] Belastingdienst, *Tarieven voor de vennootschapsbelasting (2024)*, Dutch Tax Administration website page listing CIT brackets and rates, 2024.

[127] Intratec. "Gasoline price in the netherlands." Accessed 27 January 2026, Accessed: Jan. 27, 2026. [Online]. Available: https://www.intratec.us/solutions/energy-prices-markets/commodity/gasoline-price-netherlands.

[128] International Air Transport Association (IATA). "Jet fuel price monitor." Accessed 2026-02-25. [Online]. Available: https://www.iata.org/en/publications/economics/fuel-monitor/.

[129] Market data source as used in workbook. "Title transfer facility (ttf) natural gas price, annual average (2024)." Workbook uses an annual average of 34.65 EUR/MWh (converted with 1 MWh = 3.6 GJ). Replace this placeholder with the exact data provider and dataset used.

[130] Intratec. "Industrial hydrogen price in the netherlands." Accessed 29 May 2025, Accessed: May 29, 2025. [Online]. Available: https://www.intratec.us/solutions/industry-economics-worldwide/utility/industrial-hydrogen-price-netherlands.

[131] European Central Bank (ECB). "Euro foreign exchange reference rates." Reference rates for 2026-02-25, accessed 2026-02-25. [Online]. Available: https://www.ecb.europa.eu/stats/shared/pdf/eurofxref.pdf.

[132] CBS (Statistics Netherlands). "Prices of energy." Accessed 29 May 2025, Accessed: May 29, 2025. [Online]. Available: https://www.cbs.nl/en-gb/figures/detail/85666ENG.

[133] Intratec. "Industrial steam cost in netherlands." Accessed 29 July 2025, Accessed: Jul. 29, 2025. [Online]. Available: https://www.intratec.us/solutions/industry-economics-worldwide/utility/industrial-steam-cost-netherlands.

[134] Intratec. "Cooling water cost in netherlands." Accessed 29 May 2025, Accessed: May 29, 2025. [Online]. Available: https://www.intratec.us/solutions/industry-economics-worldwide/utility/cooling-water-cost-netherlands.

[135] STOWA, "Symbaal zuivering: Theoretische verkenning van de haalbaarheid," STOWA, 2013, Accessed via Wageningen UR e-depot.

[136] Y. Zhu, S. T. Rahardjo, C. Valkenburg, L. Snowden-Swan, S. Jones, and M. Machinal, "Techno-economic analysis for the thermochemical conversion of biomass to liquid fuels," Pacific Northwest National Laboratory (PNNL), Washington, USA, 2011, Cited in workbook as basis for heavy purge disposal cost (USD basis), converted using ECB FX.

[137] S. Jones et al., "Process design and economics for the conversion of lignocellulosic biomass to hydrocarbon fuels: Fast pyrolysis and hydrotreating bio-oil pathway," National Renewable Energy Laboratory (NREL), NREL/TP-5100-61178, Nov. 2013, Accessed 27 January 2026.

[138] Chemical Engineering, *Economic indicators: Ce plant cost index (cepci) updates (june 2024 preliminary / may 2024 final)*, ChemEngOnline Economic Indicators / CEPCI update, Aug. 2024.

[139] AACE International, *Recommended practice 18r-97: Cost estimate classification system – as applied in engineering, procurement, and construction for the process industries*, AACE Recommended Practice, 1997.

[140] CME Group. "European naphtha cargoes cif nwe (platts) futures – quotes." Accessed 2026-02-25. [Online]. Available: https://www.cmegroup.com/markets/energy/refined-products/european-naphtha-calendar-swap.html.

[141] Organization of the Petroleum Exporting Countries (OPEC). “Conversion factors (volume to mass and vice versa).” Accessed 2026-02-25. [Online]. Available: https://www.jodidata.org/_resources/files/events/joint-apec-jodi-training-workshop-on-oil-and-gas-statistics/04.-conversion-factors-volume-to-mass-and-vice-versa.pdf.

[142] M. van der Spek, A. Ramirez, and A. Faaij, *Supplementary material for: Improving model uncertainty evaluation by using pedigree matrices*, Supplementary information / appendix material, 2016.

A

Supplementary Excel workbooks and traceability

A.1. Appendix roadmap

This thesis is accompanied by two Excel workbooks that implement the steady-state gate-to-gate model (Areas A100–A400) and the screening techno-economic assessment (TEA) and discounted cash flow (DCF) calculations used in Chapter 6, Chapter 7, and Chapter 8. The appendix is written to support verification of reported results while avoiding duplication of large calculation tables that are already supplied in the workbooks.

What is contained in the PDF appendix

The PDF appendix provides (i) a workbook architecture map, (ii) a compact traceability convention and audit path for Chapter 6 to Chapter 8, and (iii) a small set of high-value disclosure tables that improve auditability of the economic basis and sensitivity implementation without reproducing the full Excel calculation layers.

What remains in the Excel workbooks

The Excel workbooks contain the complete intermediate calculations, including the full stream lists, area-level mass and energy balance sheets, utility integration logic, cost build-ups, the DCF timeline used for MSP closure, and the pathway-specific pedigree reporting sheets (`PA - Results`). These layers are intentionally not reproduced in full in the PDF to preserve readability.

A.2. Supplementary file identifiers

Two workbooks are submitted alongside the PDF.

- **Supplementary File S1:** `Complete Model - Jet fuel BASE.xlsx` (jet-fuel pathway workbook)
- **Supplementary File S2:** `Complete Model - Naphtha BASE.xlsx` (naphtha pathway workbook)

A.3. Traceability convention and audit path

A.3.1. Reference format

Workbook references are written in a compact form:

```
S#:Sheet!Cell
```

where S# is S1 or S2, Sheet is the Excel sheet name, and Cell is the Excel cell address. If a named range is used, the named range replaces Cell.

A.3.2. Audit path for Chapters 6--8

Chapter 6
Values reported in Chapter 6 are consolidated in Chapter 6 Results. This sheet reports each KPI together with a *Source* pointer that identifies the originating calculation sheet and cell or the relevant stream list entry. Verification should therefore start at Chapter 6 Results and then follow the *Source* pointer into the deeper area sheets or the Master Stream List.

Chapter 7
Values reported in Chapter 7 are consolidated in Chapter 7 Results. DCF construction and the derivation of NPV and IRR are implemented in DCF. The MSP closure convention is implemented by solving for a product-price scaling factor such that NPV at the defined reference point equals zero; the corresponding solve factor is located in Economic Inputs, and the resulting NPV can be verified on DCF.

Chapter 8
The one-at-a-time sensitivity analysis in Chapter 8 varies a small set of high-leverage parameters while holding all other assumptions fixed. In the workbooks, these parameters map to a small number of input cells (or to multipliers applied to those cells). The baseline values correspond to the Chapter 7 BASE case (see Table 7.2 and Table 7.3); the sensitivity ranges are defined in Table 8.1. Appendix Table A.4 provides the cell-level implementation references used for reproducibility.

A.3.3. Worked examples (stable cell references)

- **Annual throughput (Chapter 6 reporting layer):** S1:Chapter 6 Results!E4 reports annual plastic throughput; the calculation source is shown in S1:Chapter 6 Results!H4 and traces to S1:Master Stream List!B12 and S1:Economic Inputs!B8.
- **NPV consistency between reporting and DCF sheets:** S1:Chapter 7 Results!B5 reports NPV (PV at year 0) and matches S1:DCF!B56.
- **A market-facing coefficient used in Chapter 7 and Chapter 8:** the baseline hydrogen unit price is S1:Economic Inputs!B61; the OAT hydrogen-price cases in Chapter 8 apply multipliers to this coefficient while holding consumption constant.

A.4. Workbook architecture map

Both workbooks implement the same modelling logic and use the same sheet names for the reporting and area calculation layers, although sheet ordering differs between files. Table A.1 summarises the workbook structure and indicates which sheets serve as the reporting layer for thesis values.

A.5. DCF conventions and economic basis as implemented in Excel

The DCF basis used in Chapter 7 is defined in Table 7.2. For auditability, Table A.2 reports the corresponding workbook entries and references to the cell locations used in Supplementary Files S1–S2.

A.6. Key economic input coefficients used in Chapter 7 and Chapter 8

Table 7.3 reports the unit coefficients used to monetise material and utility flows at battery limits. Table A.3 provides the corresponding workbook cell references for the coefficients used directly in the OAT sensitivity levers in Chapter 8.

Table A.1: Workbook architecture and navigation map for Supplementary Files S1–S2. Sheet names are reported verbatim.

Layer	Sheets and purpose
Reporting layer	`Chapter 6 Results` (consolidated technical KPIs and *Source* pointers); `Chapter 7 Results` (consolidated economic indicators); `CAPEX`, `OPEX` (cost build-ups); `DCF` (cash-flow timeline, NPV, IRR, MSP closure); `Results` (pedigree summary tables, see Appendix B).
Inputs and global data	`README` (navigation); `Process Description` (high-level process narrative); `Technical Inputs` (technical assumptions and constants); `Economic Inputs` (financial basis, coefficients, and DCF parameters); `Master Stream List` (stream table backbone); `Yield & Composition Data` and `Boiling Point Data` (property and yield inputs); `Equipment List` (equipment inventory for CAPEX); `Energy Balance Formulas` (shared energy-balance logic); `General Overview` (system-level summary checks).
Area-level overview sheets	`A100 - Overview`, `A200 - Overview`, `A300 - Overview`, `A400 Overview` (area-level closure checks and summaries used as integrity indicators in Chapter 6).
Area-level detailed calculation sheets	**A100:** `A100 - Pyrolysis Energy`, `A100 Pyrolysis - Mass`, `A100 - FGH & Furnace Mass + En`, `A100 - Pyrolysis Reactor`. **A200:** `A200 HTU - Energy`, `A200 HTU - Mass`, `A200 - HTU Reactor`. **A300:** `A300 HCU - Energy`, `A300 HCU - Mass`, `A300 - Distillation Collumn`, `A300 - HCU Reactor`. **A400:** `A400 - Utilities Mass`, `A400 - Utilities Energy`.
Pedigree module sheets	`Pedigree Analysis Guidelines` (criteria guidance); `PA - Technical Model` and `PA - Economic Model` (documentation layer for scoring logic); `PA - Results` (consolidated pedigree outputs for each pathway workbook, including reviewer scores, mean score, and reviewer deviation).

Table A.2: DCF conventions and financial basis as implemented in the Excel workbooks (baseline). Values correspond to Table 7.2; references indicate where they are set in `Economic Inputs`.

Parameter	Value	Unit	Excel reference
Discount rate (real)	0.15	–	`S1:Economic Inputs!B14`, `S2:Economic Inputs!B14`
Analysis horizon	25	years	`S1:Economic Inputs!B15`, `S2:Economic Inputs!B15`
Construction period	2	years	`S1:Economic Inputs!B16`, `S2:Economic Inputs!B16`
Construction CAPEX split (year -2 / -1)	0.40 / 0.60	–	`S1:Economic Inputs!B17--B18`, `S2:Economic Inputs!B17--B18`
Start-up utilisation (year 0)	0.80	–	`S1:Economic Inputs!B19`, `S2:Economic Inputs!B19`
Depreciation method and period	straight-line, 25	years	`S1:Economic Inputs!B21--B23`, `S2:Economic Inputs!B21--B23`
Corporate income tax rate	0.258	–	`S1:Economic Inputs!B25`, `S2:Economic Inputs!B25`
Working capital fraction (shortcut)	0.15	–	`S1:Economic Inputs!B43`, `S2:Economic Inputs!B43`
NPV reference point	year 0 (start of operation)	–	`S1:Economic Inputs!B26`, `S2:Economic Inputs!B26`
Cash-flow timing	end-of-year convention	–	`S1:Economic Inputs!B27`, `S2:Economic Inputs!B27`

Table A.3: Selected market-facing coefficients and their Excel locations (baseline). Values correspond to Table 7.3 and the BASE case described in Chapter 7.

Coefficient	Value	Unit	Excel reference
Fuel-gas export price (Stream 423 credit)	9.63	EUR/GJ	`S1:Economic Inputs!B59`, `S2:Economic Inputs!B59`
Plastic feedstock gate price	0	EUR/t	`S1:Economic Inputs!B60`, `S2:Economic Inputs!B60`
Hydrogen price	0.6846	EUR/kg	`S1:Economic Inputs!B61`, `S2:Economic Inputs!B61`

A.7. Sensitivity parameter implementation map

The OAT sensitivity ranges are defined in Table 8.1. Table A.4 adds the cell-level mapping required to reproduce each lever in the Excel workbooks under the Chapter 7 MSP closure convention.

Table A.4: Sensitivity levers, ranges (from Table 8.1), and Excel implementation references. All other assumptions remain at baseline during each OAT run.

Lever	Unit	Low	Base	High	Excel implementation reference
Plant capacity (annual throughput)	kt/y	20	40	80	Adjust plastic feed rate in `Master Stream List!B12` (Stream 101 total, kg/h) and verify annual throughput in `Chapter 6 Results!E4`; CAPEX scaling follows the workbook rule in `CAPEX`.
Feedstock price at battery limits	EUR/t	-100	0	$+100$	Modify `Economic Inputs!B60` (plastic feedstock gate price).
Hydrogen price multiplier	–	0.5×	1.0×	1.5×	Apply the multiplier to `Economic Inputs!B61` (hydrogen unit price) while holding consumption constant.
Fuel-gas export monetisation (Stream 423 credit)	–	0%	100%	150%	Apply the multiplier to `Economic Inputs!B59` (fuel-gas export price coefficient).

B

Pedigree analysis summary

B.1. Purpose and scoring approach

This thesis applies a pedigree analysis to transparently communicate the strength of the evidence base behind (i) the technical steady-state model in Chapter 6 and (ii) the screening techno-economic model in Chapter 7. The pedigree approach and scoring procedure are defined in subsection 4.3.2 and are based on the pedigree-criteria definitions reported by van der Spek et al. and their supplementary material [114], [142].

The pedigree scoring in this thesis is based on two independent reviewers (Reviewer A: author; Reviewer B: supervisor). The submitted Excel workbooks contain the underlying reviewer scores and the consolidated pedigree summaries on the `PA - Results` sheet for each pathway workbook. Because the scores are ordinal, the reported summary consists of the mean score and the reviewer deviation (absolute difference between reviewers) for each criterion and assessed model element.

B.2. Implementation in the submitted Excel workbooks

The pedigree module is included in Supplementary Files S1–S2 to keep the documentation and consolidated outputs traceable to the same workbook versions used for Chapter 6 to Chapter 8. Guidance is provided in `Pedigree Analysis Guidelines`, and consolidated outputs are presented on `Results`. The tables below reproduce the consolidated *Mean* and *Std. Dev.* values as reported on `Results`; these summary statistics describe the central tendency and spread of the underlying scored items within each evidence category.

B.3. Implications for interpreting Chapters 7 and 8

The pedigree results support two interpretation points that are carried forward into Chapter 8. First, screening-level CAPEX estimation and fixed-cost modelling exhibit comparatively weaker empirical support than the DCF framework itself, and they contribute materially to scale effects in the capacity lever. Second, boundary-credit and co-product monetisation is comparatively weakly supported and commercially contingent, motivating its explicit inclusion as an OAT lever in the sensitivity analysis.